ResearchGate

See discussions, stats, and author profiles for this publication at: https://www.researchgate.net/publication/324125814

The primate fovea: Structure, function and development

Article *in* Progress in Retinal and Eye Research · March 2018

DOI: 10.1016/j.preteyeres.2018.03.006

CITATIONS
98

READS
2,624

7 authors, including:

Steffen Syrbe
Universität Heidelberg
126 PUBLICATIONS **1,704** CITATIONS
SEE PROFILE

Mike Francke
University of Leipzig
82 PUBLICATIONS **3,734** CITATIONS
SEE PROFILE

Peter Wiedemann
University of Leipzig
597 PUBLICATIONS **16,788** CITATIONS
SEE PROFILE

Andreas Reichenbach
University of Leipzig
293 PUBLICATIONS **13,074** CITATIONS
SEE PROFILE

Some of the authors of this publication are also working on these related projects:

glutathion in mammalian retina View project

Cellular responses in MNU-induced retinal degeneration View project

All content following this page was uploaded by Mike Francke on 06 June 2019.

The user has requested enhancement of the downloaded file.

Progress in Retinal and Eye Research 66 (2018) 49–84

Contents lists available at ScienceDirect

Progress in Retinal and Eye Research

journal homepage: www.elsevier.com/locate/preteyeres

The primate fovea: Structure, function and development

Andreas Bringmann[a], Steffen Syrbe[b,1], Katja Görner[b,2], Johannes Kacza[c], Mike Francke[b,c], Peter Wiedemann[a], Andreas Reichenbach[b,*]

[a] Department of Ophthalmology and Eye Hospital, Medical Faculty, University of Leipzig, 04103 Leipzig, Germany
[b] Paul Flechsig Institute of Brain Research, Medical Faculty, University of Leipzig, 04103 Leipzig, Germany
[c] Saxon Incubator for Clinical Translation (SIKT), Leipzig University, 04103 Leipzig, Germany

ARTICLE INFO

Keywords:
Fovea
Glia
Müller cell
Astrocyte
Optics
Primate

ABSTRACT

A fovea is a pitted invagination in the inner retinal tissue (fovea interna) that overlies an area of photoreceptors specialized for high acuity vision (fovea externa). Although the shape of the vertebrate fovea varies considerably among the species, there are two basic types. The retina of many predatory fish, reptilians, and birds possess one (or two) convexiclivate fovea(s), while the retina of higher primates contains a concaviclivate fovea. By refraction of the incoming light, the convexiclivate fovea may function as image enlarger, focus indicator, and movement detector. By centrifugal displacement of the inner retinal layers, which increases the transparency of the central foveal tissue (the foveola), the primate fovea interna improves the quality of the image received by the central photoreceptors. In this review, we summarize – with the focus on Müller cells of the human and macaque fovea – data regarding the structure of the primate fovea, discuss various aspects of the optical function of the fovea, and propose a model of foveal development. The "Müller cell cone" of the foveola comprises specialized Müller cells which do not support neuronal activity but may serve optical and structural functions. In addition to the "Müller cell cone", structural stabilization of the foveal morphology may be provided by the 'z-shaped' Müller cells of the fovea walls, via exerting tractional forces onto Henle fibers. The spatial distribution of glial fibrillary acidic protein may suggest that the foveola and the Henle fiber layer are subjects to mechanical stress. During development, the foveal pit is proposed to be formed by a vertical contraction of the centralmost Müller cells. After widening of the foveal pit likely mediated by retracting astrocytes, Henle fibers are formed by horizontal contraction of Müller cell processes in the outer plexiform layer and the centripetal displacement of photoreceptors. A better understanding of the molecular, cellular, and mechanical factors involved in the developmental morphogenesis and the structural stabilization of the fovea may help to explain the (patho-) genesis of foveal hypoplasia and macular holes.

1. Introduction

Vertebrate species possess a retina which is inverted with respect to the light path. The inverted structure allows an efficient trophic and structural support of photoreceptors by the retinal pigment epithelium (RPE). However, it has the disadvantage that the incoming light has to traverse the entire neural retina before it arrives at photoreceptors. Cellular elements with dimensions within or near the wavelength range of visible light, e.g., cell processes and organelles, are phase objects that reflect and scatter light (Zernike, 1955; Land, 1972; Tuchin, 2000). Light scattering by the retinal tissue in the living eye is evidenced by the fact that optical coherence tomography (OCT) delivers images of retinal layers. In OCT images, the highest light reflectivities are found in the nerve fiber (NFL) and inner plexiform layers (IPL), the outer plexiform (OPL) and Henle fiber layers (HFL), the outer limiting membrane (OLM), and the transition zone between the inner and outer photoreceptor segments (Fig. 1Ba and 2A). Light reflection within the NFL, plexiform (synaptic) layers, and HFL suggests that a substantial portion of the incident light is scattered at neuronal and photoreceptor cell axons and synapses. Retinal light scattering is expected to reduce visual

Abbreviations: ACL, amacrine cell layer; BCL, bipolar cell layer; FGF, fibroblast growth factor; GCL, ganglion cell layer; GFAP, glial fibrillary acidic protein; HFL, Henle fiber layer; ILM, inner limiting membrane; INL, inner nuclear layer; IPL, inner plexiform layer; NFL, nerve fiber layer; OCT, optical coherence tomography; OLM, outer limiting membrane; ONL, outer nuclear layer; OPL, outer plexiform layer; PDGF, platelet-derived growth factor; RFL, radial fiber layer; RPE, retinal pigment epithelium; VEGF, vascular endothelial growth factor

* Corresponding author. Paul Flechsig Institute of Brain Research, University of Leipzig, Liebigstraße 19, D-04103 Leipzig, Germany.
E-mail address: reia@medizin.uni-leipzig.de (A. Reichenbach).
[1] Center for Paediatric and Adolescent Medicine, Division for Neuropaediatrics and Metabolic Medicine, Heidelberg University Hospital, 69,120 Heidelberg, Germany.
[2] Median Klinik Bad Sülze, 18334 Bad Sülze, Germany.

https://doi.org/10.1016/j.preteyeres.2018.03.006
Received 17 November 2017; Received in revised form 20 March 2018; Accepted 27 March 2018
Available online 30 March 2018
1350-9462/ © 2018 Elsevier Ltd. All rights reserved.

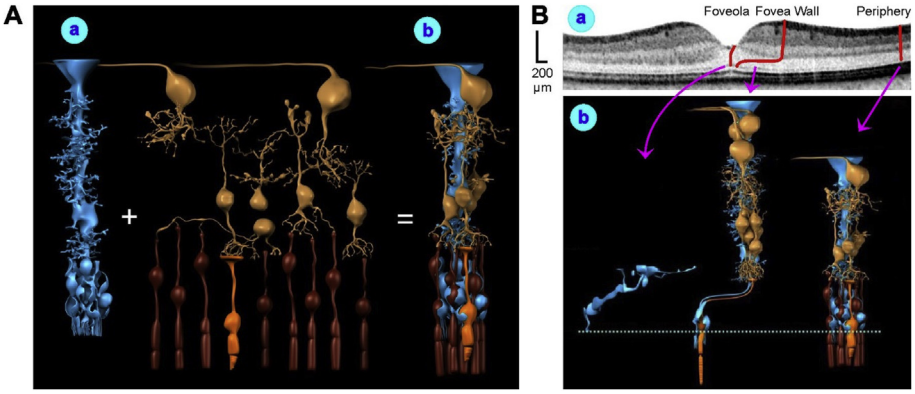

Fig. 1. Müller cells of the primate retina. **A.** Müller cells form the cores of the functional units of retinal information processing. Every Müller cell is surrounded by a distinct group of photoreceptors and neurons (**a**) with which it interacts specifically during development and mature functioning (**b**). *Blue*, Müller cells. *Yellow*, neurons. *Orange*, cones. *Brown*, rods. **B.** Morphological diversity of Müller cells in the human retina. **a.** OCT image of a human fovea. Note that the image is optically inverted, i.e., light-reflecting structures appear *dark*. **b.** Müller cells as well as photoreceptors and neurons of their columns in three parts of the retina. In the foveola (*left side*), where the inner retinal layers are shifted peripherally and the light nearly directly hits the photoreceptor cells, short specialized Müller cells extend from the vitreal (inner) surface of the retina to the outer limiting membrane (*dashed line*). These cells do not form a functional column with photoreceptors and neurons. In the fovea walls and parafovea (*middle*), very long Müller cells display a z-shaped morphology because (within the Henle fiber layer) Müller cell processes run centrifugally in association with photoreceptor cell axons. In the retinal periphery (*right side*), shorter and thicker Müller cells run roughly straight through the tissue. While the overall number of photoreceptors and neurons per Müller cell does not change from the fovea wall to the retinal periphery, there is an alteration in the composition of the functional unit, i.e., peripheral units contain more rods and fewer neurons than more central units. Modified after Reichenbach and Bringmann (2010, 2017).

sensitivity and acuity, and decreases the signal-to-noise ratio of the visual image (Agte et al., 2011). In addition, angioscotomas produced by light scattering and absorption at blood vessels decrease the quality and brightness of the visual image (Weale, 1966).

Various retinal adaptations developed during the evolution of the vertebrate eye in order to minimize retinal light scattering and to increase the visual resolution. It has been shown for the retina of nonprimate mammals (Franze et al., 2007; Agte et al., 2011; Labin et al., 2014), and proposed for the human and avian retina (Labin et al., 2014; Zueva et al., 2014), that Müller cells act as living optical fibers which guide the light with minimal intensity loss through the inner retinal layers toward the photoreceptors. Müller cells, the principal macroglial cells of the vertebrate retina (Müller, 1851; Bringmann et al., 2006; Reichenbach and Bringmann, 2010), are specialized radial glial cells which span the whole thickness of the neural retina, from the vitreal surface to the subretinal space (Müller, 1856; Reichenbach and Bringmann, 2017). The endfeet and inner main processes of Müller cells are light-guiding fibers (Franze et al., 2007) which bypass the light-scattering nerve fibers and synapses in the inner retina. The image, which is transported to the photoreceptors by a population of Müller cells, is resolved in 'pixels' corresponding to individual Müller cells (Franze et al., 2007). Because the local densities of cone photoreceptors and Müller cells are roughly equal in many species (Reichenbach and Robinson, 1995; Agte et al., 2011), every cone may have its 'private' Müller cell which delivers the appropriate pixel of the image, while several rods (up to 10 in the peripheral human retina; Reichenbach and Bringmann, 2010) are illuminated by one Müller cell. Through the thick, multilayered outer nuclear layer (ONL) of the peripheral retina of nocturnal mammals, in which the outer Müller cell processes are very thin, light is transported by the nuclei of rod photoreceptor cells which are arranged in linear vertical rows and thus form chains of lenses which transmit the light delivered by Müller cells and direct it to the receptor segments (Solovei et al., 2009; Kreysing et al., 2010).

In addition to optical image magnification factors like eye size, lens radius, and anterior segment light refraction, visual acuity mainly depends on the density of photoreceptors and the ratio between the numbers of photoreceptors and ganglion cells (Wässle and Boycott, 1991). (The acuity of stereoscopic vision also depends on the central visual information processing). Across the vertebrate species, the density of retinal cells may be increased in the central retina, the temporal retina, and/or the horizontal meridian of the retina (Müller, 1861; Walls, 1942). In areas of high cell densities, the retina is thickened, and photoreceptors may show a bouquet-like spatial arrangement (Franz, 1913). The retina of nonprimate mammals does not contain a fovea but may have specialized areas of high cell densities like a concentrically organized area centralis (predators like the cat), a visual streak (as in rabbits and tree shrews) which lies along the horizontal meridian of the retina, or a combination of a visual streak and an area centralis (Reichenbach and Robinson, 1995; Ahnelt and Kolb, 2000). The different morphologies of these regions are adaptations to the feeding behavior and habitats of the animals. The visual streak of rabbits, for example, is a high-density area that scans the horizon without the need of extensive head movements. The retina of dogs contains a fovea externa, i.e., a central area without a foveal pit which contains a fovea-like bouquet of cone photoreceptors and a high ganglion cell density (Franz, 1913; Beltran et al., 2014).

A further retinal specialization which minimizes light scattering and increases the visual acuity is the presence of a fovea. The retinas of various vertebrate species possess one or two foveas (Müller, 1861, 1862, 1863). A fovea is a pitted invagination in the inner retina (fovea interna) that overlies an area of photoreceptors specialized for high acuity vision (fovea externa). A fovea contains particularly high numbers of photoreceptors and neurons, and provides the highest visual resolution (Walls, 1942; Polyak, 1957). The foveal pit may improve the local visual acuity by magnifying the image and/or by improving the transparency of the retinal tissue due to lateral displacement of the light-scattering inner retinal layers. Although the foveal shape varies considerably across the species, there are two basic types of the vertebrate fovea. The typical fovea of many predatory teleosts, reptilians (lizards, certain snakes), and birds, which have avascular retinas, is the convexiclivate fovea (Slonacker, 1897; Wood, 1917; Walls, 1942; Duke-Elder, 1958). A convexiclivate fovea is a funnel-shaped fovea (Fig. 3A) and is localized in the near-central and/or temporal retina. The pit of the convexiclivate fovea can be shallow, medium, or deep (Fig. 3C) (Slonacker, 1897). The walls of deep-pit foveas have a convex shape, and the slope of the pit is more or less steep (Fig. 3A,C). In many species with deep foveas, the foveal center does not contain light-scattering ganglion cell somata and axons (Fig. 3C); depending on the depth of the pit, the foveal center may lack further inner retinal layers like the IPL and inner nuclear layer (INL), and may also show a (partial) displacement of the ONL (Fig. 3A) (Fite and Rosenfield-Wessels, 1975). However, many birds and teleosts possess a fovea in which all retinal layers are present in the foveal center, albeit with reduced thickness (Walls, 1942). It has been proposed that light refraction at the vitreoretinal border of the convexiclivate fovea provides a local magnification of the image (Fig. 3B and C; see 3.) that (in addition to the high density of photoreceptors and the 1:1:1 ratio between photoreceptors, bipolar cells, and ganglion cells (Ramón y Cajal, 1891) underlies the high

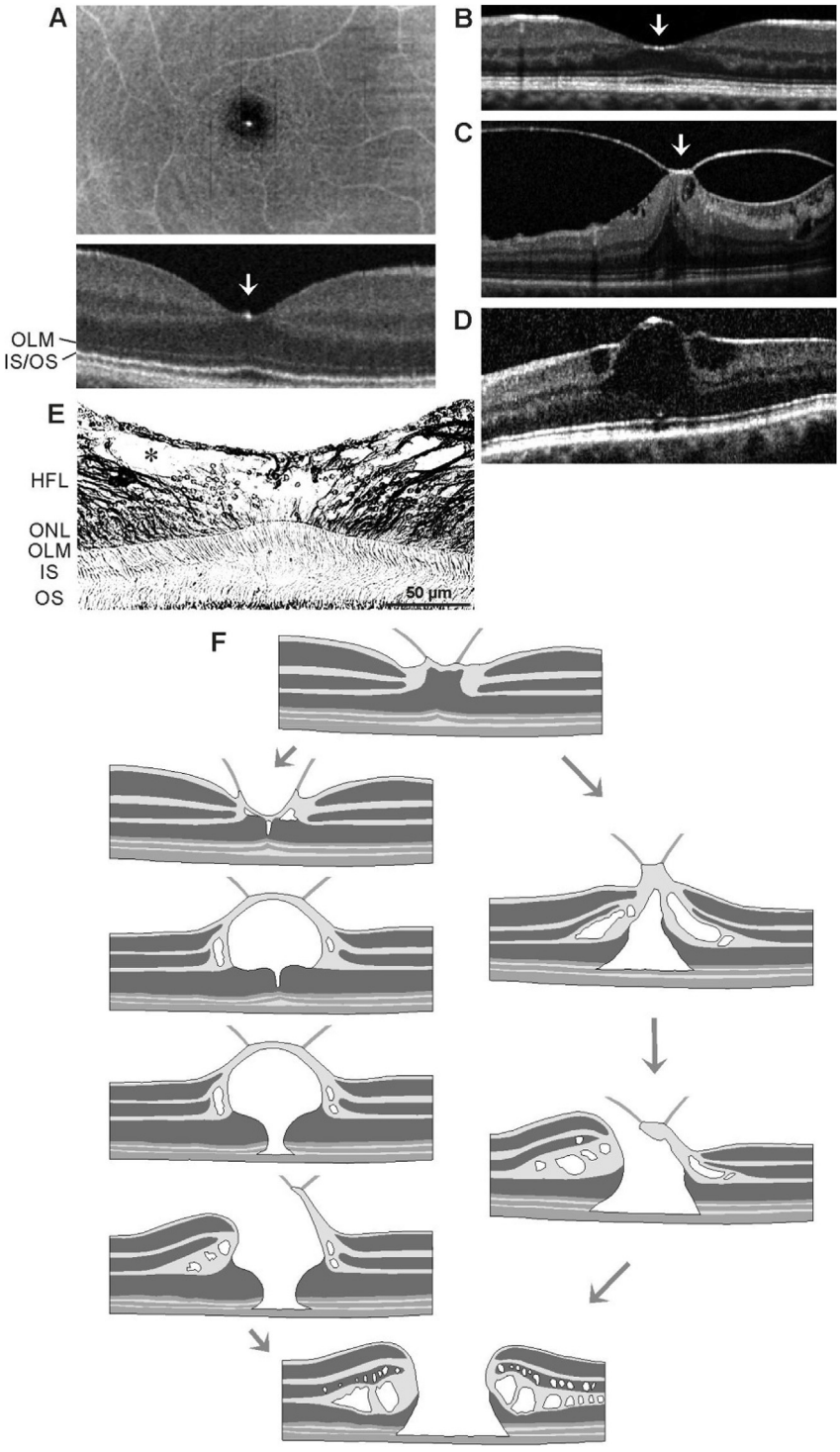

Fig. 2. Pathology of the foveola. **A.** OCT images of horizontal (*above*) and vertical sections (*below*) through the center of the foveola of a normal human subject (22 years, male). Note the hyperreflective dot in the inner layer of the central foveola (*arrow*) which is the central light reflex at the deepest point of the foveal pit (Tick et al., 2011). The position of the dot coincides with the tip of the fovea externa, i.e., the central 'photoreceptor pyramid' created by the elongated photoreceptor segments which is recognizable at the oblique arrangements of the outer limiting membrane (OLM) and the inner/outer segment (IS/OS) boundary. **B.** Fovea of a 60 year-old female with Müller cell sheen dystrophy. Note that the inner Müller cell layer of the foveola contains multiple hyperreflective dots (*arrow*). **C.** Fovea of a 58 year-old female with vitreoretinal traction syndrome. The foveola is detached because of tractional forces from membranes which adhere at the edges of the foveola. Note the strong hyperreflectivity of the inner Müller cell layer of the foveola which contains many hyperreflective dots (*arrow*). Note also that the foveola is detached at the boundary between the outer nuclear layer (ONL) and OLM. **D.** Fovea of a 71 year-old female with Müller cell sheen dystrophy. The inner layer of the foveola is detached from the ONL by a large cyst. The detached inner layer is connected to the fovea walls by Müller cell processes to the nerve fiber and inner plexiform layers. The ONL of the foveola is well preserved while the fovea externa is flattened. **E.** Hematoxylin/eosin-stained section through the foveola of a rhesus macaque. Note the tissue disruptions between the inner Müller cell layer and Henle fiber layer (HFL) in the more peripheral foveola (*), and between the inner layer and OLM in the central foveola. The locations of tissue disruptions suggest that these regions have a low resistance against mechanical stretch. Disruptions of the tissue at these sites are often seen before the development of macular holes (Chung and Byeon, 2017). **F.** Development of macular holes, as suggested by Chung and Byeon (2017). There are (at least) two modes of macular hole formation which differ in the early stage. Macular hole formation is often caused by anteriorposterior vitreoretinal traction resulting from perifoveal posterior vitreous detachment. Vitreoretinal traction produces a tissue disruption and cyst formation within the foveola (*left side*) or a detachment of the foveolar neuroretina (*right side*). In cases of intrafoveolar tissue splitting and cyst formation (*left*), there are often horizontal cleavages at the boundary between the inner Müller cell layer and HFL of the peripheral foveola, and a vertical cleavage in the center of the foveola. Disruption or loss of the “Müller cell cone” in the foveola precedes the development of a full-thickness macular hole. After formation of a full-thickness macular hole, the foveolar ONL degenerates within several days after loss of the “Müller cell cone” (*left*) (Byon et al., 2014). Radial tension from the nerve fibers may produce an elevation of the retinal tissue around the hole. The edematous cysts in the HFL and INL are caused (at least in part) by the Müller cell dysfunction of water transport (Bringmann et al., 2004). The area of the full-thickness macular hole is limited by the perifoveal blood vessels which mechanically interfere with the centrifugal displacement of the retinal tissue. When vitreoretinal traction produces a detachment of the inner Müller cell layer from the ONL (*left*), the operculum contains the tissue of the inner layer of the foveola; after detachment of the foveolar tissue (*right*), the operculum may contain the whole foveolar tissue. Images are modified after OCT images shown by Chung and Byeon (2017).

acuity of foveal vision (Walls, 1942).

Retinas of nonprimate mammals do not possess a fovea; a fovea was ‘reinvented’ by higher primates (Slonacker, 1897). Most prosimian primates are nocturnal and have an area centralis with higher photoreceptor and neuron densities in which large blood vessels are absent; several species also have elongated photoreceptors in the central retina. Higher diurnal primates (haplorrhines: tarsiers, monkeys, apes) have a concaviclivate fovea (Walls, 1942). The concaviclivate fovea is a dish- or bowl-shaped fovea (Fig. 1Ba, 2A,B, and 3A); this fovea is a specialization of the area centralis that lies along the horizontal meridian of the retina (Fig. 4A) (Polyak, 1957). The fovea is situated slightly temporal to the retinal center near the optic axis where chromatic aberration is least (Pumphrey, 1948; Polyak, 1957). In the center of the concaviclivate fovea (the foveola or 'little fovea'), all inner retinal layers are shifted peripherally (Fig. 3A) and blood vessels are absent (the foveal avascular zone; Fig. 4B) (Müller, 1856). (However, there are variations in the morphology of the foveola; see 4.5.) Nocturnal tarsiers have a foveal pit from which blood vessels and most ganglion cells, but

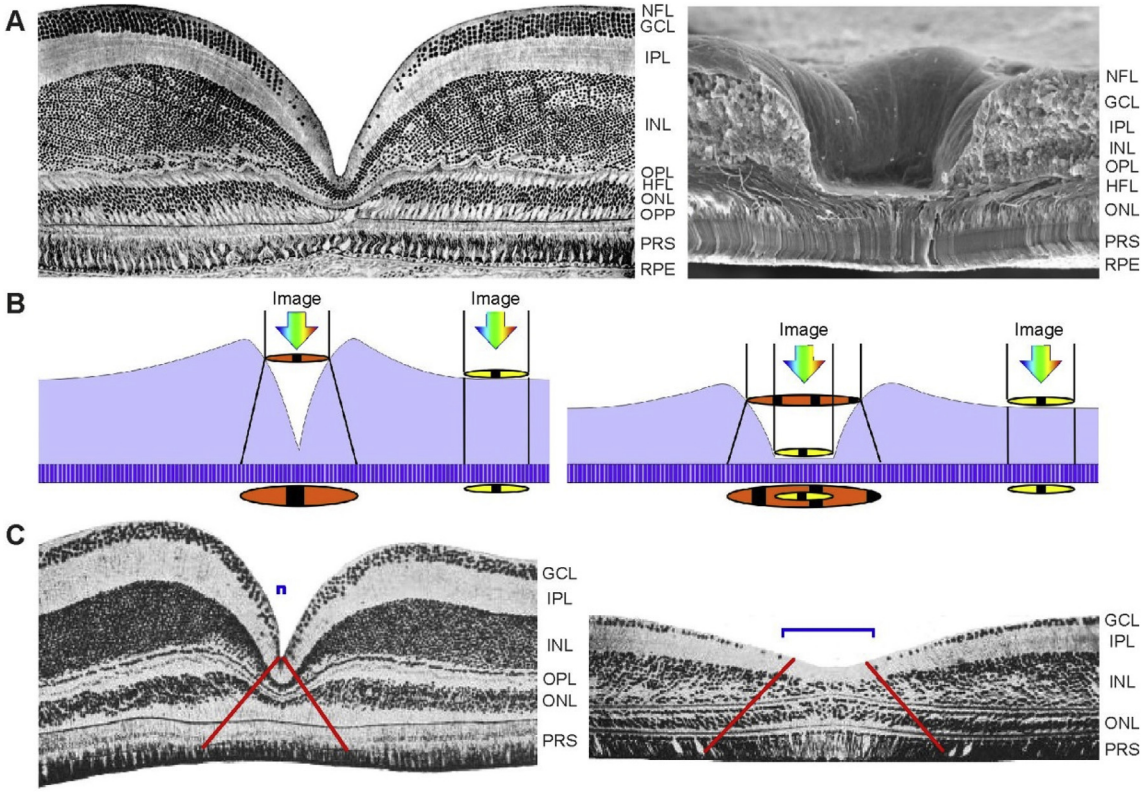

Fig. 3. Convexiclivate and concaviclivate fovea. **A.** Histological section through the central convexiclivate fovea of an American golden eagle (*left*) and scanning electron microphotograph of the fovea of a macaque monkey (*right*). Note the different shapes of the pits of both fovea types. In the eagle fovea (*left*), all inner retinal layers, with the exception of the ganglion cell layer (GCL), are present up to the center of the pit, although at lower thickness. In the macaque fovea (*right*), the nerve fiber layer (NFL), GCL, inner plexiform (IPL), inner nuclear (INL), and outer plexiform layers (OPL) are absent in the foveola. Note the extremely high packing density and elongation of cone photoreceptor segments (PRS) in the central foveola and the centrifugal course of cone cell axons in the Henle fiber layer (HFL). **B.** Presumed optics of both fovea types. *Left:* As hypothesized by Walls (1942), the steep walls of the convexiclivate fovea constitute a means to expand the image on its way through the retinal tissue and thus to generate a magnified image at the level of the photoreceptor cells. The peripheral retina does not provide image magnification. *Right:* A similar image-magnifying function may have the central walls of the concaviclivate fovea (which may be rather steep, too) whereas the flat foveola proper allows a short, direct pathway of the image to the central cones, without light-scattering at inner retinal layers. **C.** Presumed optics of deep and shallow convexiclivate foveas. The images show cross-sections through the deep fovea of the European bank swallow (*left*) and the shallow fovea of a tuatara (*right*). As suggested by Snyder and Miller (1978), the deep fovea with steep fovea walls (*left*) provides a huge magnification of a small part of the foveal image. The steeper the slope of the central fovea walls, the steeper is the curvature of the ganglion cell-free (*bracket*) concave bottom of the foveal pit, and the higher is the magnitude of image magnification. In the shallow fovea (*right*), the ganglion cell-free zone (*bracket*) is wider than in the deep fovea; however, the foveal image is less magnified compared to the deep fovea. Note the shallow bowl formed by the OPL below the base of the foveal pit of the deep fovea (*left*) which likely serves as projection area for the magnified image. In birds, deep foveas are used fo lateral high-acuity monocular vision in great distances, while shallow foveas are used for binocular vision in near distances with lower acuity (Müller, 1863; Tucker, 2000). ONL, outer nuclear layer; OPP, outer photoreceptor cell processes; RPE, retinal pigment epithelium. The images of **A** (*left*) and **C** are modified from Polyak (1957) and Walls (1942), respectively.

not INL cells, are excluded (Rohen and Castenholtz, 1967; Wolin and Massopust, 1970; Ross, 2004). Night monkeys (*Aotes*) vary in respect to the presence of a fovea; there are species in which a fovea is absent, rudimentary, or present in 10% of the individuals (Moritz et al., 2014). The owl monkey *Aotes*, which evolved from a diurnal ancestor and returned to a nocturnal lifestyle, has a fovea externa and a fovea-like thinning of the ganglion cell layer (GCL) and INL; however a foveal pit, a foveal avascular zone, and true midget ganglion cells (see 2.4.1.) are absent (Woollard, 1927; Kolmer, 1930; Webb and Kaas, 1976). In addition, the retina of owl monkeys lacks blue cones (Jacobs, 1998).

The centrifugal displacement of inner retinal layers in the central primate fovea greatly reduces the light scattering at neuronal structures and blood vessels, and allows a nearly direct illumination of photoreceptors (Müller, 1856; Polyak, 1957; Duke-Elder, 1958; Weale, 1966). The degree of light scattering in the human retina is least at the fovea and increases more peripherally; the retina is most transparent in the fovea (Gorrand, 1979). The advantage of the displacement of the inner retinal layers is also suggested by the reduced visual acuity of many individuals with foveal hypoplasia which contain all retinal layers in the foveal center (Thomas et al., 2011; Wilk et al., 2014; McCafferty et al., 2015). The shallow bowl of the foveola is surrounded by convex fovea walls (Figs. 3A and 5A,B). The extreme packing of cone photoreceptors in the fovea externa in association with the midget system of photoreceptors and neurons in the fovea walls, i.e., the 1:2:2 circuitry between cones, midget bipolars, and midget ganglion cells (see 2.4.) (Polyak, 1941), is the main basis of the high-acuity vision provided by the primate fovea (Hendrickson, 2005). In this review, we summarize – with the focus on Müller cells of the human and macaque fovea – data regarding the structure of the primate fovea, discuss certain aspects of the optical function of the fovea, and propose a model of foveal development in which Müller cells and astrocytes contribute to the formation of the foveal pit.

2. Structure of the primate fovea

The presence of the human macula lutea was discovered by Buzzi (1782). The presence of the human fovea was discovered in 1791 and described by Sömmerring (1795) as 'foramilunum centrale retinae'. Shortly after, Buzzi (1795) described that the fovea centralis is not a hole, but a localized thinning of the retinal tissue (Belloni, 1983).

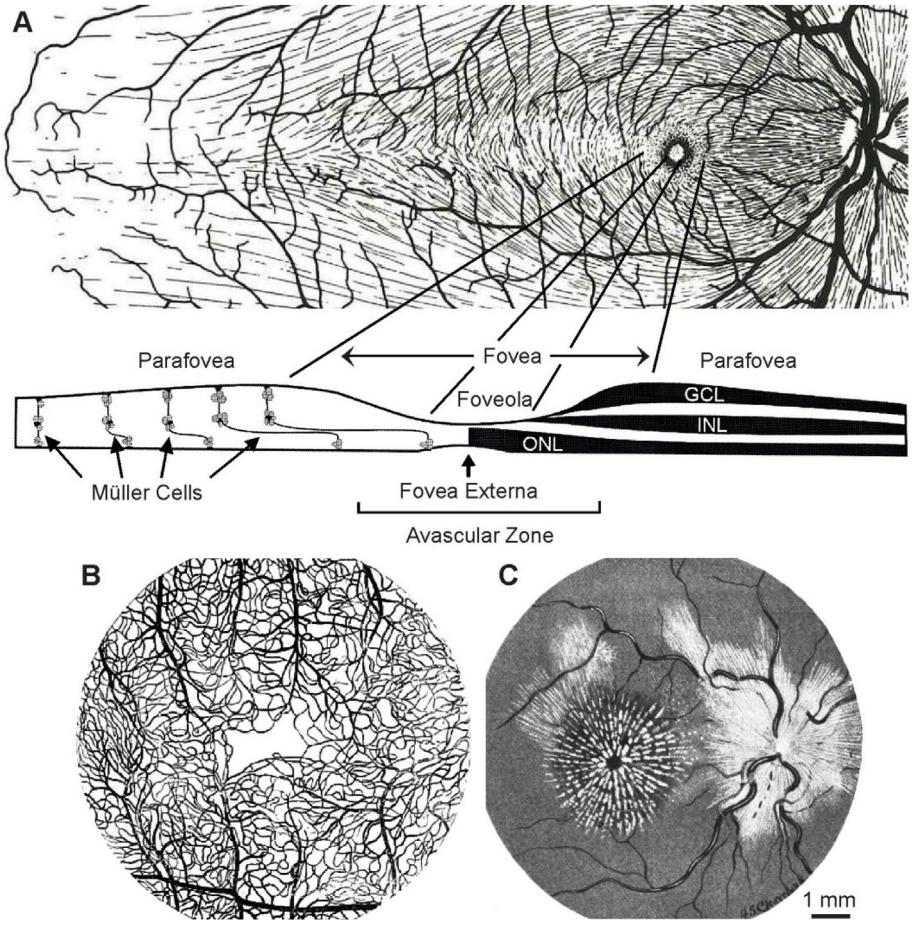

Fig. 4. Nerve fiber bundles, blood vessels, and Henle fibers around the primate fovea. **A.** *Above:* Horizontally placed area centralis, which produces a bilateral symmetry of the retina, in the fundus of the rhesus macaque. The horizontal meridian of the retina extends from the fovea to the temporal margin of the retina (*left*). Note the similar spatial arrangements of large blood vessels (*thick lines*) and nerve fiber bundles (*thin lines*). Thinner arteries and thicker veins emerge from the optic disc (*right*). The area centralis is supplied with blood by the superior and inferior vascular arcades. Nerve fiber bundles draw above and below from the horizontal meridian. *Below:* Schematic representation of the macular region of primates. Note that the foveal slope is steeper in the nasal hemimeridian than in the temporal hemimeridian. **B.** Blood vessels supplying the human foveal region, drawn from an injected preparation by Heinrich Müller. **C.** Appearance of the ocular fundus of a human subject with albuminuric retinitis. The degenerative patches arranged in a stellate fashion around the fovea (*left*) reflect exudates localized in the Henle fiber layer caused by leakage of the outer capillary plexus (located at the border between the inner nuclear and outer plexiform layers). Note the large area of the Henle fiber layer around the fovea. The stellate structure around the optic disk (*right*) are light reflexes or exudates in the nerve fiber layer. Images are modified after Piersol (1897), Wood and Woodruff (1904), and Polyak (1957).

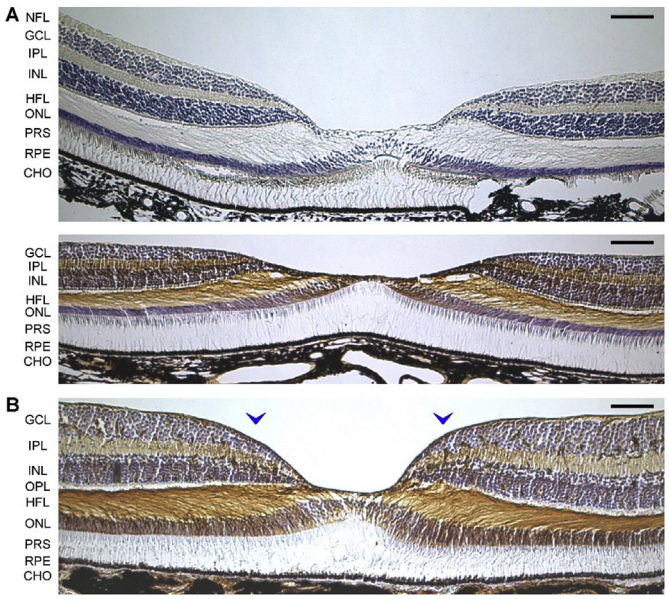

Fig. 5. Morphological variation of the primate fovea. **A.** Cross-sections through two foveas of the common squirrel monkey (*Saimiri sciureus*). Note the different thickness and shapes of the outer nuclear (ONL) and Henle fiber layers (HFL) in the center of the foveola. **B.** Cross-section through the fovea of a siamang (*Symphalangus syndactylus*). Müller cells are visualized by vimentin immunohistochemistry (*brown*); cell nuclei are stained with hematoxylin-eosin (*blue*). *Arrowheads*, centralmost blood vessels. CHO, choriocapillaris; GCL, ganglion cell layer; INL, inner nuclear layer; IPL, inner plexiform layer; NFL, nerve fiber layer; OPL, outer plexiform layer; PRS, photoreceptor segments; RPE, retinal pigment epithelium. Bars, 100 µm.

In humans, the macula lutea is an elliptically shaped area, about 5.5 mm in diameter, which includes the foveal, parafoveal, and perifoveal retina (Fig. 6). The fovea (delimitated by the rim of the foveal pit) comprises the foveola proper and the central fovea walls (Fig. 4A), the parafovea includes the peripheral fovea walls, and the perifovea is the area between the margins of the parafovea and the macula (Fig. 6). The more or less flat foveola proper, which is elliptical with a long horizontal axis of about 300 µm and a vertical axis of about 200 µm (Detwiler, 1943), is the central fovea which does not contain inner retinal layers (Polyak, 1957). The foveal pit has a diameter of about 0.8–1.5 mm, and the parafovea is a 0.5 mm-wide annular zone surrounding the fovea (Polyak, 1957). The fovea walls are the sites of the thickest retina (thickness, 275–410 µm on the temporal side and 220–350 µm on the nasal side) (Duke-Elder, 1958). The human fovea lies 3.5–5.5 mm temporal to the optic disk and 0.6–0.8 mm below the center of the optic disk (Figs. 4A and 6) (Detwiler, 1943). The foveas of pigtail and stumptail macaques lie 3.60 and 3.15 mm, respectively, temporal to the optic disk (Schein, 1988; Packer et al., 1989).

The movements which create the primate fovea during the ontogenetic development involve a centrifugal displacement of the inner retina (see 4.3.) and a centripetal displacement of the outer retina (see 4.4.). The former produces the foveola, and the latter produces the fovea externa. Both movements causes the formation of the HFL. The HFL contains the axons of photoreceptor cells which draw from the photoreceptor cell somata in the ONL to the OPL where they make synapses with bipolar cells; the axons are surrounded and bound together by the outer processes of Müller cells (Fig. 7I). Thus, the foveal photoreceptor cell axons and the local Müller cell processes follow the same 'z course' (Fig. 1Bb, 8A–D, and 9C). The displacement of the inner retinal layers at the foveola produces a thickening of the inner retinal layers in the foveal walls and parafovea (Fig. 1Ba). The parafovea has

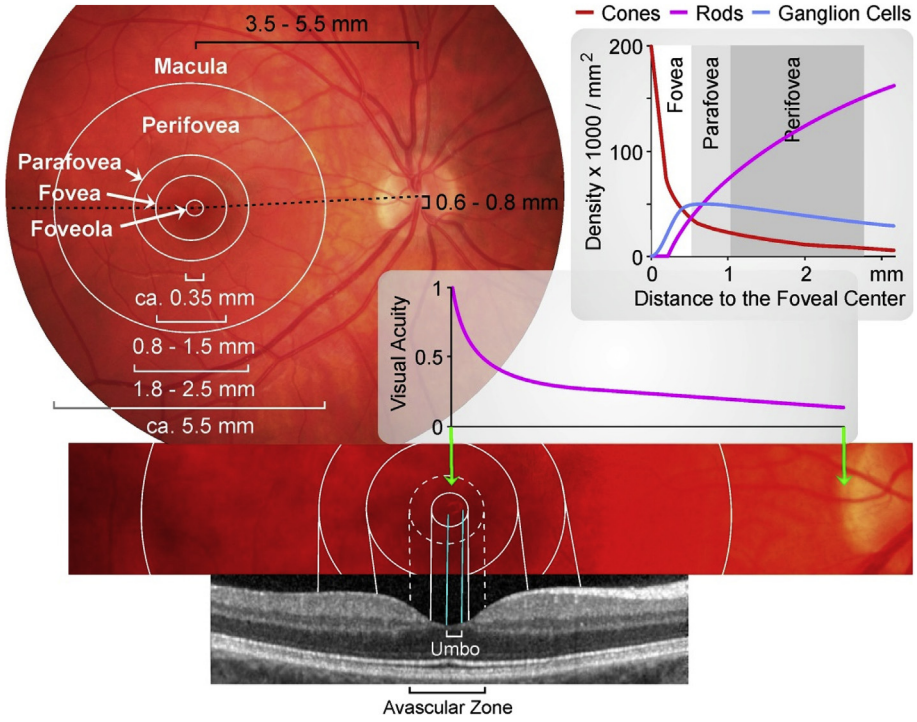

Fig. 6. Human macula. The macular region includes the fovea (i.e., the foveal pit) with the foveola (the area of the highest visual acuity and the highest density of cone photoreceptors), the parafovea (the area of the highest cell density and the thickest retina), and the perifovea. The rim of the avascular zone is located at the slope of the foveal pit. The location and size of the umbo (the area of the light reflex at the central concavity of the floor of the foveal pit) depend upon the shape of the foveal pit and the angle of the incoming light.

the largest accumulation of neurons in the retina; the INL of the parafovea consists of up to 12 rows of cells (Fig. 5A and B and 10Ja). The GCL forms up to 9 rows of closely packed cells at the foveal edge; the thickness of the GCL decreases to 4 cell layers at the peripheral edge of the parafovea, and to a monolayer of cell somata at the peripheral edge of the perifovea (Hendrickson, 2005). Thus, the macula is characterized by containing two or more ganglion cell layers.

The fovea externa, i.e., the pyramid-like indention into the foveolar tissue which is created by the elongated central cone receptors (Schultze, 1866) (Fig. 2A,E, 4A, 10A, and 11B), contains the foveal cone mosaic and corresponds with the rod-free site of the highest visual acuity (see 2.3.). The tip of the fovea externa, which is located in the foveolar center (the site of the smallest thickness of the foveola; Fig. 2A,E, 10A, and 11B), indents the foveola resulting in a decreased length of the light path between the inner retinal surface and the receptor segments. Because the foveola is largely rod-free (Fig. 7A) (Ahnelt, 1998; Provis et al., 2005; Bumsted O'Brien, 2008), the primate fovea is blind at night (with the exception of the fovea of nocturnal tarsiers in which rods are present at significant densities throughout the central retina [Polyak, 1957; Hendrickson et al., 2000]).

Most mammals but primates are dichromates; they possess two types of cones, middle-wavelength (green light)-sensitive (M) cones (termed in the following text as 'green cones'), used for shape and contrast detection, and a minority of short-wavelength (blue light)-sensitive (S) cones ('blue cones'), used for color information. Simian primates add a third type of long-wavelength (red light)-sensitive (L) cones ('red cones'); a splice mutation of the gene encoding the green-sensitive cone photopigment generated a long wavelength-sensitive photopigment (Lamb et al., 2007; Lamb, 2013). This improvement in color vision has evolved three separate times in simian primates (Jacobs, 1998; Jacobs and Deegan, 2001). However, many primate species have more than two alleles for the M/L photopigments and a polymorphic color vision comprising populations of di- and tichromatic individuals.

The central fovea of primates is also free of blood vessels (Fig. 4B) (Müller, 1856; Polyak, 1957; Duke-Elder, 1958). The foveal avascularity removes angioscotomas from the visual image (Weale, 1966). Circularly arranged capillaries at the GCL-IPL, IPL-INL, and INL-OPL boundaries, which form anastomoses and join as a single layered ring, delimitate the foveal avascular zone in the foveal slope. In the macaque fovea, the vascular coverage of the photoreceptor layer is zero in the foveal avascular zone, 30% at 1 mm from the foveal center (the edge of the foveal pit), and 45% at 2 mm from the foveal center (Snodderly et al., 1992). In macaques, the foveal avascular zone has a diameter of 500–650 µm (Snodderly et al., 1992; Provis et al., 2000). In human subjects, the foveal avascular zone may have diameters between 200 µm and 1 mm (Adler, 1929; Dubis et al., 2012a); most subjects have a 400–600 µm-wide avascular zone (Weale, 1966; Mansour et al., 1993). In the sample of the human fovea shown in Fig. 7J, the centralmost vessel is located at around 250 µm from the foveal center; Müller cell processes cover the outer surface of the vessel (Syrbe et al., 2018). The central fovea of primates is also free of astrocytes (Fig. 12B and C) and microglia (Schnitzer, 1987; Penfold and Provis, 1991; Distler et al., 1993; Provis et al., 2000).

Among most primates, from marmosets to humans, the absolute dimensions of the fovea externa (foveal cone density and areas of the foveal cone mosaic and rod-free zone), the diameter of the foveal pit, and the relative position of the fovea in the temporal retina remain constant despite a fivefold variation in eye size and retinal area (with the exception of the howler monkey which has a small rod-free zone associated with a very high central cone density) (Franco et al., 2000). Thus, in larger eyes, the fovea subtends a decreasing visual angle. About 50% of the primary visual cortex processes information provided by the fovea (Wässle et al., 1989). It has been suggested that larger foveas may not be possible without enlarging the brain beyond its cranial capacity (Hendrickson, 2005). In addition, the absence of blood supply in the foveal center may restrict the size of the fovea (Franco et al., 2000).

2.1. Foveola

The foveola is formed by cone and Müller cells (Yamada, 1969). In addition, few dispersed ganglion cell and interneuron somata (Fig. 7F), as well as few cone pedicles, may be present (Polyak, 1957; Leventhal et al., 1988; Fukuda et al., 1989; Savy et al., 1991; Ahnelt, 1998; Hendrickson, 2005; Rudich et al., 2013; Syrbe et al., 2018). The human foveola has an average diameter of 350 µm (Curcio et al., 1990) and a

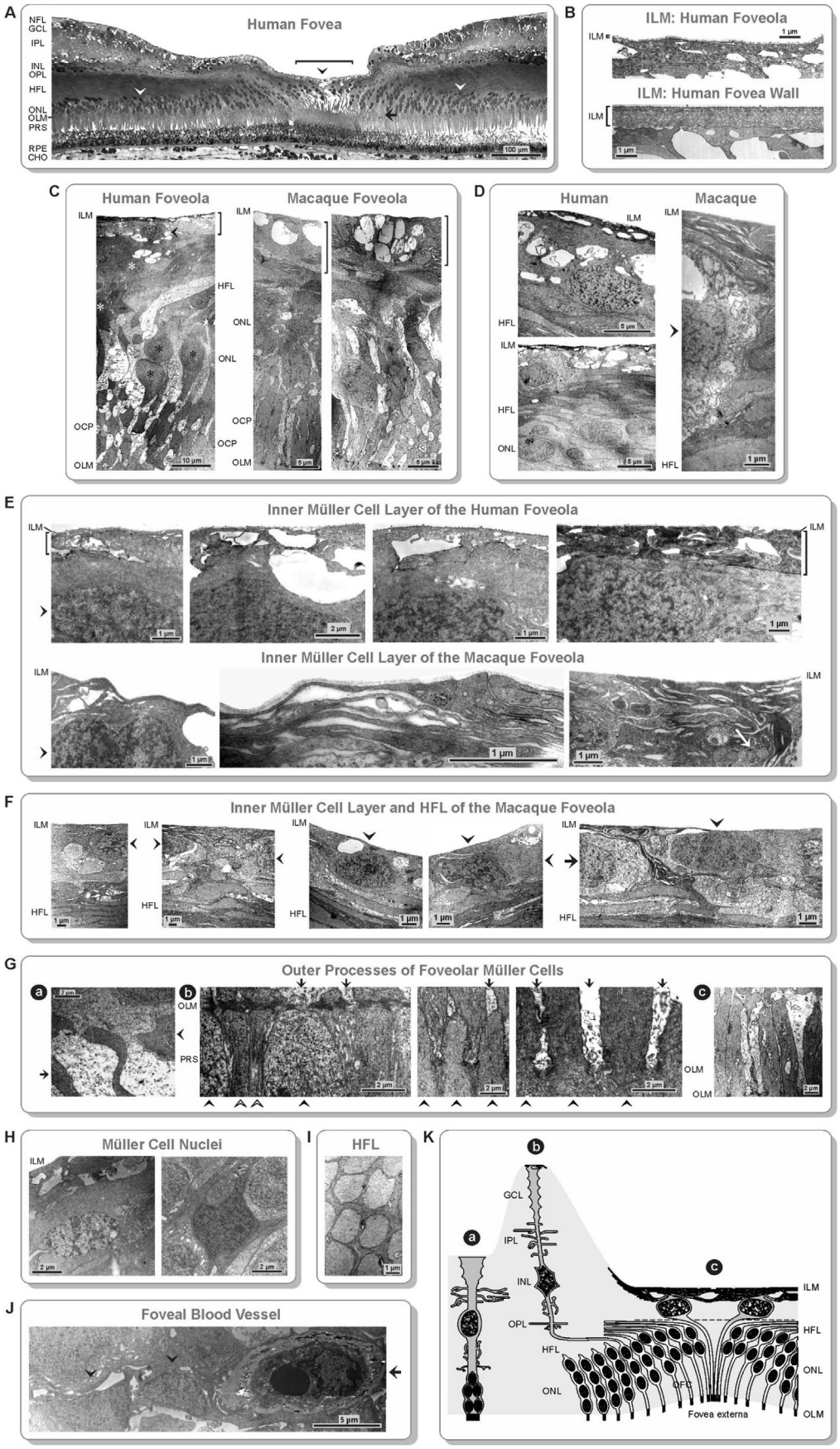

(caption on next page)

Fig. 7. Ultrastructure of Müller cells in the central foveas of a 40 years-old human male without apparent intraocular disease and an adult cynomolgus monkey (*Macaca fascicularis*). **A.** Semithin cross-section through the human fovea. The foveola is composed of a thin inner layer which contains the somata and inner processes of specialized Müller cells. The inner Müller cell layer lies in front of the outer nuclear layer (ONL) and the central bouquet of cone photoreceptors (*bracket*). The ONL of the foveola is composed of obliquely arranged rows of cone cell somata (including nuclei) which are separated from the outer limiting membrane (OLM) by a layer which contains outer cone processes (OCP) and Müller cell processes (*arrow*). *White arrowheads* indicate the centralmost rod nuclei which are located at 270 and 370 μm, respectively, from the foveal center. The *black arrowhead* indicates the deepest point of the foveal pit. **B.** Different morphologies of the inner limiting membrane (ILM) in the human foveola (*above*) and fovea walls (*below*). In the foveola, the basal lamina of the ILM (*bracket*) is very thin (about 40 nm). Depending on the distance to the foveola, the thickness of the basal lamina increases (about 900 nm). The Müller cell processes, which contact the basal lamina, contain smooth endoplasmic reticulum and mitochondria. **C.** Cross-sections through the foveola of the human (*left*) and macaque retina (*right*). The tissue composition is similar in the human and macaque foveola. The foveola of both species is composed of four layers which lie in front of the fovea externa, i.e., the inner layer, the Henle fiber layer (HFL), the ONL, and the layer of the outer cone cell processes. The inner layer, which mainly contains the cytoplasm, nuclei, and inner processes of specialized Müller cells, as well as watery cysts, overlies the central Henle fibers and ONL. *Arrowhead*, Müller cell nucleus. *Black and white asterisks*, nuclei of cone cells. In the center of the foveola, 2–3 cone cell somata are stacked. Above the cone cell nuclei, Henle fibers are bended centrifugally. The cytoplasm of the outer Müller cell processes becomes less electron-dense (brighter) and more loosely distributed in the course from the inner Müller cell layer to the OLM. Müller cell processes which accompany the cone cell axons in the HFL of the foveola also display a relatively electron-lucent cytoplasm. In the macaque foveola, the outer cone cell processes have a diameter of about 2.2 μm at the OLM; the cone inner segments have a diameter of about 2.8 μm. The length of the outer cone cell processes (between the cone cell nuclei and OLM) is ≥ 15 μm. Note that the thickness of the foveola is smaller in the macaque compared to the human tissue. **D.** Cross-section through the inner layers of the transition zone between the foveola and the fovea wall. The innermost layer contains numerous watery cysts and thin Müller cell processes, which run below the ILM. The human tissue contains Müller cell (*above*) and neuronal cell nuclei (*below*) which lie near the HFL. The macaque tissue contains a neuronal cell nucleus (*arrowhead*). **E.** Cross-sections through the inner Müller cell layer of the foveola. The composition of the inner layer of the foveola is similar in the human and macaque tissues. The thickness of the basal lamina of the ILM is less than 40 nm. The tissue between the ILM and Müller cell nuclei (*arrowheads*) is composed of numerous lamelliform and tubular Müller cell processes, which form an elaborated plait below the basal lamina; the Müller cell processes surround fluid-filled cysts (*brackets*). Many Müller cell processes have a thickness similar to that of the basal lamina. The Müller cell cytoplasm contains abundant smooth endoplasmic reticulum. The *arrow* points to cross-sections through tubular Müller cell processes with diameters between 30 and 500 nm. **F.** Cross-sections through the inner layer and the HFL of the macaque foveola. Note the presence of thin Müller cell processes and cystoid spaces between the ILM and Müller cell nuclei (*arrowheads*). The *right image* shows a Müller cell nucleus (*arrowhead*) and a neuronal cell body (*arrow*) in the inner layer of the foveola, located at 45 μm from the foveal center. **G.** Outer processes of foveolar Müller cells. **a.** Section through the ONL of the human foveola. *Arrow*, cone cell axon. *Arrowhead*, cone cell soma. Note that the cytoplasm of Müller cell processes becomes more electron-lucent and more loosely distributed in the course towards the OLM (*below*). **b.** OLM of the human parafovea (*left*) and foveola (*middle* and *right*). The section through the parafovea (*left*) shows (thicker) cone segments (*filled arrowheads*) and (thinner) rod segments (*unfilled arrowheads*). The cone processes in the sections through the foveola (*middle* and *right*) have diameters between 1.9 and 2.1 μm at the OLM. Note that the cytoplasm of Müller cell processes (*arrows*) near the OLM of the foveola is less electron-lucent, loosely distributed, and contains membranous and vesicular structures, while the cytoplasm of cone processes is electron-dense and contains fibrillar structures. **c.** Outer Müller cell and cone cell processes near the OLM of the macaque foveola. **H.** Different morphologies of Müller cell nuclei in the human foveola near the ILM (*left*) and in the inner nuclear layer (INL) of the fovea wall (*right*). The nucleus in the foveola has an oval shape, while the Müller cell soma and nucleus in the fovea wall are polygonal because they are impressed by the surrounding neuronal somata. **I.** Cross-section through the HFL in the wall of the macaque fovea. The diameter of a Henle fiber is about 2 μm. The fibers are separated by Müller cell processes. **J.** Cross-section through the centralmost blood vessel (*arrow*) located around 250 μm from the center of the human fovea. At the *left side*, two Müller cell nuclei are visible (*arrowheads*). The processes of the right Müller cell run along the ventral surface of the vessel. An erythrocyte is visible in the vessel lumen. **K.** Schematic representation of the Müller cell morphology in the peripheral retina (**a**), fovea walls (**b**), and foveola (**c**). Müller cells in the fovea walls (**b**) display a 'z-shape' because of the elongation of their outer processes which run obliquely or horizontally through the HFL. The somata of the specialized Müller cells in the foveola (**c**) lie in the innermost layer. The thin lamelliform and tubular inner processes of these cells form an elaborated plait along and below the ILM, and surround the cystoid spaces in this layer. The outer processes run through the ONL of the foveola up to the OLM and thus form the stalk of the “Müller cell cone”. The cytoplasm of these processes becomes increasingly dispersed and electron-lucent in their course to the OLM. The fovea externa is the indention into the foveolar tissue caused by the elongation of the central cone photoreceptors. CHO, choriocapillaris; GCL, ganglion cell layer; IPL, inner plexiform layer; NFL, nerve fiber layer; OPL, outer plexiform layer; PRS, photoreceptor segments; RPE, retinal pigment epithelium. Modified after Syrbe et al. (2018).

thickness of 90–130 μm (Polyak, 1957; Yamada, 1969; Burris et al., 2002; Yanni et al., 2012). However, there is a high interindividual variability in the dimensions of the foveola. There are individuals with a small and thick foveola; here, the ONL is thickest in the center of the foveola, and the central fovea may contain remnants of inner retinal layers (Fig. 13D) (Tick et al., 2011). In individuals with a wide, flat, and thin foveola, the central ONL is v-shaped and thickest in the periphery of the foveola (Fig. 13D) (Tick et al., 2011). A v-shaped central ONL is also found in the monkey foveola (Figs. 5A and 10A). In a specimen of a macaque fovea, the local density of ONL nuclei peaks between 100 and 120 μm from the foveal center (Fig. 10E). In the sample of the human fovea shown in Fig. 7C, the foveola has a thickness of about 65 μm (measured between the inner limiting membrane [ILM] and OLM) while the fovea walls have a thickness of 220 μm (Fig. 7A) (Syrbe et al., 2018). The foveola of cynomolgus monkeys has a thickness of 45–67 μm (Fig. 7C) (Schein, 1988; Syrbe et al., 2018). (However, it cannot be ruled out that the foveal thickness in these specimens is decreased due to tissue dehydration during histological processing.)

The foveola is composed of four layers which lie in front of the fovea externa, i.e., the inner layer, the HFL, the ONL, and the layer of the outer cone cell processes. The inner layer of the foveola, which fills the bottom of the foveal pit, is mainly composed of Müller cell somata and processes (Fig. 14A–C). This layer has a thickness of 10–12 μm in the human foveola and 5.5–9.5 μm in the foveola of cynomolgus monkeys (Fig. 7C) (Syrbe et al., 2018). The thin HFL runs between the inner Müller cell layer and the ONL in the more peripheral foveola (Fig. 14A). The obliquely oriented outer processes of cone cells connect the perikarya in the ONL with the inner segments at the OLM (*arrow* in Fig. 7A; Fig. 7C,G, 10A, and 13C). The ONL of the foveola contains obliquely arranged rows of stacked cone cell somata (Fig. 5A and B, 7A, 10A, and 11A); the cone cell somata are separated by the outer processes of Müller cells of the fovea walls (Figs. 1B and 7K). The foveola contains the greatest accumulation of cone cell somata in the entire retina (Polyak, 1957; Lujan et al., 2011). In individuals with a v-shaped ONL, 2–3 loosely scattered cone cell somata are stacked in the center of the foveola while up to 8–10 somata are stacked in the peripheral foveola (Figs. 5A, 7A and 10A, and 11A) (Polyak, 1957; Yuodelis and Hendrickson, 1986; Syrbe et al., 2018). Individuals with more shallow foveal pits have the greatest accumulation of cone cell somata in the center of the foveola (Fig. 13D). The outer cone cell processes are longest in the center of the foveola; along with the increase of the number of stacked cone cell somata, the length of the outer cone cell processes decreases (Figs. 7A, 10A and 11A, and 13C).

2.1.1. Basal lamina of the ILM

The ILM consists of the vitreal surface of Müller cell endfeet and the overlying basal lamina (Reichenbach and Bringmann, 2010). The basal lamina is morphologically different in the foveola and the fovea walls.

The basal lamina in the foveola is a thin sheet of extracellular matrix, while the basal lamina in the fovea walls and the parafovea is much thicker (Foos, 1972; Henrich et al., 2012). In the human and macaque foveola, the thickness of the basal lamina is less than 30–40 nm (Fig. 7B,E) (Syrbe et al., 2018). Depending on the distance to the foveola, the thickness of the basal lamina increases; the thickness of the basal lamina in human fovea walls ranges from 900 nm to 1 µm (Fig. 7B) (Syrbe et al., 2018). The basal lamina in human fovea walls is composed of a thick layer which contains numerous horizontally aligned fibers and a thin dark layer at the vitreal surface which displays a higher electron density; many small dark knobs are integrated in the thin surface layer (Fig. 7B) (Almeida et al., 2015; Syrbe et al., 2018). The knobs likely represent remnants of vitreous collagen fibrils normally adhered to the basal lamina (Gandorfer et al., 2004). In contrast to the basal lamina of the fovea walls, the basal lamina of the foveola does not contain an electron-dense vitreal layer (Fig. 7B,E) (Syrbe et al., 2018). The basal lamina of the human foveola consist of a thin, electron-lucent (bright) layer in which single scattered electron-dense (dark) knobs are integrated (Fig. 7B) while the basal lamina of the macaque foveola consists only of a thin electron-lucent layer (Fig. 7E) (Syrbe et al., 2018). The basal lamina in the fovea walls has a smooth vitreal surface; the retinal surface of the basal lamina is irregular and follows the contour of the underlying Müller cell processes (Fig. 7B) (Halfter et al., 2014; Syrbe et al., 2018).

2.1.2. Müller cells of the foveola

An inverted cone-like structure composed of Müller cells overlies the area of high photoreceptor density in the primate foveola (Fig. 11A) (Yamada, 1969; Gass, 1999). The foveola is formed by the centrifugal displacement of the inner retinal layers; this also causes a centrifugal displacement of the somata and inner processes of the centralmost Müller cells (Fig. 11C). The base of the “Müller cell cone” lines the floor of the foveal pit (Fig. 14A) and extends laterally into the area of the slope of the central fovea walls; the central stalk of the “Müller cell cone”, which is 20–50 µm thick, reaches up to the OLM (Fig. 11A,C). The apex of the “Müller cell cone” lies in front of the region with the highest photoreceptor density which is within 40 µm of the foveal center in the macaque retina (Fig. 11B) (Packer et al., 1989). In the human retina, the apex of the “Müller cell cone” lies in front of the central bouquet of about 500 cone photoreceptors (Rochon-Duvigneaud, 1907; Ahnelt, 1998). The “Müller cell cone” is free of photoreceptor cell processes except near its apex (Gass, 1999; Rudich et al., 2013).

The foveola of humans and macaques contains 25–35 specialized Müller cells (Fig. 14B) (Syrbe et al., 2018) which form the “Müller cell cone”. These specialized Müller cells are atypical because their processes do not leave the foveola (Fig. 14C and D). A ‘typical’ Müller cell of the fovea has a characteristic ‘z-shape’ with a soma in the INL of the fovea wall and an outer process that runs obliquely or horizontally through the HFL towards the ONL of the foveola (Figs. 1B, 7K and 8A, and 11C). The outer processes of the specialized foveolar Müller cells do not leave the foveola and fail to join the course of the photoreceptor axons into the HFL; instead, they run rather straight within the stalk of the “Müller cell cone” from the inner layer of the foveola, where the somata are located, through the ONL to the OLM (Figs. 1B and 7C,K, 11C, and 14D) (Syrbe et al., 2018). The specialized Müller cells of the foveola have no contact to synapses or neuronal elements other than central cones which are surrounded by the outer processes of typical Müller cells (Fig. 7K), i.e., the foveolar Müller cells do not form a functional column with photoreceptors and neurons (Fig. 1Bb). It fits to the fact that these cells do not contact synapses and that key enzymes of the glio-neuronal transmitter recycling, the glutamate uptake transporter GLAST and glutamine synthetase (Bringmann et al., 2013), are expressed at lower levels by foveolar Müller cells (Fig. 12D) (Nishikawa and Tamai, 2001; Nishikawa, 2006–07). Müller cells in the central foveola do not express glutamine synthetase (Fig. 12D).

The inner layer of the foveola mainly consists of somata (including nuclei) and inner processes of the 25–35 specialized Müller cells (Fig. 7C,E,F and 14A,B) (Syrbe et al., 2018). The nuclei of these Müller cells have an oval shape (Fig. 7F,H) (Syrbe et al., 2018) while the nuclei and somata of the typical Müller cells in the fovea walls are polygonal (Fig. 7H) because they are impressed by the surrounding neuronal somata (Lu et al., 2006). The somata of the specialized foveolar Müller cells extend numerous thin lamelliform and tubular inner processes which form an elaborated plait which spreads along and below the basal lamina of the ILM and thus covers the vitreal surface of the foveola (Fig. 7E and F) (Syrbe et al., 2018). The complex network formed by the inner Müller cell processes extends into the transition zone between the foveola and the fovea walls (Fig. 7D). Thin Müller cell processes also cover the retinal surface of the basal lamina in the fovea walls (Fig. 7B). The Müller cell processes, which run along the inner surface of the foveola, are often very thin and display a thickness similar to that of the basal lamina of the ILM (Fig. 7E). The cytoplasm of Müller cells in the inner layer of the foveola is densely packed with smooth endoplasmic reticulum (Fig. 7B) (Syrbe et al., 2018), likely to produce secretory proteins including components of the basal lamina (Ponsioen et al., 2008; but see Halfter et al., 2014).

The spaces between the thin inner Müller cell processes are commonly very narrow, but at many locations, they are expanded and form small watery cysts (Fig. 7B,E) (Syrbe et al., 2018). In addition, larger cystoid spaces are present in the inner layer of the foveola (Fig. 7B,C,E,F). Small and large watery cysts are also present in the transition zone between the foveola and the fovea walls (Fig. 7D), and in the innermost layer of the fovea walls (Fig. 7B) (Syrbe et al., 2018).

The outer processes of the foveolar Müller cells run from their somata between the somata and outer processes of the central cone cells to the OLM (Fig. 7C,K and 14A,D). The cytoplasm of these Müller cell processes becomes increasingly dispersed and electron-lucent in the course from the inner layer of the foveola to the OLM (Fig. 7C,G) (Syrbe et al., 2018). In addition, the cytoplasm of the processes of ‘typical’ Müller cells which enwrapp the axons, somata, and outer processes of central cone cells are electron-lucent (Fig. 7C,G). Near the OLM, the cytoplasm of Müller cell processes displays a watery appearance and contains only dispersed membranous and vesicular structures (Fig. 7C,G). In contrast, Müller cells in the fovea walls (Fig. 7D,H) and Müller cell somata and processes in the inner layer of the foveola (Fig. 7E and F) have an electron-dense cytoplasm. A watery cytoplasm of the outer Müller cell processes within the central 50 µm of the foveola was also described by other authors, e.g., Nishikawa (2006–07).

The retina is structurally and functionally compartmentalized into cellular columns which represent the smallest functional unit of the forward processing of visual information (Fig. 1A) (Reichenbach et al., 1994; Reichenbach and Robinson, 1995). In many species, the core of the columns is constituted by one Müller cell in association with one cone photoreceptor (Fig. 1B) (Reichenbach and Robinson, 1995; Agte et al., 2011). Each Müller cell is responsible for all functional and metabolic interactions with the photoreceptors and neurons of the column (Bringmann et al., 2006; Reichenbach and Bringmann, 2010). However, because the photoreceptor cells in the foveola are surrounded by the outer processes of Müller cells of the fovea walls (Figs. 1B and 7C,G), the centralmost specialized Müller cells, which form the “Müller cell cone”, are likely not involved in supporting photoreceptor cell function. Therefore, the centralmost Müller cells in the foveola seem to be additionally inserted into the tissue. It is probable that the two Müller cell populations in the fovea may have different metabolism because the Müller cells of the fovea walls support the activities of photoreceptors and neurons and have contact to retinal vessels whereas the foveolar Müller cells apparently do not support neuronal activity (as suggested, for example, by the low expression of GLAST and glutamine synthetase) but may serve optical and structural functions.

2.1.3. Possible functional roles of foveolar müller cells

The specialized Müller cells of the foveola may have various functional roles. These cells contain macular pigment at high density. Depending on the cone cell distribution in the foveola, there is a sharp peak of macular pigment density in the center of the foveola (Fig. 11B) or (in subjects with a v-shaped ONL) there is an annular distribution of macular pigment in the foveola (Elsner et al., 1998). In the fovea walls, macular pigment is preferentially deposited in the IPL and HFL. Macular pigment reduces the effects of chromatic aberration on the visual acuity and protects the central photoreceptors from light damage by absorbing short-wavelength (blue-violet) light (Reading and Weale, 1974; Snodderly et al., 1984). The density of macular pigment decreases at the border between the nonvascularized and vascularized parts of the fovea because blood vessels form a yellow screen which also acts as a short-wavelength light filter (Schultze, 1867; Balaratnasingam et al., 2015). The high density of macular pigment in Müller cells of the foveola (Fig. 11B) is one reason for the facts that the central 100–200 µm of the human retina contain only few blue cones (see 2.3.1.) and that the foveal center is largely insensitive to blue light (König, 1894; Wilmer and Wright, 1945). The density of macular pigment is inversely related to the central foveal thickness (Balaratnasingam et al., 2015). The density is higher in subjects of African descent than in subjects of Caucasian ancestry (Wolf-Schnurrbusch et al., 2007; Ctori and Huntjens, 2017); subjects of African ancestry have a thinner foveola than subjects of Caucasian descent (Wagner-Schuman et al., 2011). Possibly, the density of macular pigment increases in thin foveolas to compensate the higher levels of blue light that reaches the photoreceptors.

The pale outer processes of the foveolar Müller cells, which surround the somata and outer processes of cone cells in the central foveola (Yamada, 1969; Hogan et al., 1971), are characterized by a low density of the cytoplasm (Fig. 7C,G) (Nishikawa, 2006–07; Syrbe et al., 2018). The low density of the cytoplasm may reflect the very thinness of these processes which allows the high packing density of central cones. In addition, the watery cytoplasm may support the light transmission through the foveola (see 3.).

The basal lamina of the ILM functions as a barrier to the vitreous cavity; it prevents the passage of cells (e.g., hyalocytes and blood cells in the case of blood-ocular barrier breakdown) and of molecules larger than 15–20 nm (Balazs, 1984). One function of the plait of the thin inner Müller cell processes, which spreads along the basal lamina of the foveola (Fig. 7E), may be the formation of additional diffusion and cell passage barriers to the vitreous cavity; these Müller cell barriers compensate the thinness of the basal lamina of the foveola (Syrbe et al., 2018). The numerous thin inner Müller cell processes as well as the watery cysts in the inner layer of the foveola (Fig. 7B,C,E) largely increase the surface area of Müller cells and thus the area for the insertion of receptors which recognize physiological and pathogenic signaling molecules, and for the release of secretory proteins.

It has been proposed that one function of the deep convexiclivate fovea of birds is image magnification resulting from light refraction at the vitreoretinal border of the central fovea walls (Fig. 3B) (Walls, 1942). This mechanism requires that the retinal tissue displays a higher refraction index than the vitreous; indeed, this has been demonstrated (Valentin, 1879; Franze et al., 2007). In the fovea walls, the basal lamina of the ILM is thick and has a smooth surface towards the vitreal cavity (Fig. 7B) (Halfter et al., 2014; Syrbe et al., 2018). A smooth retinal surface minimizes image distortions which result from varying light refraction angles at uneven surfaces. On the other hand, in the foveola, the basal lamina of the ILM is very thin (Fig. 7B,E) and seems not to be capable to mechanically maintain an even retinal surface. Therefore, another function of the elaborated plait of thin Müller cell processes, which run horizontally below the basal lamina, is to smooth the inner surface of the foveola and thus to minimize image distortions in the area of high-acuity vision (Syrbe et al., 2018). It is conceivable that the thick basal lamina of the fovea walls has light-scattering properties and thus may contribute to the hyperreflection of the NFL outside of the foveola in OCT images (Fig. 1Ba and 2A). It could be that the basal lamina in the foveola is very thin in order to avoid light scattering at the inner retinal surface; therefore, the thickness of the basal lamina is far below the wavelength range of visible light. For the same reason, the thickness of many inner Müller cell processes which form the elaborated plait below the basal lamina is smaller than the wavelength range of visible light (Syrbe et al., 2018).

In addition to improving the optical properties of the foveola, the specialized foveolar Müller cells may provide the structural stability of the central fovea (Gass, 1999). Generally, the neuroretina is mechanically stabilized by the glial cell network, in particular, by Müller cells; neurons do not provide much structural support to the tissue (Müller, 1856; MacDonald et al., 2015). Structural tissue stabilization is supported by the strands of microtubules and intermediate filaments in Müller cells (Reichenbach, 1989; Röll, 2001) as well as by adherent junctions which are present between astrocytes and Müller cells, but not between glial cells and neurons or among neurons (with the exception of the junctional coupling between Müller and photoreceptor cells; see 4.4.) (Holländer et al., 1991; Ramírez et al., 1996; Omri et al., 2010; Matet et al., 2015). The only type of macroglial cells in the center of the fovea is the Müller cell (Distler and Dreher, 1996). The plait of the thin inner Müller cell processes, which spreads along and below the basal lamina of the foveola (Fig. 7E and F) (Syrbe et al., 2018), may provide increased resistance against mechanical stretch resulting from horizontal and vertical tractional forces. Tractional forces onto the central fovea may occur, for example, in cystoid macular edema and after partial detachment of the posterior vitreous. In cystoid macular edema, fluid-filled cysts may be present in the foveola resulting in a detachment of the inner Müller cell layer; the detached Müller cell layer often holds the foveal walls together (Fig. 2D). Disruption of the foveolar Müller cell layer results in macular hole formation (Fig. 2F) (Gass, 1999). The structural support of the fovea is supported by the extension of the inner Müller cell processes into the central fovea walls (Fig. 7D). The inner layer of the foveola contains numerous small and larger watery cysts (Fig. 7B,C,E) (Syrbe et al., 2018). It could be but remains to be proven that the small cysts between the inner Müller cell processes allow displacements of single or several Müller cell processes against the others and thus alterations of the shape of the foveola, i.e., flattening and deepening of the foveal pit, depending on the extent of shearing stress. Larger watery cysts make the tissue softer and thus may increase the capability of adaptive tissue deformations.

Tractional forces onto the foveola (vitreomacular traction) induces gliosis of the specialized foveolar Müller cells. Müller cell gliosis is associated with a hypertrophy of cell processes and upregulation of intermediate filaments (Bringmann et al., 2009). Gliosis of the specialized Müller cells is recognizable in OCT images by the presence of multiple hyperreflective dots in the inner layer of the foveola (Fig. 2B and C). The dots are produced by light reflection at optically dense structures of Müller cells (Yokotsuka et al., 1997).

A further role of the centralmost Müller cells may be the vertical mechanical stabilization of the fovea externa, i.e., the pyramid-like arrangement of the elongated cone segments in the center of the foveola (Fig. 11D). The involvement of tractional forces by the centralmost Müller cells is suggested by the colocalization of the deepest point of the foveal pit (*black arrowhead* in Fig. 7A) which lies in front of the tip of the fovea externa (Figs. 2E and 10A); the deepest point of the foveal pit can be identified at the central light reflex in OCT images of many human subjects (Fig. 2A) (Tick et al., 2011). However, the mechanisms of central cystoid macular edema and macular hole formation (the latter may involve a detachment of the inner layer from the ONL of the foveola [Fig. 2D,F]; Byon et al., 2014) may rather suggest a mechanical instability of the pale outer processes of central Müller cells which seems to easily disrupt in the presence of anteriorposterior tractional forces. The low density of the cytoplasm of outer Müller cell processes, which does not contain glial filaments or microtubules (Fig. 7G), may

be one reason for the low vertical stability of the foveola, and may explain the tissue disruption between the inner layer and the OLM in the central foveola often seen in cystoid macular edema (Fig. 2D). Another reason may be the absence of cellular connections between the atypical foveolar Müller cells and the typical Müller cells of the fovea walls; therefore, the border between the inner layer and the HFL in the more peripheral foveola has a low resistance against mechanical stretch (Fig. 2E) which may be produced by the outer processes of Müller cells in the fovea walls (Fig. 11D). The sites of low mechanical stability may explain the locations of tissue disruptions in central cystoid macular edema and early stages of macular holes (*left side* of Fig. 2F) (Chung and Byeon, 2017).

2.2. Müller cells of the fovea walls and parafovea

The photoreceptor cells of the foveola are surrounded by the outer processes of the 'typical' Müller cells of the fovea walls. The fovea is formed by a centrifugal displacement of the inner retina and a centripetal displacement of the outer retina. Both movements result in a radial displacement of the inner retinal neurons away from the photoreceptor cell somata by up to 150–675 µm in the human and macaque fovea (Polyak, 1941; Ahnelt and Pflug, 1986; Schein, 1988; Wässle et al., 1989; Sjöstrand et al., 1999b; Drasdo et al., 2007) and cause the z-shape of the Müller cells in the fovea walls and parafovea (Figs. 1B, 7K and 8A,B,D, and 11C). The somata of the 'typical' Müller cells lie in the INL (Figs. 7K and 8B,C). The outer processes of the cells surround the axons (Figs. 7I and 8B,D, 9C, and 14A), somata (Fig. 8D and E and 12A), and outer processes of the central photoreceptor cells (Fig. 7C). These processes draw obliquely or horizontally through the HFL towards the ONL of the central fovea (Figs. 3A, 8A and 11C, and 14A) and are centripetally bended in association with the oblique or curved rows of photoreceptor somata and outer cone cell processes in the foveola and central fovea walls (Fig. 5A and B, 7A, 10A,B, and 11C). The columnar rows of cell somata in the GCL and INL run roughly parallel to the main Müller cell processes in the IPL (Schein, 1988), suggesting that these cellular columns are arranged and mechanically stabilized by the processes of Müller cells.

The length of the outer Müller cell processes in the HFL depends on the distance to the foveal center. In the example of the macaque fovea shown in Fig. 10A, the centrifugal displacement of the Müller cell somata in the INL from the outer Müller cell processes in the ONL was measured; this distance reflects the horizontal length of Henle fibers (Fig. 4C). The distance between the Müller cell somata and the Müller cell processes in the ONL increases roughly linearly from less than 50 µm in the foveal center up to 300–330 µm within a distance of 500 µm from the foveal center (i.e., within the central fovea walls) (Fig. 10C). In more peripheral areas of the fovea walls and parafovea, the displacement of the Müller cell somata from the Müller cell processes in the ONL decreases more or less continuously up to a distance of 2.5–3 mm from the foveal center (Fig. 10C). In a human fovea, the horizontal length of Henle fibers increases up to a distance of 400 µm from the foveal center (Fig. 15A). Similar horizontal extensions of the Henle fibers, with a maximal extension between 0.5 and 0.8 mm and a steep decline in the extension between 2.0 and 2.5 mm from the foveal center, were described by other authors (Schein, 1988; Sjöstrand et al., 1999b). These values of the horizontal length of Henle fibers correspond well with the thickness of the HFL and of the fovea walls (Fig. 1B) found in OCT images. Here, the thickness of the HFL increases continuously from the foveal center up to a distance of about 400 µm from the foveal center, peaks between 400 µm and 0.7–1 mm, and decreases up to about 3 mm from the foveal center (Curcio et al., 2011). The OPL in the region of the peak extension of the Henle fibers contains the highest density of cone pedicles (in macaques, 25,000–36,000 per mm^2 between 0.5 and 0.8 mm from the foveal center) (Schein, 1988; Wässle et al., 1989; Krebs and Krebs, 1989).

The horizontal extension of the HFL (i.e., the distance to the foveal center up to which a HFL is present) is not uniform. In the human tissue, the horizontal extension of the HFL is greatest in the temporal retina (mean ± S.D.; 2.51 ± 0.21 mm; n = 3) and smallest in the nasal retina (1.89 ± 0.29 mm); the extensions in the superior (2.12 mm) and inferior retinas are between these two values. These values are in agreement with previous studies which show an asymmetry of the fovea walls (Fig. 4A) (Curcio et al., 1987; Tick et al., 2011). The different horizontal extensions of the HFL in the nasal and temporal retina suggest that the temporal retina is more stretched than the nasal retina during the postnatal growth of the eyeball (see 4.2.). It has been shown that during the postnatal development of the macaque retina, the dimension of the posterior pole (between the fovea and optic disk) remains stable although the area of the whole retina increases (Packer et al., 1990). The different developmental expansions of the retinal tissue may also explain the higher photoreceptor and ganglion cell densities in the nasal compared to the temporal retina (Perry and Cowey, 1988; Wässle et al., 1989; Curcio and Allen, 1990; Curcio et al., 1991; Finlay et al., 2008).

In addition to the displacement of the outer Müller cell processes, there is a centrifugal displacement of the inner Müller cell processes which draw from the Müller cell somata within the INL to the endfeet in the GCL (Fig. 8A) (Schein, 1988). The displacement of the inner Müller cell processes is rather small (< 50 µm) and disappears at a distance of 1.3–1.4 mm from the foveal center in a macaque fovea (Fig. 10C) and at a distance of 1.6–1.8 mm from the foveal center in a human fovea (Fig. 15A). More peripherally, the inner Müller cell processes draw rather straight through the tissue (Figs. 8A and 10I). The peak of the displacement of the inner Müller cell processes coincides with the peak length of the Henle fibers in a human fovea (Fig. 15A) and is more peripherally located than the peak Henle fiber length in a macaque fovea (Fig. 10C).

The local density of Müller cells in the human and macaque fovea is similar in the peripheral foveola and central fovea walls (around 15,000 per mm^2; Figs. 10D and 15B). The density of Müller cell processes is decreased in the ONL of the central foveola (Figs. 10D and 15B). This corresponds with the low density of cone cell nuclei in the central foveola (Fig. 5A and B, 7A, 10A,E, 11A, and 15C). However, because the outer Müller cell processes were counted in the ONL of the foveola, the decreased density of Müller cells in the central foveola results from the oblique arrangement of the processes in the layer of the outer cone cell processes and does not reflect a decreased density of Müller cell processes at the OLM. In sections through the central foveola of rhesus macaques, densities of Müller cell processes at the OLM of 32,000–58,000 per mm^2 were counted; the mean distance between two Müller cells was 4.46 ± 1.30 µm (mean ± S.D.).

Depending on the high density of cones in the foveola, the ONL (which contains the cone cell somata) is thickened. In individuals with a wide foveola, the central ONL is v-shaped (Figs. 11B and 13C,D) and contains only few cell somata at which light can scatter (Fig. 5A and B, 7A, 10A,E, 11A, and 15C). The central widening of the ONL is caused by the centrifugal displacement of the cone pedicles which is followed by a displacement of the cone cell somata from the foveal center (Detwiler, 1943); the stalk of the “Müller cell cone” fills the space left by the displaced somata (Fig. 11C). A large centrifugal displacement of the central cone cell somata is associated with the formation of outer cone cell processes which draw from the cone cell somata to the OLM of the foveola (Fig. 7A,C, 10A, 11A, and 13C). The centrifugal displacement of the cone pedicles may be mediated by horizontal tractional forces which originate in Müller cells and are transmitted by their outer processes in the HFL (see below). This displacement also causes the oblique or curved arrangement of the photoreceptor cell somata rows in the ONL of the foveola and fovea walls (Figs. 5A, 7A and 10A,J, 11A,B, and 13C).

The conspicuous shape of the fovea, with the almost full absence of inner retinal layers in the foveola, is expected to need particular structural stabilization. It has been shown that intermediate filaments

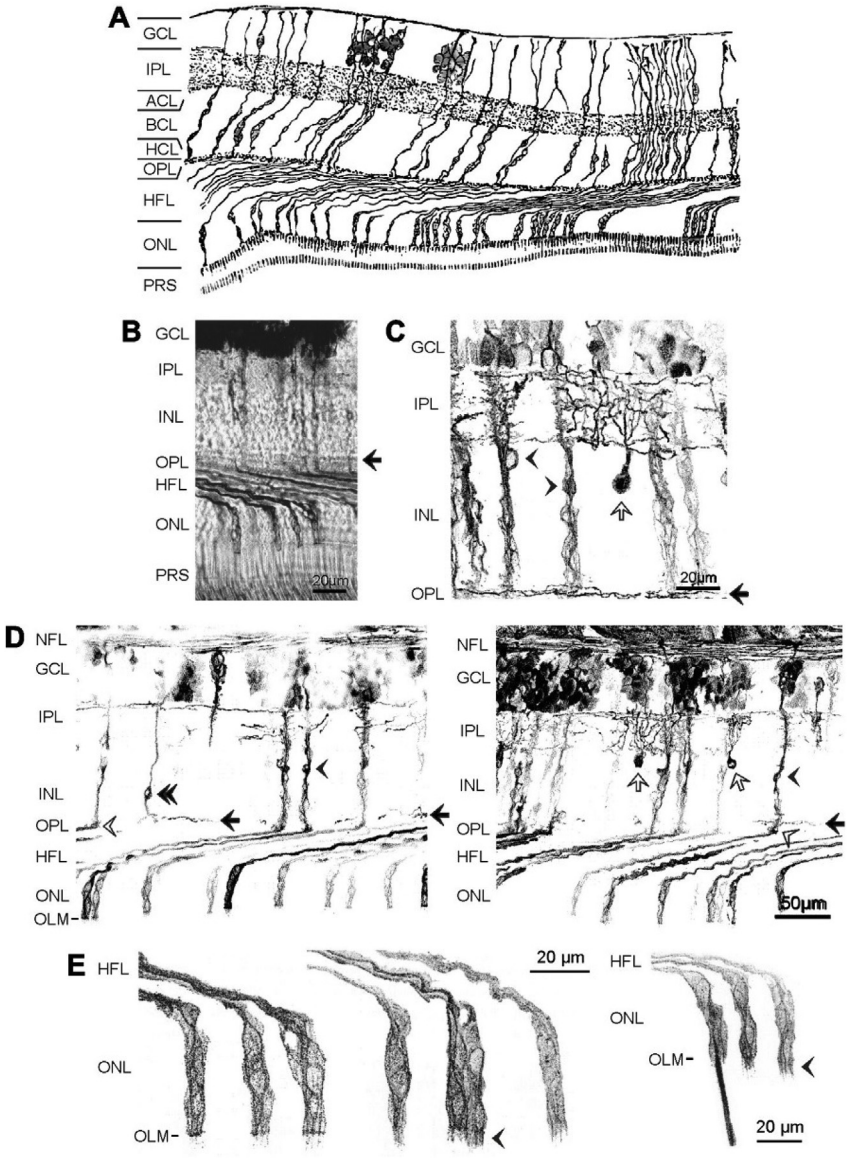

Fig. 8. Typical Müller cells of the primate fovea. **A.** Cross-section through the human parafovea, showing the spatial arrangement of Müller cell processes. Note the oblique arrangement of the outer Müller cell processes in the Henle fiber layer (HFL). The inner Müller cell processes show a centrifugal displacement between the bipolar cell layer (BCL) and ganglion cell layer (GCL) near the central foveal wall (*left*); the processes are bended at the boundary between the BCL and amacrine cell layer (ACL). More peripherally, inner Müller cell processes draw rather straight through the tissue (*right*). Note also the side processes of Müller cells in the inner (IPL) and outer plexiform layers (OPL). Image modified from Piersol (1897). **B–E.** Golgi-stained Müller cells in sections through the parafovea of a cynomolgus macaque (*Macaca fascicularis*) (courtesy of H. Wässle and B. Boycott). **B.** Section through the neuroretina. Note the horizontal layering of the inner fibrous part of the OPL (*arrow*). **C.** Section through inner retinal layers. In addition to Müller cells, an amacrine cell and somata of GCL neurons are stained. The soma of the amacrine cell (*white arrow*) lies in the inner nuclear layer (INL); the amacrine cell processes form a tree in the IPL. *Arrowheads*, Müller cell somata containing the nuclei. Note that the nucleus of the left marked cell is located out of the cell axis. The *black arrow* indicates side processes of Müller cells which draw horizontally through the inner part of the OPL. Further side processes of Müller cells draw horizontally through the IPL. **D.** Sections through the neuroretina. The radial extension of the outer Müller cell processes in the HFL is 175 (*left*) and 190 µm (*right*), respectively. *Black arrowheads*, Müller cell somata. *White arrows*, amacrine cell somata. *Double arrowhead*, soma of a midget bipolar cell. Note the horizontal Müller cell side processes in the inner part of the OPL (*black arrows*) and the thickening of Müller cell processes in the outer part of the OPL (*white arrowheads*), likely representing glial baskets around cone pedicles. Note also the wave-like appearance of the Henle fibers. **E.** Sections through the outer retina. In the outer nuclear layer (ONL), glial processes surround the somata of photoreceptor cells. The *arrowheads* indicate microvilli of Müller cells (length, 4–6 µm) which extend from the outer limiting membrane (OLM) into the subretinal space. In the *right image*, the microvilli of a Müller cell surround the inner segment of a cone cell. HCL, horizontal cell layer; NFL, nerve fiber layer; PRS, photoreceptor segments.

like glial fibrillary acidic protein (GFAP) contribute to the biomechanical properties of Müller cells. Reactive gliosis is characterized by an upregulation of intermediate filaments (Bringmann et al., 2009), cell process hypertrophy, and an increased stiffness of Müller cells; the increased stiffness correlates with the increased density of intermediate filaments (Lu et al., 2011). Intermediate filaments provide resistance to mechanical stress; after retinal detachment, for example, the absence of GFAP and vimentin results in a shearing of the Müller cell endfeet away from the rest of the retina or even in a separation of the endfeet from the retina (Lundkvist et al., 2004; Verardo et al., 2008). Under normal conditions, GFAP is constitutively expressed by astrocytes while Müller cells are largely devoid of GFAP (Figs. 9A and 12E,F) (Reichenbach and Bringmann, 2016). In the peripheral retina, GFAP in Müller cells is downregulated after birth, and is upregulated under pathological or stressful conditions (Distler and Dreher, 1996; Provis et al., 2000; Bringmann et al., 2009; Reichenbach and Bringmann, 2016). In contrast, Müller cells within the fovea express GFAP throughout life (Gariano et al., 1996; Distler et al., 2000; Provis et al., 2000), suggesting that their cellular environment is different (Hendrickson, 2005). In the fovea walls and peripheral retina, inner Müller cell processes express low levels of GFAP (Figs. 9B and 12C,F) while outer Müller cell processes, that draw through the HFL and ONL, contain elevated levels of GFAP (Fig. 9C). In addition, Müller cells express GFAP in the inner fibrous part of the OPL (Fig. 9C); this part of the OPL contains a horizontal layering structure (Fig. 8B) formed by neuronal processes and horizontal side processes of Müller cells (Fig. 8C and D). The outer part of the OPL is largely devoid of GFAP (Fig. 9C); here, synaptic terminals of photoreceptor cells are arranged in a monolayer (Polyak, 1941) and processes of several Müller cells form glial baskets around each cone pedicle (Fig. 8D) (Burris et al., 2002; Hendrickson, 2005). Because expression of GFAP in Müller cells is a very sensitive 'retinal stress' indicator (Bringmann et al., 2009), the expression of GFAP may indicate the presence of mechanical stress in these layers. The distribution of GFAP may support the assumption that tractional forces provided by Müller cell processes in the OPL on the Henle fibers underlie the structural stability of the fovea. In addition to Müller cells of the fovea walls, Müller cells in the foveola and the lower fovea walls express GFAP (Fig. 12A,C,D and 14C,E). Outside of a diameter of 300–600 µm from the foveal center, the GFAP expression by Müller cells disappears (Fig. 12A,C,D and 14C,E). These data may suggest that the foveola and lower fovea walls are areas which are subjects to mechanical stress.

There are three morphological subclasses of retinal astrocytes: elongated bipolar astrocytes with processes which run in association with nerve fiber bundles, perivascular astrocytes which surround

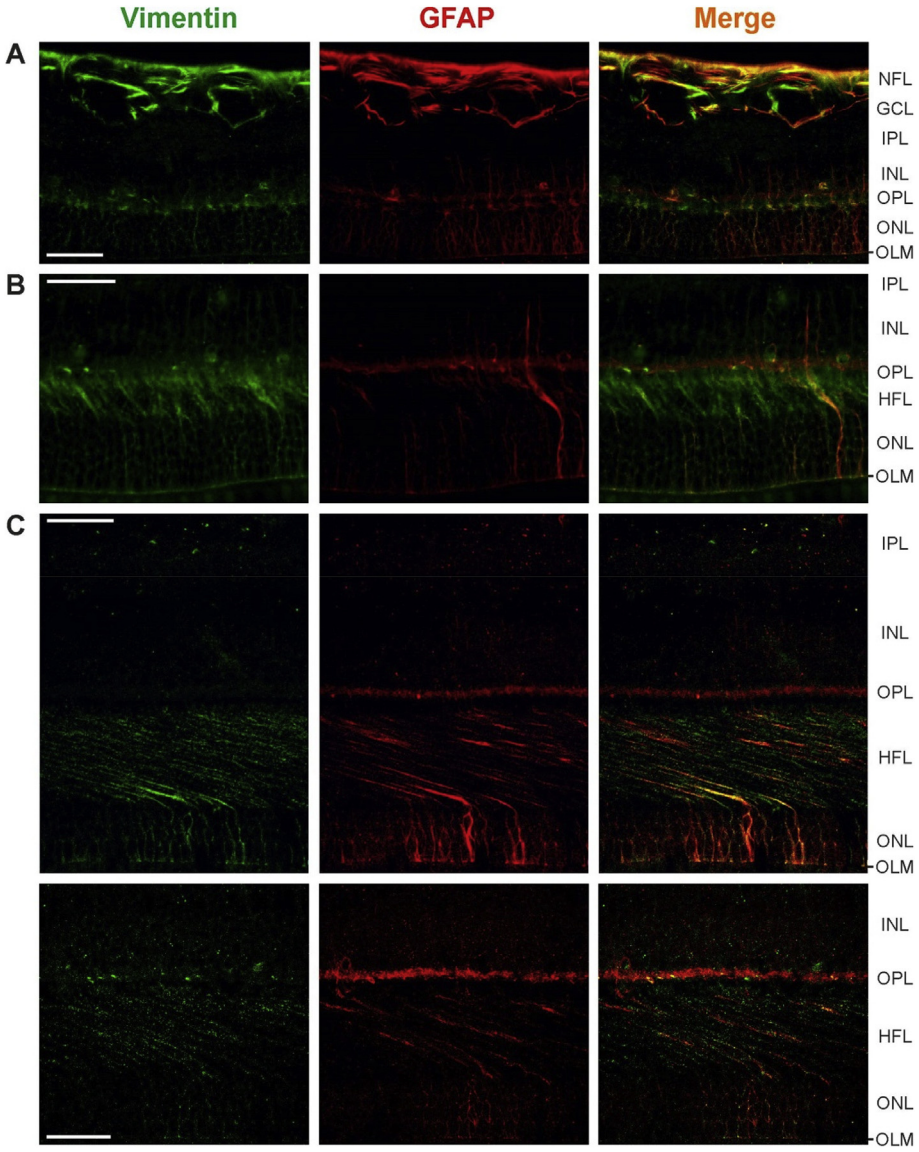

Fig. 9. Glial intermediate filaments in the fovea of a rhesus macaque (*Macaca mulatta*). Cross-sections through the peripheral retina (**A**; 3.5 mm from the foveal center), parafovea (**B**; 2.5 mm from the foveal center), and fovea walls (**C**; 700 µm from the foveal center) were immunostained for vimentin (*green*) and GFAP (*red*). Colabeling yielded a *yellow* merge signal. Note the expression of GFAP in the inner part of the outer plexiform layer (OPL) and in the Henle fiber layer (HFL) of the fovea walls (**C**). In the nerve fiber (NFL) and ganglion cell layers (GCL), GFAP is expressed by astrocytes (**A**). In the section of the peripheral retina (**A**), no HFL is present, and the retinal tissue has a thickness of 160 µm. In the section of the parafovea (**B**), the thickness of the retina and HFL are 205 and 25 µm, respectively; the radial displacement between Müller cell inner and outer processes is 23 µm. In the sections of the fovea walls (**C**), the thicknesses of the retina and HFL are 290 and 75 µm, respectively; the radial displacement between Müller cell inner and outer processes is 270 µm. INL, inner nuclear layer; IPL, inner plexiform layer; OLM, outer limiting membrane; ONL, outer nuclear layer. Bars, 50 µm.

retinal vessels, and stellate astrocytes which fill the spaces between the vessels and nerve fiber bundles in the GCL (Reichenbach and Bringmann, 2016). Stellate astrocytes form a three-dimensional network (Fig. 12F and G); their processes are connected by adherent and gap junctions (Burns and Tyler, 1990; Holländer et al., 1991; Ramírez et al., 1996). GFAP-expressing astrocytes are circularly arranged in the fovea walls outside of 0.57–1.1 mm from the foveal center (Fig. 12C,D,E); the distance of astrocytes from the foveal center is smaller in the nasal than in the temporal fovea. Single GFAP-labeled astrocytic processes are also found between 400 and 800 µm from the foveal center (Fig. 12D).

Müller cells of the fovea walls may play a role in morphological alterations of the tissue which adapt the position of the central photoreceptors to changes in the angle of the incoming light. Fortin (1925; cited in Kolmer and Lauber, 1936) suggested that horizontal movements of Henle fibers play a role in accomodation and fixation, by causing flattening and deepening of the foveal pit. Müller cells of the fovea walls are connected by horizontal side processes within the inner part of the OPL (Fig. 8C and D); these side processes (in addition to neuronal processes) form a horizontal layering structure in the OPL (Fig. 8B). Horizontal contraction of Müller cell processes within the OPL will produce traction on the Henle fibers; centrifugal displacement of Henle fibers will alter the slope of the OLM in the foveola, i.e., the shape of the fovea externa (Fig. 11D). Perhaps, the wave-like appearance of Henle fibers, often seen in histological sections (Fig. 8A,D), indicates the capability of a displacement of Henle fibers. A steeper slope of the OLM may be also produced by a vertical contraction of the specialized Müller cells which form the stalk of the “Müller cell cone” in the center of the foveola (Fig. 11D). The Müller cell-mediated displacement of foveal photoreceptors is supported by tight junctions between Müller cells and photoreceptor cell axons in the HFL (Matet et al., 2015), as well as by tight-like junctions between Müller cells and photoreceptor cells within the ONL and at the OLM (Omri et al., 2010). This mechanism may be one basis of the remarkable capacity of photoreceptors to realign themselves towards the pupil after retinal detachment and pupil displacement, for example (Enoch et al., 1973; Bonds and MacLeod, 1978). Müller cells express myosin VI which may play a role in these movements in response to changes in light conditions (Breckler et al., 2000). Horizontal traction exerted by Müller cells in the fovea walls on the central photoreceptor cells may contribute to the widening of the ONL during foveal development and macular hole formation (Fig. 2F) (Gass, 1999). Mechanical forces provided by foveal Müller cells are also suggested to be involved in the restoration of the foveal shape after macular hole surgery (Chung and Byeon, 2017).

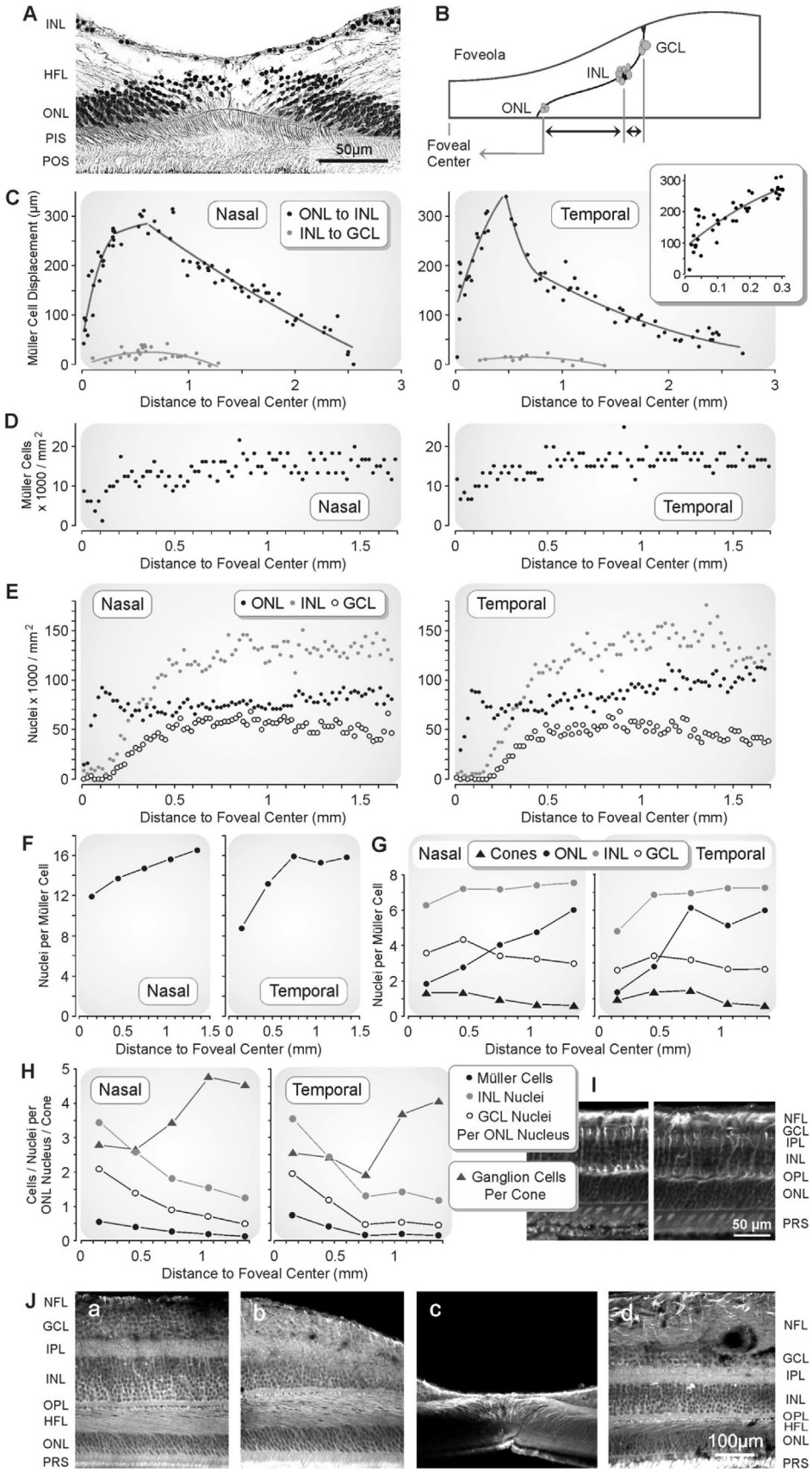

Fig. 10. Cellular composition of the fovea of the rhesus macaque (*Macaca mulatta*). **A.** Cross-section through the foveola of a 19 years-old female animal. Cell nuclei were counted in hematoxylin/eosin-stained, 10-µm thick foveal sections along the nasal and temporal hemimeridians. Müller cell processes were counted in vimentin-immunolabeled sections. Data are not corrected for tissue shrinkage. The ratios between the numbers of cell nuclei and Müller cells were determined with consideration of the displacement of the Müller cell somata from the outer Müller cell processes in the outer nuclear layer (ONL), and were calculated with consideration that the retinal area increases with the distance to the foveal center (the raw data were multiplied by the magnification of the retinal area from the ONL to the inner nuclear layer [INL] and ganglion cell layer [GCL], as described by Schein [1988]). **B.** Schematic representation of the measurement of the distance of Müller cell processes between the nuclear layers. **C.** Centrifugal displacement of foveal Müller cells between the nuclear layers. *Left side*: nasal fovea. *Right side*: temporal fovea. The distance between the outer Müller cell processes in the ONL and the Müller cell somata in the INL, and the distance between the Müller cell somata in the INL and the inner Müller cell processes in the GCL, are shown as a function of the distance of the outer Müller cell processes to the foveal center. **D.** Number of Müller cells per mm^2 retinal area as a function of the distance to the foveal center. Müller cell stem processes were counted in the foveolar ONL and the inner plexiform layer (IPL) of the fovea walls, respectively. **E.** Numbers of cell nuclei in the ONL, INL, and GCL per mm^2 as a function of the distance to the foveal center. **F.** Total numbers of cell nuclei per Müller cell in relation to the distance to the foveal center. **G.** Numbers of cone, ONL, INL, and GCL nuclei per Müller cell in relation to the distance to the foveal center. The number of cones was estimated according to the cone-rod ratio described by Wikler et al. (1990). In **F** and **G**, the numbers of cell nuclei were determined in 300 µm-wide sections for Müller cells according to the location of their outer processes in the ONL. **H.** Ratios of Müller cells, INL nuclei, and GCL nuclei per ONL nucleus, and of ganglion cells per cone, in relation to the distance to the foveal center. The number of ganglion cells was estimated in consideration of the fact that 5% of the GCL neurons in the central retina are displaced amacrines (Wässle et al., 1989; Sjöstrand et al., 1999a). **I.** Vertical sections through the peripheral retina of another macaque. The thickness of the retina is about 140 µm. **J.** Vertical sections through the parafovea 400 µm temporal from the foveal center (**a**), fovea wall (**b**), foveal center (**c**), and perifovea 2.4 mm nasal from the foveal center (**d**) of another animal. The thickness of the para- and perifovea is 260 µm. The centrifugal displacement of the inner retinal tissue from the outer retinal tissue within the Henle fiber layer (HFL) is 270 µm in the parafovea (**a**), 235 µm in the inner fovea wall (**b**), and 70 µm in the nasal perifovea (**d**). The nasal perifovea (**d**) contains a very thick (90 µm) nerve fiber layer (NFL). OPL, outer plexiform layer; PIS, photoreceptor inner segments; POS, photoreceptor outer segments; PRS, photoreceptor segments.

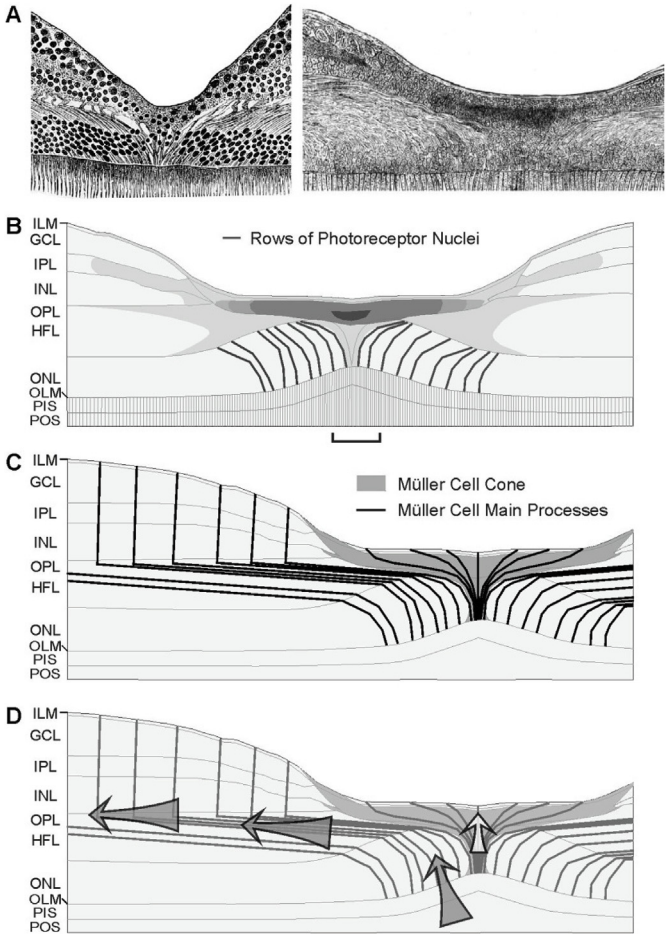

Fig. 11. "Müller cell cone" in the primate foveola. **A.** Cross-sections through the human fovea shown by Franz (1913) (*left*) and Babbitt (1878) (*right*). Note the presence of an inverted cone-like structure in the center of the fovea. **B.** Distribution of the blue light-absorbing macular pigment in a cross-section of a macaque fovea. The drawing represents the author's interpretation of an image shown by Snodderly et al. (1984). Note that the horizontal layer of the "Müller cell cone" contains macular pigment at high density. The highest density is localized in the center of the "Müller cell cone" that lies in front of the region of the highest cone density which is within 40 µm of the foveal center in the macaque retina (*bracket*) (Packer et al., 1989). The density of the macular pigment decreases continuously from the center to the periphery of the foveola. The stalk of the "Müller cell cone" as well as Müller cell processes in the nerve fiber layer, inner plexiform layer (IPL), outer plexiform layer (OPL), and Henle fiber layer (HFL) in the central fovea walls also contain macular pigment, albeit at lower density. **C.** Arrangement of the Müller cell main processes in the fovea. In the center of the foveola, Müller cells which run vertically from the inner (ILM) to the outer limiting membrane (OLM) create the stalk of the "Müller cell cone". In the periphery of the foveola, the outer processes of Müller cells run through the stalk of the "Müller cell cone", while the inner parts of the cells are shifted towards the fovea walls. Müller cells in the fovea walls have the characteristic 'z-shape' caused by the centrifugal shift of the inner Müller cell processes and the centripetal shift of the outer retina, resulting in the formation of the HFL. In the HFL, the outer Müller cell processes run obliquely or horizontally from the OPL to the outer nuclear layer (ONL). **D.** Müller cells may regulate the slope of the OLM in the foveola according to the angle of the light path. In the inner part of the OPL, Müller cells are interconnected; horizontal contraction of Müller cell processes in this layer may produce a centrifugal displacement of Henle fibers resulting in a steeper slope of the OLM in the foveola. A steeper slope of the central OLM may be also produced by vertical contraction of the specialized Müller cells in the center of the foveola. GCL, ganglion cell layer; INL, inner nuclear layer; IPL, inner plexiform layer; PIS, photoreceptor inner segments; POS, photoreceptor outer segments.

2.3. Photoreceptors of the fovea

The primate fovea has evolved under the selective pressure favoring high spatial resolution. High spatial resolution is provided by the high density of central photoreceptors and the increased ratio of ganglion cells to photoreceptors (Wässle and Boycott, 1991). The spatial resolution provided by the human foveola (about 60 cycles per degree) is limited by the cone spacing that correlates with the receptive field density of midget ganglion cells (Rossi and Roorda, 2010). It has been suggested that the optics of the eye do not allow sharp image gratings of greater than 60 cycles per degree (Campbell and Gubisch, 1966). Outside the foveola, the visual resolution does not match with the cone spacing but with the receptive field density of midget ganglion cells (Rossi and Roorda, 2010). In humans, the acuity sufficient for reading is provided by the foveola and the lower fovea walls, up to about 600 µm from the foveal center. Because this region is small, the eyes must constantly shift their gaze when an object is large, to bring different portions of the image into the fovea (as in reading).

2.3.1. Cones

More than 90% of the cones in the human retina are red and green cones (Ahnelt, 1998). Both cones types are not morphologically different. There are approximately equal numbers of randomly distributed red and green cones in the central fovea (Roorda et al., 2001; Mollon and Bowmaker, 1992); however, interindividual differences in the ratio between red and green cones were described for the human retina. In the fovea externa, the very thin and long red and green cones are arranged in a regular hexagonal mosaic (Fig. 16B and C); cones of the same type may form clusters. Foveal cones are packed very close together (with about 2.5 µm intercone spacing). The diameter of the inner segments of human foveal cones is 1.6–2.2 µm (Fig. 7G) (Detwiler, 1943; Curcio et al., 1990; Syrbe et al., 2018). The inner segments of human central foveal cones are up to 30–35 µm long, and the outer segments have a length of up to 50–65 µm (Greeff, 1900; Salzmann, 1912; Polyak, 1941; Yamada, 1969; Yuodelis and Hendrickson, 1986; Hendrickson and Provis, 2006). The length of cone segments is inversely related to the thickness and packing density of the receptors.

Blue cones are morphologically distinct; they have longer inner segments than the other cones, and the diameter of the inner segments is similar across the whole retina, thus they are thicker in the central fovea and thinner in the peripheral retina than red and green cones (Ahnelt et al., 1987). In the fovea externa, more than 6 red and green cones surround a blue cone (Pum et al., 1990); this causes disruptions of the regular cone mosaic (Fig. 16C) (Ahnelt et al., 1987). Blue cones have also a different retinal distribution than red and green cones. The density of blue cones is 3–5% of all cones in the foveola and 15% on the foveal slope (with a peak density of 2000 per mm^2 200–300 µm distant from the foveal center); in more peripheral areas, 7% of all cones are blue cones (De Monasterio et al., 1985; Ahnelt, 1998). The very center of the foveola is almost devoid of blue cones. However, the blue cone topography in the fovea differs among primate groups. In common marmosets and capuchin monkeys, blue cones are found throughout the foveola at relatively high densities (Martin and Grünert, 1999). Chimpanzees and orangutans have a small blue cone-free zone, similar to humans (Hendrickson, 2005). There are contrary data regarding the presence or absence of a blue cone-free zone in macaques (Martin and Grünert, 1999; Bumsted and Hendrickson, 1999).

For the human foveola, a high interindividual variability in the peak cone density was described (98,000–324,000 per mm^2); beyond 1 mm from the foveal center, all human eyes have similar cone densities (Curcio et al., 1987, 1990). A substantial variation of the peak cone density (84,000–260,000 per mm^2) was also found in the macaque fovea (Fig. 16A) (Perry and Cowey, 1985; Packer et al., 1989, 1990; Wässle et al., 1989; Wikler et al., 1990; Finlay et al., 2008). The peak cone density of the marmoset fovea is 133,000–211,000 per mm^2 (Wilder et al., 1996; Franco et al., 2000; Finlay et al., 2008), and the

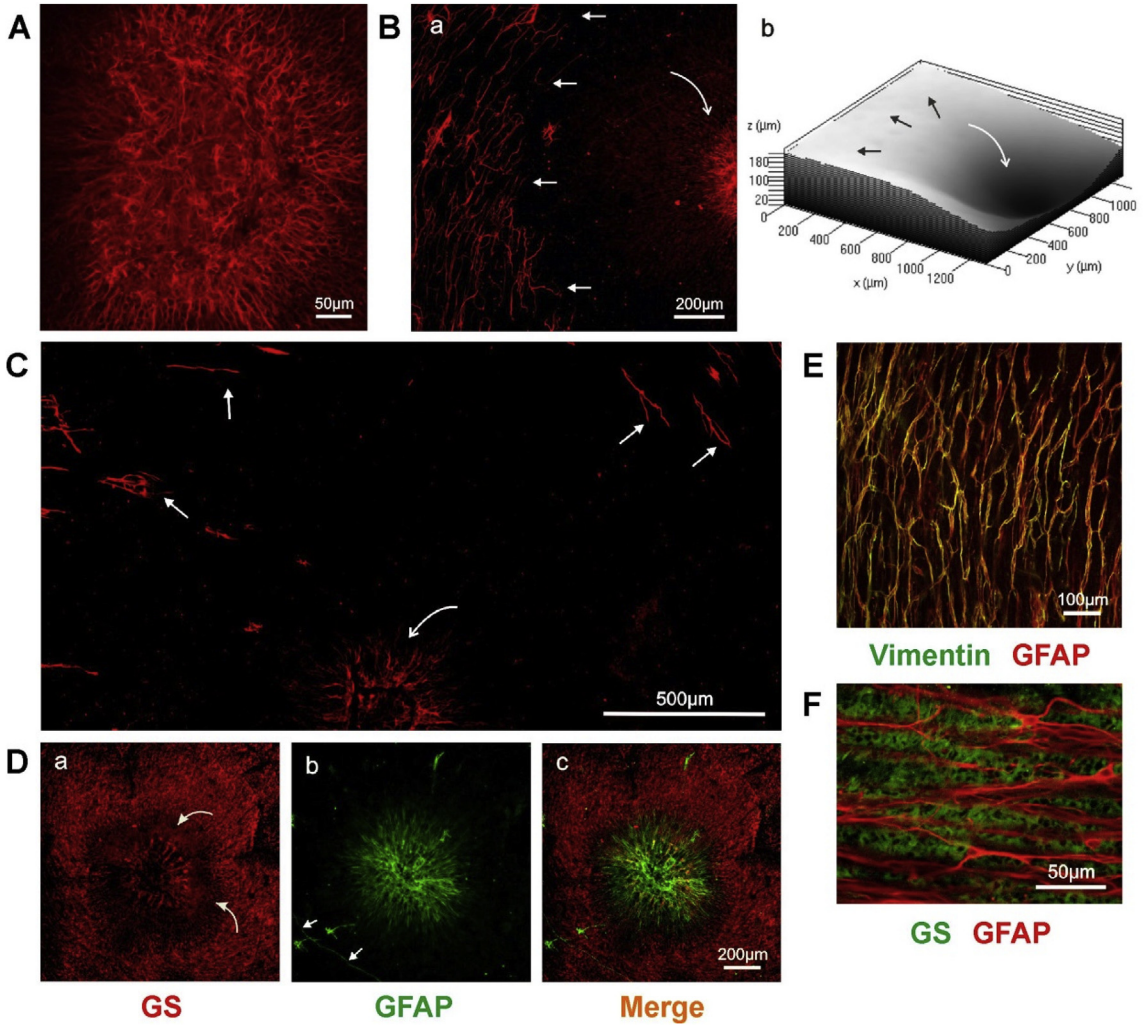

Fig. 12. Astrocytes and Müller cells in the foveola of the rhesus macaque (*Macaca mulatta*). Images from immunohistochemically stained retinal wholemounts were obtained with a confocal laser scanning microscope. **A.** Supervision on the foveal center of one animal. Müller cells are immunostained against GFAP (*red*). Müller cell processes in the foveola are irregularly arranged whereas Müller cell processes which surround the rows of photoreceptor cell somata in the outer nuclear layer of the fovea walls display a centrifugal direction. The GFAP staining intensity of Müller cells decreases outside of a diameter of about 400 µm from the foveal center. **B.** Supervision on a fovea of another animal immunostained against GFAP (*red*). (**a**) The *right side* of the image displays GFAP-expressing Müller cells in the foveola (*curved arrow*) while the *left side* shows GFAP-expressing astrocytes in the fovea wall which are circularly arranged around the foveal pit (*straight arrows*). (**b**) Reconstruction of the fovea. *White arrow*, arrangement of Müller cell main processes. *Black arrows*, circularly arranged astrocytes. **C.** Supervision on the fovea of another animal which was immunostained against GFAP (*red*). The GFAP-expressing region, which involves the foveola and the lower part of the fovea walls, has a diameter of about 600 µm (*curved arrow*). GFAP-expressing astrocytes (*straight arrows*) are found at distances of about 600 µm (*left side*) and 1.1 mm (*right side*) from the foveal center. **D.** Supervision on a fovea which was immunostained against glutamine synthetase (**a**; *red*) and GFAP (**b**; *green*). Colabeling yielded a *yellow* merge signal (**c**). Note the decrease in the level of the glutamine synthetase staining in the foveal center (*curved arrows*) and the GFAP expression by Müller cells in the central 600–700 µm of the fovea. GFAP-expressing astrocytes (*straight arrows*) are located at a distance of about 570 µm from the foveal center. Note also that Müller cell endfeet in the fovea walls do not express GFAP. Astrocytes in the fovea walls and Müller cells in the central foveola do not express glutamine synthetase (**c**). On the other hand, outer processes of Müller cells of the fovea walls, which are radially arranged in the foveola, express both glutamine synthetase and GFAP (**c**). **E.** Supervision on the astrocytic network in the ganglion cell/nerve fiber layers of the peripheral retina. Astrocytes were immunostained for both vimentin (*green*) and GFAP (*red*); costaining yielded a *yellow* merge signal. **F.** Supervision on astrocytes and Müller cell endfeet in the ganglion cell/nerve fiber layers of the peripheral retina. Astrocytes express GFAP (*red*), and Müller cell endfeet express glutamine synthetase (*green*).

peak cone density among other primate species ranges from 110,000 to 200,000 per mm^2 (Schein, 1988; Wilder et al., 1996; Franco et al., 2000; Finlay et al., 2008). The highest peak cone density among primates was found in the fovea of the howler monkey (357,000–429,000 per mm^2) (Franco et al., 2000). Because howler monkeys also have a small rod-free zone (250 µm diameter instead of 500 µm in other New World primates) (Franco et al., 2000), it is likely that the very high cone density in the foveola results from a strong developmental displacement of the outer retina towards the foveal center (see 4.4.). The lowest yet described peak cone density in primate foveas (50,000–85,000 per mm^2) was found in the nocturnal tarsier *Tarsius spectrum*; throughout the foveal cone mosaic, rods are present at significant densities (Hendrickson et al., 2000). The nocturnal owl monkey *Aotes*, which has a very high density of rods in the central retina and no fovea interna, has a peak cone density of 7000–17,000 per mm^2 (Wikler and Rakic, 1990; Finlay et al., 2008).

The human fovea contains a central bouquet of about 500 cones (Rochon-Duvigneaud, 1907; Ahnelt, 1998). In the foveolar center of the baboon retina, there is a distinct group of about 500 cones which have a density of 385,000 per mm^2 (Krebs and Krebs, 1989). In the macaque retina, the highest photoreceptor density is within 40 µm of the foveal center (Fig. 11B) (Packer et al., 1989). The centralmost 100 µm of the

human fovea contains 2000 cones (Polyak, 1957), the central 300 µm contain 7000–10,000 cones, and the central 2 mm of the human retina contain 90,000 cones (Curcio et al., 1990; Wässle et al., 1990). Thus, the highest visual acuity depends on the function of several thousands cones.

The local density of cones steeply decreases from the center to the periphery of the foveola (Curcio et al., 1990); at the transition zone between the foveola and fovea walls, the cone density is half of the peak density (Fig. 16A). In the fovea walls, the distance-dependent decrease of the cone density is less steep (Figs. 6 and 16A). Superimposed on this gradient is a streak of high cone density along the horizontal meridian of the retina; along the nasal hemimeridian, the cone density is 40% higher than along the temporal hemimeridian (Perry and Cowey, 1988; Packer et al., 1989; Curcio et al., 1990, 1991; Finlay et al., 2008). Along with the steep decrease of the cone density from about 200,000 to about 35,000 per mm^2 up to a distance of 600 µm from the foveal center, the visual acuity of humans falls from 1 to about 0.4 (Fig. 6). However, the pattern of cone density alterations in the foveola displays individual variations. While the animal shown at the *right side* of Fig. 16A apparently had a central bouquet of cones within the centralmost 50 µm of the foveola, the cone density falls rather continuously from the center to the periphery of the foveola in the animal shown at the *left side* of Fig. 16A.

The peripheral cone density in all primates ranges between 2000 and 4000 per mm^2; this value is little different from that of many other mammals like mice (Ahnelt and Kolb, 2000). The total number of foveal cones is similar for eyes with widely varying peak cone density; this is consistent with the assumption that the variability of the peak cone density reflects differences in the magnitude of the centripetal displacement of photoreceptors during development (see 4.4.) rather than differences in the absolute number of cones (Curcio et al., 1990).

The steep increase in the cone density within the fovea externa occurs in association with an increase in the length of the cone outer segments (Fig. 11B) and a decrease in the thickness of the cone segments (Fig. 16B and C). The thickness of the cone segments gradually increases from the center to the periphery of the foveola (Polyak, 1957). While the foveola only contains thin cone segments (diameter, 1.6–2.2 µm; Fig. 7G) (Curcio et al., 1990), the fovea walls and parafovea contain thick cone segments and thin rod segments (Fig. 16B and C). According to Polyak (1941), the inner segments of the centralmost cones are 1.5 µm thick, and the outer segments 1 µm. In the slope of the fovea externa, the inner segments are 2.3 µm thick, and the outer segments 1.3 µm. At the edge of the fovea externa, the inner cone segments are 2.5 µm thick, and the outer segments 1.3 µm. In a fovea of a rhesus macaque, the diameter of cone inner segments is 3.34 ± 0.59 and 4.79 ± 0.81 µm at distances of 100 and 500 µm from the foveal center. In the fovea of the howler monkey, the central cone segments have an average diameter of 1.95 µm (Franco et al., 2000). At the edge of the foveola (100 µm from the foveal center), the average diameter of cones is 3.3 µm; here, the first rods appear with a mean diameter of 1.7 µm (Franco et al., 2000). At 500 µm from the foveal center, the cone diameter is 5.5 µm, and the rod diameter is 2.9 µm (Franco et al., 2000).

In the peripheral retina, the thickness of cone segments is decreased compared to that of parafoveal cones (Fig. 16D). The thickness of cone segments increases again around the optic nerve head (Fig. 16E) and near the ora serrata (Franz, 1913). The optic nerve head is surrounded by thick, irregularly formed cones (Fig. 16E). The mean density of the cones around the optic nerve head of rhesus macaques is 9300 ± 1600 per mm^2; the mean thickness of the inner cone segments is 11.0 ± 2.9 µm (means ± S.D.; n = 4).

2.3.2. Rods

There is a large interindividual variation in the diameter of the foveal rod-free zone in adult humans; values between 350 and 800 µm were described (Detwiler, 1943; Yuodelis and Hendrickson, 1986; Curcio et al., 1990). Single rods may be present up to 100 µm from the foveal center (Hendrickson, 2005). The rod-free zone of various New World monkey has a diameter of about 500 µm (Wilder et al., 1996; Franco et al., 2000; Finlay et al., 2008). Pigtail macaques have a rod-free zone with a diameter of 150–200 µm (Hendrickson and Kupfer, 1976); however, single rods may be present at distances of less than 20 µm from the foveal center (Packer et al., 1989). In the example of the human fovea shown in Fig. 7A, the centralmost rod nuclei are located 270 and 370 µm, respectively, from the foveal center (Syrbe et al., 2018).

In the fovea walls and parafovea, the density of rods gradually increases with the distance to the foveal center in parallel with the decline of the cone density (Figs. 6 and 10G). In the fovea of rhesus macaques, the ratio of rods to cones is 1:1 at a distance of 500 µm from the foveal center (with equal densities of about 40,000 per mm^2), and 10:1 at a distance of 1.5 mm (Fig. 10G) (Wikler et al., 1990). In the human fovea, a 1:1 ratio between rods and cones is found 500 µm (naso-temporal) and 400 µm (superior-inferior) from the foveal center (Curcio et al., 1990). The rod density peaks outside the macula in a ring between 4 and 6 mm from the foveal center with a 'hot spot' 3–5 mm from the fovea in the superior (or, in a minority of monkey and human eyes, in the inferior) meridian (Ahnelt, 1998). Peak rod densities between 130,000 and 190,000 per mm^2 were described for the human and macaque retina (Curcio et al., 1990; Packer et al., 1989; Wikler et al., 1990). As the rod ring crosses the horizontal meridian, the density of rods drops 15–25% (Curcio et al., 1990). Between the ring of peak rod density and the ora serrata, the rod density decreases continuously.

2.4. Second- and third-order neurons of the fovea

2.4.1. Ganglion cells

The fovea contains about 25% of all retinal ganglion cells (Curcio and Allen, 1990; Curcio et al., 1990). There are at least 15 different types of ganglion cells in the fovea of diurnal primates (Percival et al., 2013). Retinal ganglion cells are subdivided into classes according to the receptive fields, projections, and functions. The main ganglion cell types of the primate retina are small (ON and OFF) midget (parvocellular) cells (about 80% of foveal ganglion cells), large (ON and OFF) parasol (magnocellular) cells (about 10% of foveal ganglion cells), and koniocellular ganglion cells (Boycott and Dowling, 1969; Perry et al., 1984; Wässle and Boycott, 1991; Percival et al., 2013).

Midget ganglion cells have the smallest dendritic trees (about 10 µm in diameter in the human fovea; pedicles of red and green cones have a diameter of 7–9 µm) and project to the parvocellular layers of the dorsal lateral geniculate nucleus. In the fovea, they are connected to midget bipolars which are linked to one cone. They respond to light with an opponent chromatic organization in their surround. There are four types of midget ganglion cells, red-ON/green-OFF, green-ON/red-OFF, blue-ON/yellow-OFF, and yellow-ON/blue-OFF. The surround opponency of ON and OFF midget ganglion cells is produced by horizontal cell-mediated lateral feedback inhibition of cones and by amacrine cells. The contrast provided by the center-surround opponency greatly improves the resolution of the foveal image. Midget ganglion cells respond to changes in color but weakly to contrast changes (Kaplan et al., 1990). The high number of red- and green cone-driven midget ganglion cells is responsible for the high acuity color vision provided by the primate fovea.

Parasol ganglion cells have large dendritic trees (about 35 µm in diameter in the human fovea), project to the magnocellular layers of the dorsal lateral geniculate nucleus, and receive input (via bipolar cells) from many rods and cones. In the primate fovea, there is a convergence of 30–50 cones onto each parasol ganglion cell (Grünert et al., 1993). The high convergence of photoreceptors onto parasol ganglion cells provides high contrast and movement sensitivity, but low spatial resolution and color sensitivity (Kaplan et al., 1990). The surround opponency of ON and OFF parasol ganglion cells originates from lateral

inhibition of photoreceptors by horizontal cells.

Koniocellular ganglion cells, which include a large variety of morphological cell types like small and large bistratified cells (Percival et al., 2013), project to the koniocellular layers of the dorsal lateral geniculate nucleus. In the marmoset fovea, koniocellular ganglion cells (up to 540 μm from the foveal center) receive inputs from cones that are located up to a distance of 250 μm from the foveal center; more peripherally, koniocellular cells also receive input from rods (Percival et al., 2013). In the periphery, intermediate numbers of rods and blue cones provide information (via diffuse bipolar cells) to koniocellular ganglion cells. One subtype of koniocellular ganglion cells is the small bistratified blue-yellow ganglion cell.

Because the resolution limit depends both on the spacing and the dendritic field size, only cells with high density and small dendritic fields, i.e., midget ganglion cells, are capable to provide high visual acuity and can transmit fine details. The large receptive fields of parasol and koniocellular ganglion cells permit higher contrast sensitivity and movement detection.

The fovea provides the most acute color and spatial resolution. The visual resolution is dependent on various factors including the optical image magnification provided by the anterior eye structures, the central cone density, the ratio between the numbers of cones and ganglion cells, and the density of cone-driven ganglion cells (Rossi and Roorda, 2010). The foveola of most primates contains only single scattered ganglion cell somata. In a fovea of a rhesus macaque, the nasal hemimeridian was ganglion cell-free up to 120 μm and the temporal hemimeridian up to 180 μm from the foveal center. Outside the foveola, the topography of retinal ganglion cells closely follows that of cones. The density of ganglion cells gradually increases in the central fovea walls and peaks in the parafovea (Figs. 10E and 15C). Different studies described peak ganglion cell densities between 30,000 and 80,000 per mm^2 in the fovea walls of humans and macaques (Van Buren, 1963; Oppel, 1967; Perry and Cowey, 1985; Curcio and Allen, 1990; Schein, 1988; Wässle et al., 1989; Conradi and Sjöstrand, 1993; Sjöstrand et al., 1994, 1999a). In a macaque fovea, the peak density of GCL neurons of about 50,000 per mm^2 occurred between 0.5 and 1.2 mm from the foveal center (Fig. 10E), and in a human fovea, between 0.5 and 0.8 mm (Fig. 15C). A similar spatial distribution of the ganglion cell density (with a peak density of 56,000 per mm^2 between 0.6 and 0.7 mm from the foveal center) was previously described for a human retina (Sjöstrand et al., 1994). For the macaque fovea, a plateau of the maximum ganglion cell density of 60,000 per mm^2 was described to be located at around 800 μm from the foveal center (Wässle et al., 1989).

The local density of ganglion cells decreases from the central to the peripheral retina. Because the rod-driven scotopic pathway is superimposed onto the cone-driven photopic system via rod bipolars and AII amacrine cells (Kolb and Famiglietti, 1974), there is no increase in the number of ganglion cells despite the increasing number of rods. In addition, the dendritic tree size of midget ganglion cells and the convergence of cones to the midget ganglion cells increase with the distance from the foveal center (Wässle et al., 1990; Kolb and Marshak, 2003); this contributes to the decrease of the ganglion cell number in the peripheral retina. The ganglion cell density decreases to less than 3000 per mm^2 at the nasal, and to less than 2000 per mm^2 at the temporal perifoveal edge (Curcio and Allen, 1990). More peripherally, the density of ganglion cells falls continuously to a minimum of 800 per mm^2 at 12 mm from the foveal center in the nasal retina and 100 per mm^2 in the temporal retina of macaques (Perry and Cowey, 1985; Schein, 1988; Wässle et al., 1989; Sjöstrand et al., 1999a). The nasotemporal asymmetry of ganglion cell density and the presence of a streak of higher ganglion cell density along the horizontal meridian match similar structures of the cone topography (see 2.3.1.).

The density of rods gradually increases with the distance to the foveal center (Fig. 10G). Therefore, although the density of ganglion cells remains stable over a relatively wide distance from the foveal center (Figs. 10E and 15C), the ratio between the ganglion cell and photoreceptor numbers decreases with the distance to the foveal center. In a macaque fovea, the ratio decreased from about 2:1 near the foveal center to near 1:1 at 1.5 mm from the foveal center (Fig. 10H). In a human fovea, the ratio decreased from about 3:1 to 2:1 within a distance of 400–700 μm from the foveal center (Fig. 15F).

There is a long debate regarding the question 'How many ganglion cells are there to a foveal cone?' (Sjöstrand et al., 1994). In a human retina, the ratio between GCL neurons and cones in the central fovea (within a distance of 100 μm from the foveal center which only contains cones) is 2.6:1 to 3.6:1 (Fig. 15F). Near the center of a macaque fovea, the ratio between ganglion cells and cones is 2.5:1 to 3:1 (Fig. 10H). These values are similar to previous studies which described 2.8–4 ganglion cells per cone in the central fovea (Wässle et al., 1989, 1990; Curcio and Allen, 1990; Sjöstrand et al., 1994, 1999a). In the parafovea of a macaque fovea (1 mm from the foveal center), the ratio between ganglion cells and cones increased to 4–5:1 (Fig. 10H). The data may suggest that in the foveal center, one cone provides information input to two midget ganglion cells plus 0.5–1 parasol ganglion cell. Cones in the fovea walls may also provide information input to additional types of ganglion cells, i.e., various types of koniocellular cells. The fact that the proportion of koniocellular ganglion cells is decreased in the human foveola (Dacey, 1993) fits to this assumption. Because in the foveal center, each cone provides input to at least two ganglion cells (Fig. 10H), the acuity of the foveal vision is limited by the cone density (Rossi and Roorda, 2010).

More peripherally, the ratio between ganglion cells and cones decreases because of the increasing convergence of cones onto midget ganglion cells (Schein, 1988; Wässle et al., 1989, 1990; Curcio and Allen, 1990; Kolb and Marshak, 2003). In the macaque retina, the ganglion cell-to-cone ratio decreases to 1:1 at 3–4 mm from the foveal center; the peripheral retina contains more cones than ganglion cells (Wässle et al., 1990, 1994). In humans, the ratio between ganglion cells and cones is 0.5:1 at a distance of 5 mm from the foveal center (Sjöstrand et al., 1999a). Because the bipolar cell-to-cone ratio in the macaque retina is fairly constant within the central 5 mm of the fovea (Martin and Grünert, 1992), the changes in the ganglion cell-to-cone ratio are due to the convergence of bipolar to ganglion cells, rather than to a convergence of cones onto bipolar cells (Wässle et al., 1994).

2.4.2. INL neurons

There are two main parallel information pathways in the fovea: one for high resolution and color discrimination (the midget pathway), and the other for contrast sensitivity, movement detection, and luminosity perception (the diffuse pathway). Horizontal and amacrine cells provide informations regarding contrast, spatial orientation, and movement of visual objects. Color discrimination is performed by two subsystems: the red-green and the blue-yellow pathways. These subsystems are driven by different types of cones which show distinct spatial distribution and connectivity. The primate retina contains at least 9 types of midget and diffuse cone bipolar cells, and one type of rod bipolar cell (Chun et al., 1996). Small midget bipolars contact only one cone pedicle, diffuse bipolar cells (which have greater dendritic fields) contact 5 to 10 cone pedicles, and rod bipolars contact at least 15 spherules (Boycott and Wässle, 1991).

Midget bipolar cells underlie the color-opponent receptive fields of ganglion cells. In the fovea, these cells have exclusive contacts to one cone; thus, one midget bipolar cell provides the excitatory signal for the center of a midget ganglion cell, and another midget bipolar cell, connected to a spectrally different cone type, provides the signal for the inhibitory surround. (However, even foveal midget cells may have centers that are impure due to the presence of gap junctions between red and green cones.)

Each red and green cone pedicle in the primate central fovea have synaptic contacts with horizontal cell processes and three or more different bipolar cells, including an (invaginating) ON and a (flat) OFF midget bipolar cell (Polyak, 1941; Boycott and Dowling, 1969; Kolb

et al., 1969; Hendrickson, 2005). An additional population of diffuse cone bipolar cells, which contact a number of cones, innervate the remaining 20% of foveal ganglion cells which are non-midget types. Outside the central fovea, one red or green cone pedicle contacts two midget bipolar cells and 10 to 15 diffuse bipolar cells (Boycott and Wässle, 1991).

Blue cone pedicles are smaller and lie more vitread in the OPL than the other cone pedicles (Ahnelt and Kolb, 1994). Blue cones have unique connectivity with specific horizontal, bipolar, and ganglion cells (Ahnelt and Kolb, 1994; Hendrickson, 2005). In the central retina, a single blue cone contacts blue midget ON and (rare) OFF bipolar cells (Kouyama and Marshak, 1992) which provide inputs to two small bistratified ganglion cells and the giant monostratified blue ON ganglion cells (Dacey and Lee, 1994; Klug et al., 2003; Ahmad et al., 2003). These ganglion cells also receive (via other types of cone bipolars) a mixed input from red and green cones (Hendrickson, 2005). The blue-yellow ganglion cells are ON to the blue cone and OFF to yellow. The opponent yellow surround of blue-yellow ganglion cells is produced by inhibitory blue cone contacts of horizontal cells driven by red and green cones (Packer et al., 2010). An OFF yellow signal could also be provided by diffuse OFF bipolar cells. Blue cones are important for chromatic rather than spatial resolution because of their low density and because 2–4 blue cones contact one blue ON bipolar cell (Hendrickson, 2005).

Rod bipolars, which innervate AII amacrine cells (Kolb and Famiglietti, 1974), are morphologically different from cone bipolars, e.g., the dendritic trees are more bushy because they obtain information input from many rod spherules. In the central primate retina, which is cone-dominated, rod bipolar cells are less than 20% of the total bipolar cell population.

The density of INL neurons is low in the foveal center and increases up to a peak of about 130,000 cells per mm^2 at distances between 0.8 and 1.5 mm from the foveal center in a macaque fovea, and between 0.4 and 0.8 mm in a human fovea (Figs. 10E and 15C). It has been described that at a distance of 500 µm from the foveal center of cynomolgus monkeys, the density of bipolar cells is 78,000–89,000, of amacrine cells 10,000–14,000, and of horizontal cells 19,000–25,000 per mm^2 (Krebs and Krebs, 1989).

The ratio between INL neurons and photoreceptors is highest in the foveal center and decreases with the distance from the center (Figs. 10H and 15F). It has been described that the bipolar cell-to-cone ratio in the macaque retina remains fairly constant (2.4–4:1) within the central 5 mm of the fovea (Martin and Grünert, 1992). The slightly higher number of INL nuclei per ONL nucleus compared to the number of ganglion cells per cone near the foveal center (Fig. 10H) may be explained with the presence of horizontal and amacrine cells in addition to bipolar and Müller cells. Whether the higher number of INL nuclei per ONL nucleus in the human central fovea (Fig. 15F) compared to the macaque central fovea (Fig. 10H) reflects a species difference in the numbers of amacrine and horizontal cells remains to be determined.

2.5. Glio-neuronal units of the fovea

The glio-neuronal columnar units of retinal forward information processing consist of photoreceptors and neurons aligned along a Müller cell (Fig. 1A) (Reichenbach et al., 1994; Reichenbach and Robinson, 1995). The local densities of cone photoreceptors and Müller cells are roughly equal in many species (Reichenbach and Robinson, 1995; Agte et al., 2011); therefore, it has been suggested that the core of a functional unit is constituted by a Müller cell in association with a cone (Reichenbach et al., 1994; Reichenbach and Robinson, 1995). In the fovea walls of macaques, there are one Müller cell, one amacrine cell, and 0.8 horizontal cells for each cone pedicle (Burris et al., 2002; Ahmad et al., 2003).

The foveola is largely rod-free (Ahnelt, 1998; Provis et al., 2005; Bumsted O'Brien, 2008). Therefore, the cell nuclei in the ONL within a diameter of 100 µm around the foveal center are nuclei of cone cells. In two human retinas, in which the cell nuclei were counted, 0.73 ± 0.27 cone nuclei per Müller cell were found in the foveal center (Fig. 15E), suggesting a ratio between the numbers of centralmost cones and Müller cells of near 1:1. In a macaque fovea, the ratio between the numbers of centralmost cones and Müller cells was also near 1:1 (Fig. 10G). On the other hand, the peak density of cone segments in the foveola of rhesus macaques ranged between 90,000 and 166,000 per mm^2 (Fig. 16A), while the peak density of Müller cell processes at the OLM of the foveal center ranged between 32,000 and 58,000 per mm^2. These data suggest a ratio between the numbers of centralmost cones and Müller cells in the macaque fovea of about 3:1. This ratio is similar to that described for the baboon fovea (3.5 cones per Müller cell) (Finlay et al., 2005). The reason why the ratios at the levels of the ONL and OLM are different is unclear but may be explained in part by the fact that the outer cone processes are centrifugally arranged (Figs. 7A and 10A); it could be that not all outer cone processes are accompanied by outer Müller cell processes. Further investigations are required to determine the spatial relationship between cone and Müller cells in the foveola. With increasing distance to the foveal center, the ratio of Müller cells per cone increases. Using data of Packer et al. (1990) and Distler and Dreher (1996) regarding the densities of cones and Müller cells, it can be estimated that the ratio of Müller cells to cones is 1.5–2.5:1 in the peripheral retina of macaques.

The glio-neuronal units of retinal information processing in the fovea walls of humans and rhesus macaques consist of about 16 cells per Müller cell (Figs. 10F and 15D). These cells include about 4 GCL neurons, 10 inter- (INL) neurons, and 2 photoreceptors in the human fovea walls (Fig. 15E), and about 3 GCL neurons, 7 interneurons, and 6 photoreceptors in the fovea walls of a rhesus macaque (Fig. 10G). In the primate retina, central and peripheral units contain a similar total number of neurons; the cellular composition of a functional unit does not alter during retinal development, from the area centralis to the adult stage (Finlay et al., 2005). In the human retina, the number of cells per Müller cell is about 16 in the fovea walls (Figs. 15D) and 14.37 in the retinal periphery (Reichenbach and Robinson, 1995). Whether the decrease in the number of cells per Müller cell to 8–12 in the central fovea (within 300 µm from the foveal center; Figs. 10F and 15D) reflects a real decrease or is caused by the counting of Müller cell processes in the ONL of the foveola remains to be determined in future investigations. The developmental cytogenesis terminates earlier within the future foveola than in the surrounding tissue (Reichenbach and Robinson (1995); this may result in a decreased number of cells per Müller cell in the foveal center.

While the total number of cells in a columnar unit remains largely unaltered from the fovea walls to the retinal periphery, the cellular composition of the units alters with the retinal location (Finlay et al., 2005). In particular, the number of GCL neurons per unit decreases and the number of photoreceptors per unit increases in the outer fovea walls and parafovea (Fig. 10G). The number of photoreceptors per Müller cell increases from about 2 in the fovea walls (Fig. 15E) to 10.87 in the retinal periphery (Reichenbach and Robinson, 1995). Because the density of Müller cells in the fovea walls does not alter with the distance to the foveal center (Figs. 10D and 15B), the ratio between the numbers of photoreceptors and Müller cells increases in association with the steep increase of the rod number (Figs. 10G and 15E). The numbers of cones and neurons per Müller cell decrease from the fovea walls to the retinal periphery; the numbers of INL and GCL neurons decrease from about 10 to 3.2, and from about 4 to 0.3, respectively (Reichenbach and Robinson, 1995). Similar alterations in the cellular composition of the glio-neuronal units from the fovea walls to the retinal periphery were found in macaques. While the number of cells per Müller cell is similar in the fovea walls (about 16; Fig. 10F) and peripheral retina of macaques (16.32), the number of photoreceptors per Müller cell increases from about 6 (Fig. 10G) to 11.7, the number of cones per Müller cell decreases from about 1.3 to 0.4–0.7, and the numbers of INL and GCL neurons per Müller cell decrease from about 7 to 4.24, and from about 3

to 0.38, respectively, from the fovea walls to the retinal periphery (Krebs and Krebs, 1989; Packer et al., 1989; Distler and Dreher, 1996). The glio-neuronal units of the fovea and periphery of the baboon retina are composed of 12 cells per Müller cell; the cellular composition of the units alters with the retinal location similar as described above (Finlay et al., 2005). In the periphery, most cells of the retina are rod photoreceptor cells, and ganglion cells are the least cells (Reichenbach and Robinson, 1995). The data indicate that there is a tenfold increase in the number of ganglion cells and a doubling of interneurons in the fovea walls compared to the retinal periphery. The high numbers of interneurons and ganglion cells per columnar unit in the fovea is also indicated by the thick INL and GCL in the fovea walls and parafovea (Fig. 10J). In the peripheral retina, the thickness of the INL and, in particular, of the GCL is reduced compared to the foveal tissue (Fig. 10I). Thick INL and GCL are characterisics of cone-dominated photopic/diurnal mammals while the retina of rod-dominated scotopic/noctural mammals has thin INL and GCL (Reichenbach and Robinson, 1995).

3. Optics of the fovea

The optical function of both vertebrate fovea types, in particular the optical relevance of the foveal pit, is still uncompletely understood. There are no correlations between the size of the foveal avascular zone (i.e., the width of the foveal pit) and the visual acuity of human subjects (Adler, 1929) and between the depth of the foveal pit and the visual acuity of human subjects with albinism (Mohammad et al., 2011). The morphology of the foveal pit varies highly among albinotic subjects (Wilk et al., 2014). In the mean, the peak photoreceptor density is lower in human subjects with albinism compared to control subjects (Springer, 2014); in these subjects, the length of the central cone outer segments is the strongest predictor of the visual acuity (Mohammad et al., 2011). Because the length of the receptor segments is inversely related to the thickness of the segments, the length of the receptor segments is an indicator of the receptor density. Albinotic individuals who have the most developed foveal pits may have nearly normal peak cone densities and a better visual acuity, while those with less developed pits have progressively decreasing peak cone densities and visual acuities (Thomas et al., 2011; Wilk et al., 2014; McCafferty et al., 2015). These data and the assumption that the foveola does not provide image magnification (Fig. 3B) suggest that the visual acuity provided by the human fovea is mainly dependent on the density of the central photoreceptors (Wilson et al., 1988; Mohammad et al., 2011), and that the shape and depth of the foveal pit have less relevance for acuity.

It is known that avian convexiclivate foveas with a deep pit provide a very high visual acuity (Snyder and Miller, 1978). Large raptorial birds are the only animals with spatial resolution (eagles and falcons, 140 cycles per degree) higher than humans (60 cycles per degree). Convexiclivate foveas increase the visual resolution by two ways: the presence of thin photoreceptors (eagles have central cones which are thinner than the cones of the central primate fovea [Polyak, 1957]) and illumination of the central photoreceptors by a magnified foveal image. Walls (1942) proposed that the fovea of birds serves for local image magnification which results from light refraction at the vitreoretinal border of the central convex fovea walls (Fig. 3B). Later, Snyder and Miller (1978) suggested that not the central fovea walls but the concave bottom of the foveal pit acts as a diverging (negative) lens that enlarges the foveal image (Fig. 3C). They also described that the center of the deep avian fovea contains a conspicuous horizontal Müller cell structure which has a high refraction index; light refraction at this glial structure may contribute to the image-magnifying function of the avian fovea. A highly refractive Müller cell layer that lines the foveal center was not found in the primate fovea (Snyder and Miller, 1978). On the other hand, Pumphrey (1948) suggested that the convexiclivate fovea does not provide image magnification, but serves as an image fixation device. Light refraction at the vitreoretinal border may provide information on focus error (Harkness and Bennet-Clark, 1978). Pumphrey (1948) also suggested that the sloping walls of the convexiclivate fovea accentuate the angular displacement of light and thus should improve movement detection. The visual information of the fovea serves to cue the required lens accomodation to achieve a focused image which facilitates the fixation of moving targets (Pumphrey, 1948; Harkness and Bennet-Clark, 1978). In humans, the phenomenon of night myopia indicates that the focusing system is unable to correct in darkness (Toates, 1972).

The optical properties of the primate fovea are largely unclear. It has been suggested that the foveola does not provide image magnification whereas light refraction at the fovea walls may cause a magnification of the image around the foveola (Fig. 3B) (Walls, 1942; Reichenbach and Bringmann, 2010). However, many human subjects have no flat foveolas but a gently sloping inner foveolar surface (Fig. 13D) (Tick et al., 2011). In these subjects, the concave surface of the central foveola may provide image magnification, similar as the concave bottom of the pit of the avian fovea (Fig. 3C). It could be but remains to be proven that the foveolar image magnification in the latter subjects compensates the lower area of the inner foveola, enabling light guidance to the whole area of the fovea externa. The fovea externa may be formed in order to compensate the angle of centripetally refracted light. Light ray analyses using estimated light refraction at the vitreoretinal border of the primate fovea gave maximal light displacements at the photoreceptor level of about 2 µm (Ross, 2004; Frey et al., 2017); because the maximum behavioral visual acuity of macaques is 3.3 µm (Wässle et al., 1990), a light ray displacement by 2 µm is not great enough to assume an image-magnifying function of the fovea.

Image magnification provided by the central fovea walls will compensate the optical problems of the fovea walls where the retina is very thick (i.e., many light-scattering layers lie in front of the cones). However, the surface of the fovea walls is convex; a convex lens will (depending on the direction of light refraction) also cause a focusing of the light into a ring around the foveola; a directional-dependent distortion of the ring-shaped image may provide information on focus plane error, as suggested for the avian fovea (Harkness and Bennet-Clark, 1978). Focal plane analysis may be also important for the stereoscopic vision of primates. Light refraction at the fovea walls may underlie the directional sensitivity of cones at the rim of the foveola (Williams, 1980).

During tree jumping of primates, optimized visuomotor coordination is crucial for survival; however, the motor control is deprived of the input from (non-proprioreceptive) mechanosensory systems (Ahnelt and Kolb, 2000). The high spatial acuity provided by the midget system of the fovea may be favorable to achieve a maximum eye-hand coordination required for tree jumping (Ahnelt and Kolb, 2000). On the other hand, the sensitivity to rapidly varying light inputs is lower for the foveal than the peripheral vision (Hecht and Verrijp, 1933). The low temporal sensitivity of foveal vision is reflected in the refresh rates of computer monitors and movies and is an important factor in the design of visual prosthetics (Sinha et al., 2017). It has been proposed for the avian fovea that image distortion provided by the sloping central walls may improve rapid movement detection (Pumphrey, 1948). Perhaps, the central walls of the primate fovea have a similar function.

Gass (1999) suggested that the “Müller cell cone” in the foveola forms a smooth transparent plate that overlies the area of high photoreceptor density (Fig. 11A and B). Foveolar Müller cells improve the light and image transport, as their inner processes provide a plain, unruffled vitreal surface of the foveola (i.e., they form a smooth coverslide on the cone photoreceptors to avoid light scattering; see 2.1.3.). Because the central cones have elongated receptor segments (Fig. 11B), the light path from the inner retinal surface towards the receptor segments is shortest in the center of the foveola. The stalk of the “Müller cell cone”, which lies in front of the most elongated photoreceptors, has a lower optical density compared to the remaining tissue (Yamada, 1969; Hogan et al., 1971). The brighter appearance of the centralmost

foveal tissue results from the low density of cone cell nuclei at which light can scatter (Figs. 5A, 7A and 10A, and 11A) (Detwiler, 1943), and from the presence of pale outer Müller cell processes (Fig. 7C,G) (Syrbe et al., 2018). It remains to be determined in future investigations whether the vertically running pale Müller cell processes in the stalk of the "Müller cell cone" improve the light transmission towards the centralmost photoreceptors. The optical properties of the "Müller cell cone" in the foveola may alter under pathological conditions, as suggested by the presence of multiple hyperreflective dots in the inner layer of the foveola in OCT images of patients with different retinal disorders (Fig. 2B and C).

It has been shown that Müller cells in the retina of nonprimate mammals act as living optical fibers that guide the light from the inner retinal surface through their main processes towards the rows of photoreceptor cell nuclei (Franze et al., 2007; Agte et al., 2011; Labin et al., 2014). Müller cells separate between wavelengths to improve photopic vision without hampering scotopic vision (Labin et al., 2014). It has also been proposed that Müller cells in the convexiclivate fovea of pied flycatchers act as optic fibers and thus contribute to foveal image magnification (Zueva et al., 2014). The nuclei of many Müller cells are located out of the cell axis (Fig. 8C and D) which is consistent with a light-guiding function of Müller cells (Franze et al., 2007). However, the z-shaped arrangement of Müller cell main processes in the fovea walls (Figs. 1B, 8A and 11C) does not fit with the assumption that foveal Müller cells guide the light from the inner retinal surface to photoreceptor cells. If light guidance through Müller cells contributes to foveal optics, Müller cell main processes guide the light from the vitreal surface to the OPL, but not through the HFL which is a hyperreflective layer in the primate fovea (Fig. 1Ba and 2A). Perhaps, the late horizontal contraction of Müller cell processes in the OPL, which produces the erection of the inner Müller cell processes (see 4.3.), occurs to improve the light guidance through Müller cells to the HFL.

It has been suggested that the presence of a foveal pit compensates the adverse effects of chromatic aberration of the eye (Locket, 1992). Longitudinal chromatic aberration results from the fact that ocular media like the lens refract light of different wavelengths to different degrees (Sivak and Mandelman, 1982). Light of short wavelengths (blue) is more strongly refracted than green light; the least refracted light is red light. Due to chromatic aberration, the focus points of light of different wavelengths are located at different levels in the retina; when red and green light are in focus at the photoreceptor level, the focus of blue light is within the inner retina, and in the fovea at the slope of the central fovea walls. If Müller cells guide the blue light from the vitreal surface of the central fovea walls with minimal intensity loss towards the photoreceptors, the blurring effect of chromatic aberration on the images will be compensated. The foveal distribution of different cone types, i.e., the accumulation of red and green cones in the foveola and the maximum density of blue cones in a ring around the foveola on the lower foveal slope within the avascular zone (De Monasterio et al., 1985; Ahnelt, 1998), may be an adaptation to the chromatic aberration of the eye. However, it has been shown that Müller cells of nonprimate mammals guide predominantly red-green light (Labin et al., 2014); this fits to a putative light-guiding function of foveolar Müller cells rather than Müller cells in the fovea walls.

The elongation of the cone receptor segments in the fovea externa, which compensates the thinning of the segments, preserves the photopigment volume and thus the sensitivity (Ahnelt, 1998). However, in the convexiclivate fovea of many birds and chameleons, the receptor segments of the centralmost cones are thinner, but not longer than the perifoveal cone segments (Fig. 3A,C) (Ramón y Cajal, 1894). Therefore, the elongation of the receptor segments in the primate fovea externa may have also other functional roles. It is likely that the cones in the fovea externa are elongated in order to compensate the different focus planes of red and green light resulting from chromatic aberration. It has been estimated that in the human retina for small pupil (aperture) diameters, the focus plane of green light lies about 40 μm vitreally from the focus plane of red light, while blue light focusses about 33 μm vitreally from green light (K. Frey, B. Werner, M. Francke, P. Scheibe, F.G. Rauscher, A. Reichenbach, R. Brunner; unpublished data). The difference between the focus planes of red and green light is well in the range of the length of the central cone outer segments in the human fovea externa (up to 50–65 μm) (Greeff, 1900; Salzmann, 1912; Polyak, 1941; Yamada, 1969; Yuodelis and Hendrickson, 1986; Hendrickson and Provis, 2006).

4. Foveal development

To understand the developmental formation of the fovea centralis in the primate retina is a particular challenge (Provis et al., 1998). In both phylogeny and ontogeny, a fovea interna (i.e., a foveal pit) is only formed in nonvascularized retinal areas. On the other hand, a fovea externa (characterized by the high photoreceptor density) may be formed in both vascularized and nonvascularized retinal areas. The development of the fovea externa proceeds relatively independently from the morphogenesis of the fovea interna. This suggestion is supported by various facts: the fovea externa is formed by a centripetal displacement of photoreceptors, while the fovea interna is formed by a centrifugal displacement of inner retinal layers (Provis et al., 1998, 2013); the area centralis of dogs and owl monkeys contains a fovea externa but no fovea interna (Franz, 1913; Woollard, 1927; Kolmer, 1930; Webb and Kaas, 1976; Beltran et al., 2014); the developments of the fovea interna and externa of primates proceed within different time frames; the first phase of photoreceptor packing takes place before the foveal pit develops (Provis et al., 2005; Bumsted O'Brien, 2008); in the human retina, there are no correlations between the centrifugal shift of inner retinal layers and the length of central cone segments (Fig. 13D) (Tick et al., 2011), and between the size of the foveal pit and the peak cone density (Wilk et al., 2017); in prematurely born children, the fovea externa develops nearly normally while the displacement of the inner retinal layers from the foveal center is incomplete (Rosén et al., 2015); and in human eyes with a complete absence of a foveal pit, nearly normal central photoreceptor packing and receptor segment elongation can be present (Marmor et al., 2008; McAllister et al., 2010; Wilk et al., 2014).

The ontogenetic morphogenesis of the fovea interna involves the development of the rod-free zone, the area centralis, and the subsequent formation of the foveal pit and the fovea externa (Fig. 13A). The packing of central photoreceptors is initiated before the foveal pit formation, and the formation of the fovea externa is initiated during the morphogenesis of the foveola around and after birth, i.e., when the outer segments of photoreceptors become functional (Fig. 13A,C).

4.1. Cytogenesis and development of the rod-free zone

The location of the future fovea is determined by the specification of the central rod-free zone during the development of the optic vesicle at fetal week 3.4 (Provis et al., 2005; Bumsted O'Brien, 2008). A rod-free area is a precondition of the development of a foveal pit (Finlay et al., 2005). The localization of the central rod-free zone is likely determined by transcription factors which delineates the axes of the retina (Reichenbach and Pritz-Hohmeier, 1995; Schulte et al., 2005; Finlay et al., 2005) which may result in cellular accumulation in the +5a isoform of Pax6, the master regulator of eye development (Azuma et al., 2005). The region of the future fovea is devoid of rods from the beginning of retinal cytogenesis (Mann, 1964). Because there is little cell death in the ONL during development (Penfold and Provis, 1986), the rod-free zone is suggested to be produced by inhibition of the rod development from late retinal progenitor cells (LaVail et al., 1991; Reichenbach, 1993; Reichenbach and Robinson, 1995; Finlay et al., 2005; Reichenbach and Bringmann, 2010). Molecules that are associated with rod differentiation like NR2E3 are absent from the region of the future fovea (Bumsted O'Brien et al., 2004).

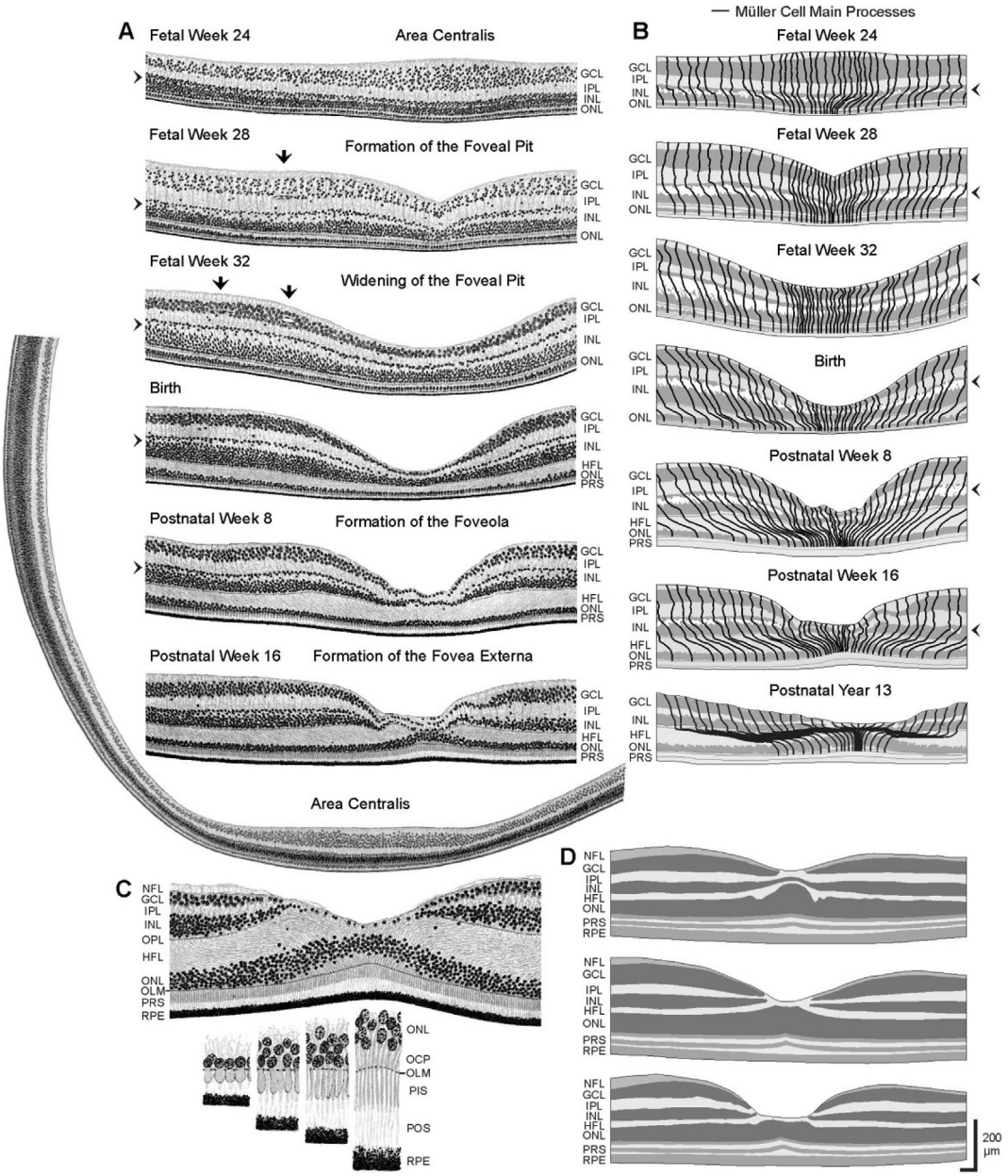

Fig. 13. Development of the human fovea. **A.** Cross sections through the developing human fovea at fetal weeks 24, 28, and 32, birth, and postnatal weeks 8 and 16. Note the presence of the area centralis with a domed ganglion cell layer (GCL) at fetal week 24 and the presence of a foveal pit at fetal week 28. The widening of the foveal pit proceeds after fetal week 28. The foveola is formed after birth, and the fovea externa after postnatal week 8. The transitory radial fiber layer between the amacrine (ACL) and bipolar cell layers (BCL) is recognizable as a layer which contains less numbers of cell nuclei (*arrowheads*). At birth, the foveal pit is a deep bowl, but still all retinal layers (with the exception of the transitory radial fiber layer) are present in the center; the central cones form a monolayer of cell somata in the outer nuclear layer (ONL), and the Henle fiber layer (HFL) begins to develop. Note that the photoreceptor somata in the ONL are earlier stacked at the foveal edge than in the foveal center. Note in the *survey image* of the retina that the retina around the area centralis is thinner than the more peripheral retina. *Arrows*, blood vessels. **B.** Spatial arrangements of main Müller cell processes and the transitory radial fiber layer between the ACL and BCL (*arrowheads*) during the development of the human fovea. **C.** Development of the fovea externa. *Above*: Foveola of an adult subject with a wide foveal pit and a v-shaped ONL. *Below*: Central cone cells at birth, postnatal weeks 8 and 16, and in the adult fovea (from *left* to *right*). **D.** Variation of the foveal morphology in three normal adult human subjects. The thickness of the central foveola is 234 µm (*above*), 215 µm (*middle*), and 180 µm (*below*), respectively. The thickness of the fovea walls is 365 µm (*above*), 378 µm (*middle*), and 339 µm (*below*), respectively. Note that a smaller diameter of the foveola is associated with a thicker foveola and a decreased steepness of the foveal slope. The morphology of the fovea externa is similar in all foveas. INL, inner nuclear layer; IPL, inner plexiform layer; NFL, nerve fiber layer; OCP, outer cone processes; OLM, outer limiting membrane; OPL, outer plexiform layer; PIS, photoreceptor inner segments; POS, photoreceptor outer segments; PRS, photoreceptor segments; RPE, retinal pigment epithelium. The images in **A** and **C** are modified from Bach and Seefelder (1914). The drawing of the postnatal year 13 fovea (**B**) represents the author's interpretation of a foveal section shown by Hendrickson (2005). The images in **D** are the author's interpretation of OCT images shown by Tick et al. (2011).

The region of the future fovea is characterized by an early cessation of precursor cell proliferation; this leads to the abundance of early-born cell types such as cones and ganglion cells, and fewer numbers of later-born cell types like rods (Reichenbach and Robinson, 1995; Finlay et al., 2005). In more peripheral retinal areas, the longer time period of cytogenesis leads to a conversion of the cone-dominated diurnal retina into a rod-dominated nocturnal retina (Reichenbach and Robinson, 1995; Finlay et al., 2005). The developmental cytogenesis is also extended in the central retina of the owl monkey (Dyer et al., 2009) which evolved from a diurnal ancestor and returned to a nocturnal lifestyle,

and which lacks a fovea interna. Many albinotic humans with impaired melanin/L-DOPA metabolism have no foveal pit (see 4.6.) and no rod-free zone (Usher, 1920; Kinnear et al., 1985; Mietz et al., 1992). This fits with the observation that L-DOPA inhibits the proliferation of late progenitor cells (Ilia and Jeffery, 2000). It has been recently shown that the formation of the area centralis in chicken is induced by a transient decrease in the level of retinoic acid which results in an increased expression of fibroblast growth factor-8 (FGF8) during the time period of cone and ganglion cell differentiation (Da Silva and Cepko, 2017). Disruption of this signaling pathway results in a loss of the central rod-free area and the area centralis with the high density of GCL neurons (Da Silva and Cepko, 2017). In addition to the inhibition of the rod generation from late progenitor cells, it is likely that there is an enhanced generation of ganglion cells and cones, and of other early-born neurons like horizontal cells, by early progenitors in the region of the future fovea (and/or an inhibition of the 'physiological cell death' resulting in an area of elevated ganglion cell density; see 4.2.). Possibly, late progenitors in the region of the future fovea undergo only two mitosis steps to generate two cone bipolar cells, one amacrine cell, and a Müller cell.

The development of the retina proceeds from the central towards the peripheral retina, and from the GCL to the ONL; therefore, the GCL in the central retina is the first retinal tissue which begin to differentiate (Chievitz, 1888). In the developing monkey retina, the first cells exit the cell cycle and differentiate to retinal ganglion cells around fetal week 7 in the region of the future fovea (Barishak, 1992). Horizontal cells are born shortly after ganglion cells in the future fovea between fetal weeks 7 and 8, followed by the generation of cone cells (between fetal weeks 11 and 14) (Hollenberg and Spira, 1973; Hendrickson and Kupfer, 1976; Provis et al., 1985a). Thereafter, amacrine and bipolar cells become postmitotic. The last cell types generated are rods and Müller cells (Rapaport et al., 1992). In the region of the future human fovea, all cells are postmitotic by fetal week 10, while in the periphery, retinal cell proliferation proceeds until fetal week 30 (Provis et al., 1985a). In humans, the location of the future fovea can be morphologically identified at fetal week 11; this site is the first part of the retina which contains three cellular and two synaptic layers, including a single layer of large, cuboidal cone cell somata (fetal week 24 in Fig. 13A) (Hendrickson, 1992).

4.2. Development of the area centralis

In primates, the area centralis lies along the horizontal meridian of the retina; the fovea is a specialization of this area near the retinal center (Fig. 4A) (Polyak, 1957). During the development, the area centralis of the future fovea is characterized by a localized doming of the retinal surface into the vitreous resulting from a thickening of the GCL (Fig. 13A) (Provis et al., 1998); in addition, the area centralis has a higher packing of photoreceptors. The GCL dome consists of rows with 7–10 stacked neuronal cell bodies (Müller, 1856). The localized thickening of the retina preceeds, during both mammalian phylo- and ontogeny, the formation of a foveal pit (Rowe and Dreher, 1982; Provis et al., 1998). The mechanism of GCL doming is unclear. Chievitz (1888) suggested a model for the formation of the GCL dome caused by the proliferation of retinal precursor cells in the more peripheral retina. Another mechanism which decreases the cell density after cessation of cell proliferation is the passive horizontal stretching of the more peripheral retinal tissue together with the growth of the eyeball (Mastronarde et al., 1984; Kelling et al., 1989; Reichenbach et al., 1991; Kuhrt et al., 2012). A third mechanism which contributes to the reduction of the GCL cell number in the more peripheral retina is the elimination of GCL neurons by apototic cell death (Provis et al., 1998). During human retinal development, the rate of cellular apoptosis peaks around fetal weeks 16–17 (Provis et al., 1998). The number of ganglion cell axons in the optic nerve reaches a maximum of 3.7 million at fetal week 17 (Provis et al., 1985b). Thereafter, the number of ganglion cell axons steadily decreases; by fetal week 30, the number of axons in the optic nerve is about one-third of that present at fetal week 17 (Penfold and Provis, 1986; Provis, 1987). In addition, there is a wave of bipolar cell death that is 2–8 times greater than that of ganglion cells (Georges et al., 1999). It has been suggested that the apoptotic elimination of bipolar cells is associated with the onset of synaptogenesis (Georges et al., 1999). In macaques, the adult synaptic density in the IPL is reached one month before birth (Nishimura and Rakic, 1985). The developmental death of GCL and INL neurons results in a thinning of the central retina compared to the peripheral retina (Fig. 13A).

All these models suggest that the number of stacked ganglion cell somata is high during the early development and decreases in the peripheral retina, but not at the site of the future fovea, during the process of GCL doming. However, Provis et al. (1985a) showed that in the developing human retina, the site of the future fovea contains fewer ganglion cells than the more peripheral retina before the development of the GCL dome, suggesting that the GCL dome is rather formed by a centripetal redistribution of ganglion and displaced amacrine cells. At fetal weeks 10–12, the central GCL contains 2–3 layers of stacked cells, at fetal weeks 14–15, 5–6 layers, and at fetal weeks 20–21, 6–7 layers (Provis et al., 1985a). The GCL dome is apparent between fetal weeks 16 and 24; the density of GCL cells increases until fetal week 17 (from 17,000 to 27,000 per mm^2) and subsequently decreases more or less continuously to about 2000 per mm^2 in the foveal center until birth (fetal weeks 37–40) (Provis et al., 1985a).

The higher packing of photoreceptors in the area centralis is produced by a centripetal displacement of the receptors (see 4.4.). The photoreceptor redistribution results in a spatial shift between the inner and outer retina which is compensated by the oblique arrangement of the bipolar cell somata rows (Fig. 13A) and Müller cell main processes (Fig. 13B) in the INL. The Müller cell main processes are centripetally bended at the outer margin of the amacrine cell layer (ACL). Between the ACL and the bipolar cell layer (BCL), a specialized Müller/bipolar cell layer is generated (Provis et al., 2000) which is recognizable in retinal sections as a layer which contains less numbers of cell nuclei (*arrowheads* in Fig. 13A; Fig. 17B). Chievitz (1887) firstly described the presence of a 'transitory radial fiber layer' (RFL) which divides the INL into two separate layers in the developing fovea of 7.5–9 months-old human fetuses. Bach and Seefelder (1914) termed this layer the 'remnant of the transient layer of Chievitz'. However, this INL sublayer is not present before the development of the area centralis (Fig. 17A) but formed during the process of GCL doming (Bach and Seefelder, 1914; Provis et al., 1998). Therefore, this layer is not identical with the early 'transient layer of Chievitz' which separates the inner and outer neuroblastic layers, and which disappears by the sclerad migration of the inner neuroblastic cells (Chievitz, 1887; Smelser et al., 1973). The transitory RFL becomes thicker in the fovea walls during the formation of the foveal pit (Figs. 13A and 17C–F) and disappears after completion of the pit formation (Hendrickson and Kupfer, 1976; Hendrickson and Drucker, 1992). In the human retina at postnatal day 5, the transitory RFL is prominent on the foveal slope and is not present at distances greater than 1.5 mm from the foveal center (Hendrickson and Drucker, 1992). In the developing marmoset retina, the transitory RFL is (at least) present from fetal day 135 to postnatal day 10, in the macaque retina from fetal day 90 to postnatal day 1, and in the human retina from fetal week 21; the transitory RFL in the human fovea disappears around postnatal week 16 (Figs. 13A and 17G) (Bach and Seefelder, 1914; Mann, 1964; Abramov et al., 1982; Provis et al., 1998, 2005; 2013; Hendrickson et al., 2006a; b; 2012; Springer et al., 2011; Dubis et al., 2012b).

The nerve fibers are symmetrically arranged at the horizontal meridian and radially around the future fovea (Fig. 4A) before the development of the foveal pit. The growth of the nerve fibers towards the optic disk is directed by (at least) two factors: (i) basal lamina-associated chondroitin-sulfate proteoglycans, which are produced by Müller cells (Ponsioen et al., 2008) and which are growth-repellent for

ganglion cell axons (Snow et al., 1991), and (ii) chemoattractive axon-guiding molecules in the optic disk (Stuermer and Bastmeyer, 2000). Chondroitin-sulfate proteoglycans are initially distributed over the center of the retina but recedes from the retinal center at the time when the first differentiating ganglion cells extend their axons (Snow et al., 1991). It has been suggested that axon growth cones move toward the optic disk because of the presence of growth-repellent proteoglycans in more peripheral locations (Snow et al., 1991). The repulsion of the nerve fibers results in the formation of a nerve fiber-free area in the center of the future fovea, making it less mechanically stiff than adjacent areas; the less mechanical stiffness supports the development of the foveal pit (Springer and Hendrickson, 2004a,b, 2005). Tractional forces provided by nerve fibers during retinal stretching may contribute to the centrifugal displacement of the ganglion cells during the widening of the foveal pit (see 4.3.).

4.3. Development of the fovea interna

The sequence of the foveal development is similar in marmosets, macaques, and humans (Hendrickson and Kupfer, 1976; Hendrickson and Yuodelis, 1984; Hendrickson et al., 2006a, 2009; Springer et al., 2011). We propose a model in which the foveal pit is formed by three consecutive movements: (Fig. 18A and B): (i) creation of the foveal pit by a vertical contraction of the centralmost Müller cells (fetal week 28 in Fig. 13A); (ii) widening of the foveal pit by a centrifugal displacement of the ganglion cells which results in a tilting of the whole inner retinal tissue (fetal week 32 until birth in Fig. 13A); and (iii) formation of the foveola by the erection of the inner retinal tissue in the fovea walls; this erection is mediated by a centrifugal displacement of the tissue in the OPL (postnatal weeks 8–16 in Fig. 13A). In humans, the development of the foveal pit starts during fetal weeks 25–26 (Provis and Hendrickson, 2008), and the foveola is formed after birth (Fig. 13A).

During the formation and widening of the foveal pit, central Müller cells heavily express GFAP (Provis et al., 2000), suggesting the presence of mechanical tissue stress. It has been shown that Müller cells provide essential tensile strength to the developing retina (MacDonald et al., 2015). Because Müller cell main processes traverse the whole neuroretina, alterations in the spatial arrangement of these processes may reflect the movements implicated in foveal development (Fig. 13B).

The widening of the foveal pit proceeds after fetal week 28 until birth by the centrifugal displacement of ganglion cells; the displacement of the inner retinal tissue is strongest at the NFL-GCL boundary (Fig. 13A and B). At fetal week 32, many bipolar cell nuclei are spindle-shaped (Fig. 17D), suggesting that the cells are mechanically stretched. The oblique arrangement of the Müller cell processes in the RFL and BCL is caused by the centripetal displacement of the photoreceptors (see 4.4.) and the centrifugal displacement of the ganglion cells. During the widening of the foveal pit, the cell nuclei rows and Müller cell processes in the GCL are obliquely arranged (Fig. 13A and B and 17D–F); such an oblique arrangement is not observed in the area centralis and during the early formation of the foveal pit (fetal weeks 24 and 28 in Fig. 13A and B; Fig. 17B and C), and is not present after the erection of the inner retinal tissue in the adult fovea (Fig. 5A and B and 10J). During the widening of the foveal pit, the IPL is less tilted than the GCL and INL (Fig. 13A and B and 17D,E). This is also recognizable at the position of the ganglion cell somata which are more peripherally located than the dendritic trees of the cells (Provis et al., 1998). During the widening of the foveal pit of rhesus macaques, the somata of ganglion cells are centrifugally displaced by 41 μm from their dendritic arbors within 1.5 mm of the foveal center; outside this region, no displacement is observed (Kirby and Steineke, 1992). The lower magnitude of tilting of the IPL in comparison to the nuclear layers may result from the higher stiffness of this layer. The IPL contains a dense network of horizontal neuronal and glial interconnections formed by the axonal and dendritic trees of bipolar, amacrine, and ganglion cells, and side processes of Müller cells (Fig. 8A,C,D). Side processes of Müller cells in the IPL are already present in the area centralis (Fig. 17B). In contrast, in the GCL and BCL, there are no cellular side processes; this makes these layers softer and supports the spatial shifts of cell somata and Müller cell processes. The transitory RFL disappears along with the erection of the inner Müller cell processes and the elongation of the Henle fibers around and after postnatal week 16 (Fig. 13A and B and 17G). This may support the assumption that the transitory RFL is mainly formed to compensate the spatial shift between the inner and outer retina before the elongated Henle fibers achieve this function.

After birth, the foveola is formed (postnatal weeks 8 and 16 in Fig. 13B). Until this stage, the inner Müller cell processes are obliquely arranged, nearly parallel to the Henle fibers in the HFL (Provis et al., 1998). During the further postnatal development (postnatal week 16 in Fig. 13B), the inner retina is centrifugally displaced at the level of the OPL, and the photoreceptors are redistributed towards the foveal center; both movements result in the elongation of the Henle fibers (from about 5 μm after synapse formation to up to 150–675 μm; postnatal year 13 in Fig. 13B). The centrifugal displacement at the level of the OPL also results in the erection of the inner retinal tissue and the inner Müller cell processes (Fig. 13B) and is likely caused by a horizontal contraction of Müller cell side processes in the inner fibrous part of the OPL (Fig. 8C and D); interconnections between Müller cells in the OPL are already present in the area centralis (Fig. 18B). The thickness of the OPL increases along with the postnatal elongation of the Henle fibers (Hendrickson and Drucker, 1992; Hendrickson et al., 2006a).

Complete displacement of all inner retinal neurons from the human foveola is achieved between 9 and 45 months postnatally (Yuodelis and Hendrickson, 1986; Dubis et al., 2012b). During the following years, the elongation of the Henle fibers and the stretching of the retinal tissue due to the eye growth are associated with a thinning and elongation of the cone receptor segments in the fovea externa (see 4.4.) and a reduction in the thickness of the fovea walls (in particular, of the IPL and INL; postnatal year 13 in Fig. 13B) (Hendrickson, 2005; Lee et al., 2015; Gong et al., 2016). The postnatal changes of the central fovea (up to 16 years of age) also include a thickening of the foveola which results from the thickening of the ONL due to the higher central cone packing (see 4.4.), a decrease of the thickness of the HFL in the foveola, and an increase in the thickness of the HFL in the fovea walls (between 0.3 and 1.5 mm from the foveal center) (Lee et al., 2015). In addition, there is a lifelong slow increase in the area of the foveal avascular zone associated with a decrease in the thickness of the foveal walls (Gong et al., 2016).

The development of the foveal pit requires the absence of retinal blood vessels. A foveal pit does not develop in vascularized retinal areas, including in many human subjects with foveal hypoplasia which lack a foveal avascular zone (Walsh and Goldberg, 2007; Querques et al., 2008). In humans, the depth of the foveal pit and the area of the foveola correlate with the size of the foveal avascular zone (Tick et al., 2011; Dubis et al., 2012a), suggesting that the size of the foveal avascular zone is related to the extent of the centrifugal displacement of the inner retinal layers. Foveal avascularity is likely induced by ganglion and Müller cells in the foveal center that express antiangiogenic molecules like pigment epithelium-derived growth factor and brain natriuretic peptide (Kozulin et al., 2010). Another possible factor which was suggested be involved in inhibiting foveal vascularization is the macular pigment (Gariano, 2010). Macular pigment is already present at fetal week 17 in the area centralis (Gariano, 2010). The size of the foveal avascular zone is correlated with the density of macular pigment (Balaratnasingam et al., 2015); human subjects with albinism or aniridia, which have no foveal avascular zone, also lack macular pigment (Gariano, 2010). Subjects of African descent which have a larger foveal avascular zone than subjects of Caucasian ancestry also have a higher macular pigment density than the latter subjects (Wolf-Schnurrbusch et al., 2007; Wagner-Schuman et al., 2011; Ctori and Huntjens, 2017). However, although lutein has been shown to suppress experimental angiogenesis through antioxidative and antiimmune actions (Chew

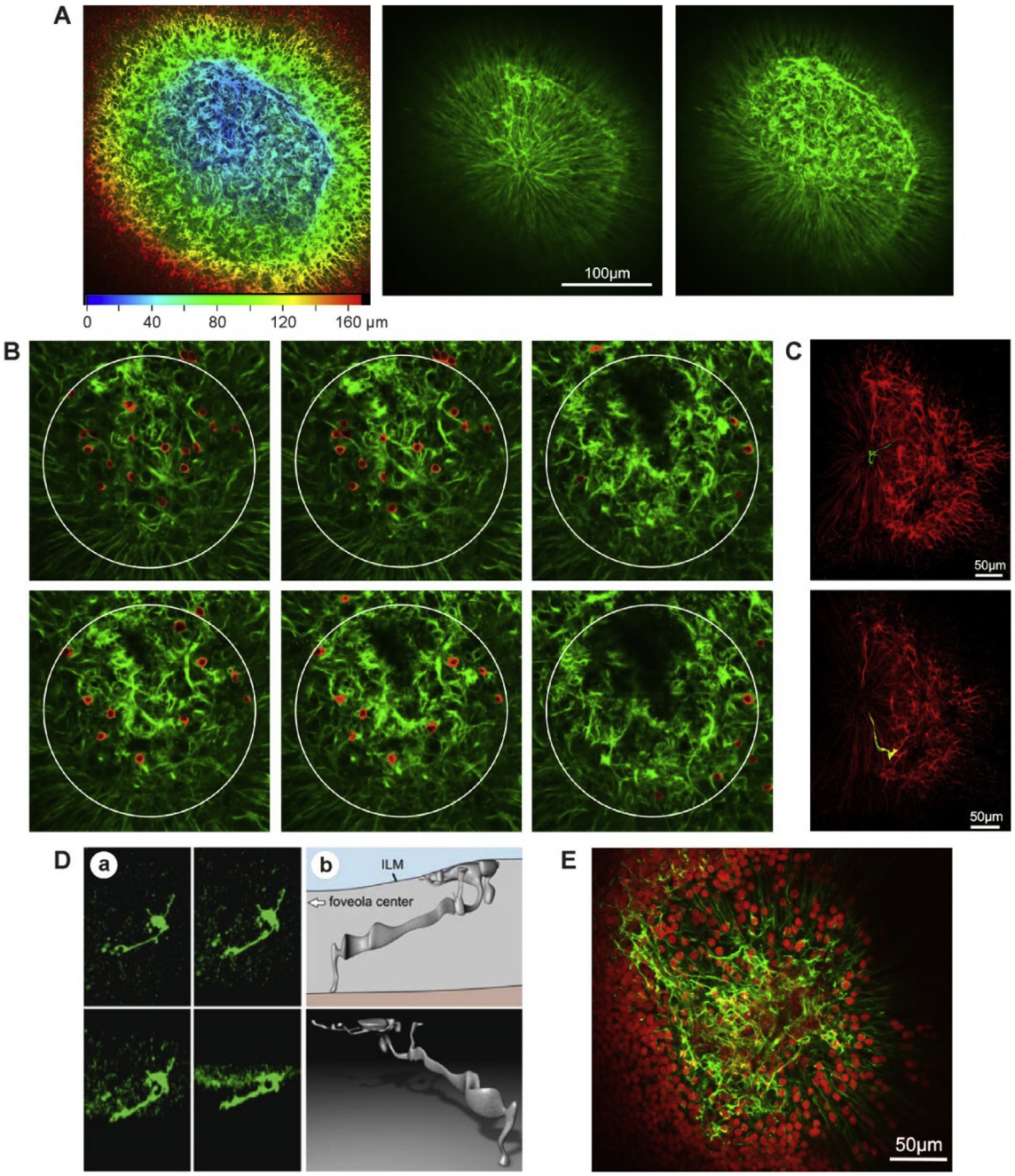

Fig. 14. Müller cells in the foveola of the rhesus macaque (*Macaca mulatta*). **A.** Horizontal sections through the central fovea of one animal. The wholemount was stained with an anti-vimentin antibody (*green*). *Left:* False-color scaling of image records from focus planes displaying the depth of the foveal pit. The foveola has a diameter of about 200 µm. *Middle:* Horizontal section through the foveola at the plane of the stalk of the "Müller cell cone" (the central 50 µm) and the Henle fiber layer in the foveolar periphery. The vimentin-expressing fibers, which are radially arranged in the Henle fiber layer, are outer processes of Müller cells of the foveal walls which surround the axons and somata of the central cone cells. Note that vimentin does not fill the whole Müller cell cytoplasm but the central axes of Müller cell processes. *Right:* Horizontal section at the plane of the inner Müller cell layer of the foveola. Vimentin-negative spherical structures are cell nuclei within the Müller cell somata which are the origin of irregular processes with varying thickness. **B.** Horizontal sections through the foveola of another animal at different focus planes within the inner Müller cell layer. The tissue was immunostained for vimentin (*green*). The somata of Müller cells are marked by *red* color. There are 28 Müller cell somata within the *white circle* of a diameter of 200 µm, indicating a mean Müller cell density of 891 per μm^2. **C.** Horizontal sections through the foveal center of a further animal. The tissue was immunostained for GFAP (*red*). Single Müller cells are marked by *green* (*above*) and *yellow* colors (*below*). The soma of the cell *above* lies near the center of the foveola. The soma of the cell *below* lies in the peripheral foveola; the outer process draws towards the center of the foveola. **D. a.** Confocal images of an 'atypical' Müller cell in the macaque foveola, filled by the fluorescent dye Lucifer Yellow. The images show horizontal (*above*) and vertical (*below*) views of the cell. **b.** 3D-Reconstruction of this foveolar Müller cell. In contrast to Müller cells of the fovea walls, the processes of this cell do not leave the foveola. ILM, inner limiting membrane. **E.** Horizontal sections through the foveal center of a further animal. The wholemount was immunostained with an antibody against GFAP (*green*); cell nuclei are *red*-stained. Note the high level of GFAP immunoreactivity in the foveola. **B** and **D** (courtesy of K. Rillich and J. Grosche) modified after Reichenbach and Bringmann (2010).

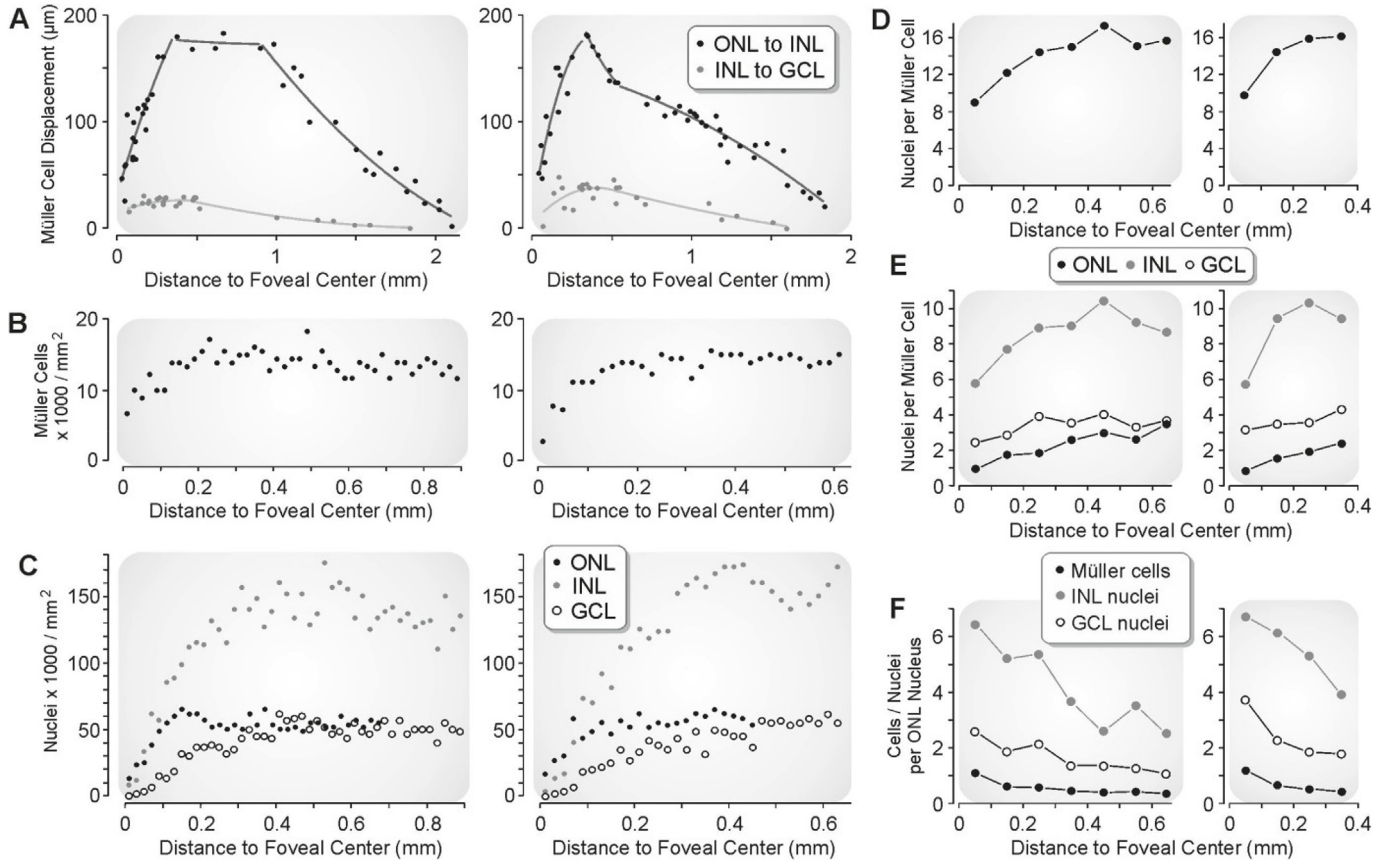

Fig. 15. Cell densities in two opposite directions around the fovea of an adult human donor. Data are not corrected for tissue shrinkage. The ratios between the numbers of cell nuclei and Müller cells were determined with consideration of the displacement of the Müller cell somata from the outer Müller cell processes in the outer nuclear layer (ONL), and were calculated with consideration that the retinal area increases with the distance to the foveal center (the raw data were multiplied by the magnification of the retinal area from the ONL to the inner nuclear layer [INL] and ganglion cell layer [GCL], as described by Schein [1988]). **A.** Centrifugal displacement of foveal Müller cells between the nuclear layers. The distance between the outer Müller cell processes in the ONL and the Müller cell somata in the INL, and the distance between the Müller cell somata in the INL and the inner Müller cell processes in the GCL, are shown in relation to the distance of the outer Müller cell processes to the foveal center. **B.** Density of Müller cells in relation to the distance to the foveal center. Müller cell stem processes were counted in the foveolar ONL and in the inner plexiform layer of the fovea walls, respectively. **C.** Density of cell nuclei in the ONL, INL, and GCL in relation to the distance to the foveal center. **D.** Total numbers of cell nuclei per Müller cell in relation to the distance to the foveal center. **E.** Numbers of GCL, INL, and ONL nuclei per Müller cell in relation to the distance to the foveal center. **F.** Ratios of Müller cells, INL nuclei, and GCL nuclei per ONL nucleus in relation to the distance to the foveal center. For comparison of cell densities in a macaque fovea, please see Fig. 10.

et al., 2003; Izumi-Nagai et al., 2007), an antiangiogenic activity of macular pigment during development has not been shown until today (Gariano, 2010). It has been suggested that ganglion cells are not essential for the development of the foveal avascularity because anencephalic human neonates, which lack ganglion cells in the central retina, may have a foveal avascular zone and a (shallow) foveal pit (Hendrickson et al., 2006b).

It is unclear why the presence of retinal vasculature inhibits the formation of a foveal pit. Springer and Hendrickson (2004a) suggested that the absence of blood vessels makes this region more elastic and malleable than the surrounding vascularized retina (similar as the absence of nerve fibers), and that the intraocular pressure acting on the foveal avascular zone initiates foveal pit formation; thus, the presence of retinal vessels will mechanically inhibit the pit formation. It has been also suggested that the formation of the foveal pit is an adaptation to the lack of intraretinal blood supply in this region which causes metabolic stress of foveal neurons (see below) (Provis, 2001). In macaques and humans, the foveal pit becomes apparent at about 90% of the caecal period that is the stage when in other species prominent waves of spontaneous activity of retinal ganglion cells are evident (Provis et al., 1998). Development of a foveal pit overcomes the metabolic stress by relocation of the neurons closer to the blood supply on the foveal rim (Provis et al., 1998, 2005); there is no need of a neuronal displacement when retinal vessels are present in the foveal center.

Whereas the formation of the foveal pit is only possible in the central avascular zone, it is likely triggered by the formation of the vascular ring around the fovea (Provis et al., 2000). The meeting of the temporal superior and inferior vascular bundles, peripheral to the fovea, coincides in time with the onset of the foveal pit formation (Provis et al., 1998). In the human retina, the vascular plexus which encircles the central avascular zone begins to form around fetal week 25, and the development of the fovel pit begins shortly after fetal week 25 (Provis and Hendrickson, 2008). In the macaque retina, the foveal avascular zone is defined at fetal day 101, and the foveal pit is visible at fetal day 105 (Provis et al., 2000).

The mechanical forces which produce the widening of the foveal pit between fetal week 28 and birth are strongest at the NFL-GCL boundary (Fig. 13A and B and 17D–F). It is unclear, which mechanism causes the centrifugal displacement of the ganglion cells. Tractional forces which mediate this displacement may have various origins: (i) the intraocular pressure acting on the foveal avascular zone (Springer and Hendrickson, 2004a, b, 2005), (ii) the horizontal stretching of the retinal tissue due to the eye growth (Mastronarde et al., 1984; Kelling et al., 1989; Reichenbach and Bringmann, 2010; Kuhrt et al., 2012), and (iii) tractional forces provided by nerve fiber bundles during retinal stretching (Van Essen, 1997). Because the superficial vascular plexus,

which develops at first, lies within the NFL/GCL (Provis et al., 2000; Provis, 2001; Reichenbach and Bringmann, 2016), it is conceivable that the displacement of these layers is also associated with the retinal vascularization.

Retinal vascularization is assumed to involve a developmental hypoxia caused by the neuronal differentiation which is associated with a switch of the neuronal metabolism from a glycolytic to an oxidative metabolism and thus with increasing oxygen demands (Provis, 2001; Reichenbach and Bringmann, 2016). Because ganglion cells differentiate at first (Chievitz, 1888), retinal hypoxia is assumed to be strongest in the central GCL. Hypoxia likely induces the expression of vascular endothelial growth factor (VEGF) in the GCL of the future fovea (Sandercoe et al., 2003) and the secretion of growth factors like platelet-derived growth factor (PDGF) from ganglion cells; these growth factors stimulate the immigration of astrocyte precursor cells that secrete VEGF (Provis, 2001; Reichenbach and Bringmann, 2016). VEGF stimulates retinal vascularization by inducing chemotactic migration of angioblasts. In the developing central retina, astrocytes are present in the NFL and GCL (Provis et al., 2005). The developing superficial retinal vessels are assumed to follow the network of astrocytes in the GCL (however, the distribution of astrocytes in the GCL does not match the pattern of developing vessels [Provis et al., 2000]). During the development of the superficial vascular plexus, astrocytes are in advance of the vascular front by 100–300 μm (Provis et al., 2000; Provis, 2001). Neither vascular endothelial cells nor astrocytes grow into the central avascular zone of the future fovea (Engerman, 1976; Gariano et al., 1994; Provis, 2001; Reichenbach and Bringmann, 2016). It is possible that central Müller cells produce factors like leukemia inhibitory factor which inhibit the migration of astrocytes (Reichenbach and Bringmann, 2016). Alternatively, the absence of vessels from the foveal center might be due to the absence of nerve fiber bundles (which may serve as guiding structures for astrocyte migration) within the region of the future fovea (Provis et al., 1998). (However, in the adult retina, the major vessels, but not the smaller vessels including such which surround the fovea follow the position of nerve fiber bundles [Fig. 4A]).

Nerve fiber bundles in the NFL are associated with elongated bipolar astrocytes, and large stellate astrocytes form a three-dimensional network in the GCL (Fig. 12F and G). The astrocytic processes are connected by adherent and gap junctions (Burns and Tyler, 1990; Holländer et al., 1991; Ramírez et al., 1996). In the developing macaque fovea at postnatal day 1, the transition zone between the central avascular zone and the more peripheral vascularized retina is marked by circularly arranged astrocytes in the GCL which form a ring around the central avascular zone (Provis et al., 2005). Shortly after the vessels reach the foveal rim, astrocytes retreat from the central retina, likely by withdrawing and not by apoptosis (Distler and Kirby, 1996; Distler et al., 2000). In the developing macaque retina, there is a withdrawing of astrocytes from the edge of the foveal pit to the parafovea by about 560 μm between postnatal day 1 and postnatal week 3, while the perifoveal blood vessels are not displaced (Provis et al., 2000). (The foveal avascular zone increases in accordance with the centrifugal displacement of the fovea walls.) Astrocyte withdrawing enlarges the diameter of the astrocyte-free zone from about 340 μm to 1.5 mm (Provis et al., 2000). The mechanism of astrocytic withdrawing is unclear. It is conceivable but remains to be proven that it is mediated by a horizontal contraction of the network of stellate astrocytes in the GCL, and of the bipolar astrocytes in the NFL; the contraction of the astrocytic network may support the centrifugal displacement of ganglion cells (Fig. 18A and B). The contraction of the astrocytic network may also cause the reduction in the thickness of the GCL which is associated with an increase in the spatial density of neuronal somata within the GCL (Fig. 17C and D). The proposed model suggests that the widening of the foveal pit is less dependent on retinal vessels but rather on the withdrawal of astrocytes from the foveal center. The finding that the depth of the foveal pit increases with the gestational age in children after preterm birth between 23 and 27 weeks (Rosén et al., 2015) may suggest that the duration (or strength) of hypoxia determines the expression levels of VEGF and chemotactic growth factors and thus the size of the astrocyte-free area; a smaller astrocyte-free area will result in a smaller avascular area (Fig. 18B). A smaller avascular area will limit the centrifugal displacement of the inner retinal layers because the presence of blood vessels mechanically interfere with their displacement (Yanni et al., 2012). The assumption of the involvement of astrocytes in the widening of the foveal pit may also explain why the pit of the convexiclivate fovea of nonmammalian species with an avascular retina, which lack retinal astrocytes but have nerve fiber bundles at the inner retinal surface, is not widened and does not contain a foveola (Fig. 3A,C).

The radial extension of the Henle fibers in adult primates (Figs. 10C and 15A) reflects the displacement between the inner and outer retina during the foveal development. The centrifugal displacement of the inner retina has a shorter duration than the centripetal displacement of the outer retina (Provis et al., 1998). In humans, the centrifugal displacement of the inner retina starts after fetal week 28 (Fig. 13A), long after beginning of the centripetal displacement of the outer retina (fetal week 8; see 4.4.), and finishes between 9 and 45 months postnatally (Yuodelis and Hendrickson, 1986; Dubis et al., 2012b). By contrast, the centripetal displacement of the outer retina continues for many years after birth (see 4.4.). Therefore, the radial extension of the Henle fibers in adult primates (Figs. 10C and 15A) may reflect a rather short displacement of the inner retina and a wide displacement of the outer retina.

The centrifugal displacement of the Müller cell processes between the INL and GCL found in the fovea of adult primates (Figs. 8A, 10C and 15A) may represent a remnant of the contraction of the astrocytic network in the GCL and NFL during the widening of the foveal pit. The displacement is rather small (< 50 μm) and peaks at around 600 μm in the macaque fovea (Fig. 10C) and at around 300 μm in a human fovea (Fig. 15A). The peak displacement at around 600 μm in the macaque fovea corresponds well with the distance of the developmental astrocyte withdrawing (Provis et al., 2000) and the distance of astrocytes to the foveal center of adult macaques (Fig. 12C,D,E). The data may suggest that in the adult macaque fovea, astrocytes within 600 μm and 1.4 mm from the foveal center (Fig. 10C) are cells which contracted during development (in the adult human fovea, astrocytes between 300 μm and 1.8 mm from the foveal center; Fig. 15A). The lower amplitude and the wider area of the tissue displacement between the INL and GCL in the temporal compared to the nasal macaque fovea (Fig. 10C) may be caused by the higher magnitude of stretching of the temporal retina during the postnatal growth of the eyeball (Mastronarde et al., 1984; Kelling et al., 1989; Reichenbach et al., 1991; Kuhrt et al., 2012). The fact that the displacement of ganglion cell somata from their dendritic tree is only observed within about 1.5 mm from the foveal center (Kirby and Steineke, 1992) seems to be not in agreement with the assumption that the widening of the foveal pit is only mediated by intraocular pessure, retinal stretching, and tension from nerve fiber bundles because these factors affect the whole retinal area.

4.4. Development of the fovea externa

The presence of thin elongated photoreceptors in the central retina of various prosimian primates suggests that the development of a fovea externa precedes the emergence of the fovea interna in phylogeny; the development of the fovea externa also preceeds the development of the fovea interna during ontogeny (Provis et al., 1998). The centripetal displacement of photoreceptors, which produces the high photoreceptor density in the fovea, proceeds during three phases. In the first phase, from fetal week 8–25 (i.e., until the onset of the foveal pit formation) (Fig. 13A), the photoreceptors in the central and peripheral retina are centripetally displaced (Franz, 1913; Provis et al., 2005, Bumsted O'Brien, 2008). The central cone density rises from about

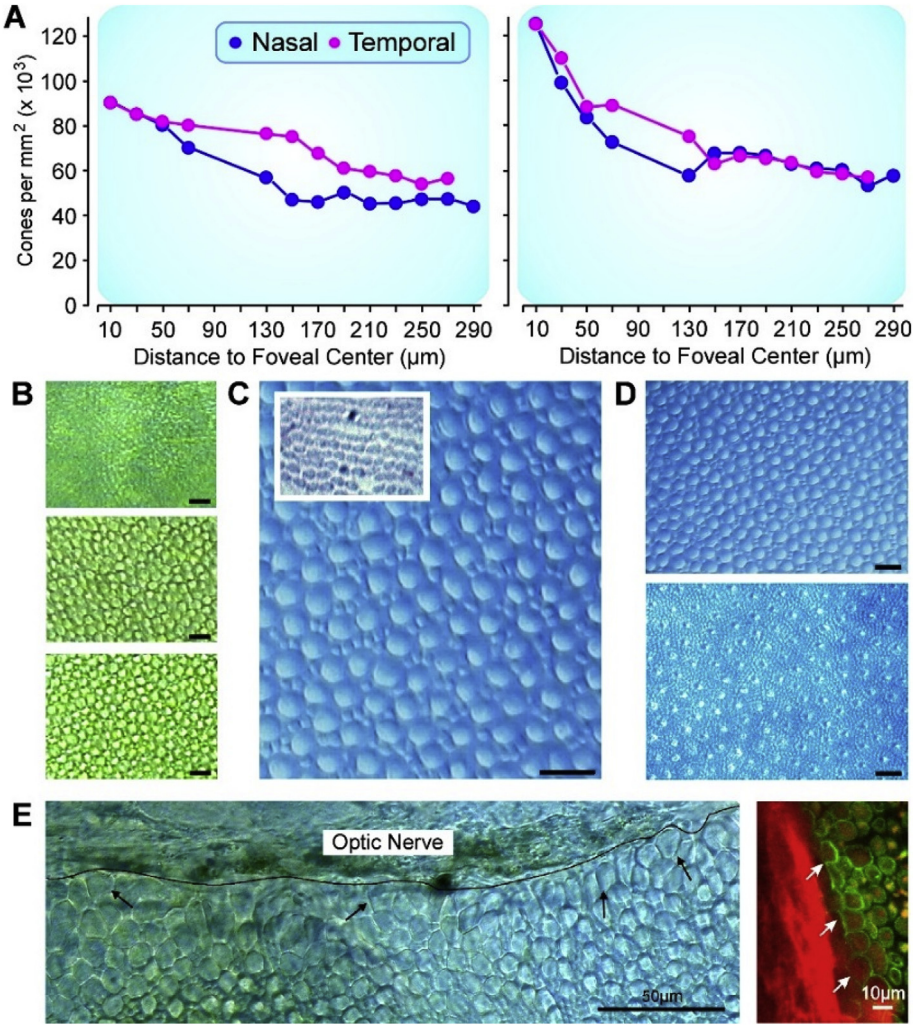

Fig. 16. Cone photoreceptors in the fovea and at the rim of the optic disk in the retina of the rhesus macaque (*Macaca mulatta*). **A.** Cone density along the nasal and temporal hemimeridians as a function of the distance to the foveal center. Cone inner segments were counted in foveal wholemounts of an 18 years-old male (*left*) and a one year-old female macaque (*right*). Data are not corrected for tissue shrinkage but for the increase of the retinal area with the distance to the foveal center. **B.** Horizontal sections through photoreceptor inner segments in a wholemount from the 18 years-old female. The images were obtained from the central foveola (*above*) and from the fovea walls at distances 150 µm (*middle*) and 290 µm (*below*) to the foveal center. Note that the foveal center contains thin cone segments while the fovea walls contain thick cone segments and thin rod segments. **C.** Horizontal sections through photoreceptor inner segments in a wholemount from a male macaque. The image was obtained from a region 800 µm distant to the foveal center. The *inset* shows the cone inner segments in the central foveola at the same magnification. Note the thinness of the cone segments in the foveola compared to that in the parafovea. In the foveola, 267 cone segments were counted within an area of 40 µm^2 (corresponding to about 166,000 segments per mm^2). Note also the distortions of the regular cone mosaic of the foveola at several sites which are likely caused by the presence of single blue cones. **D.** Photoreceptor inner segments in a wholemount from the one year-old female macaque. The images were obtained from a region 800 µm distant to the foveal center (*above*) and from the peripheral retina (*below*). Note the decreased thickness of cone segments and the highly increased number of (thin) rods in the peripheral retina compared to the more central retina. **E.** Horizontal sections through photoreceptor inner segments around the optic nerve head in retinal wholemounts of two animals. The tissue shown in the *right image* was stained with an antibody against GFAP (*red*) and fluorescent peanut agglutinin (*green*) which selectively labels cones (Kawano et al., 1984). The rim of the optic disk is only surrounded by cone photoreceptors (*arrows*). Both (thick) cone segments and (thin) rod segments are located at distances greater than 25 µm. The cone segments at the rim of the optic disk are irregularly formed and thicker than the more distant cone segments. Bars in **B–D**, 10 µm.

14,000 per mm^2 at fetal week 13 (the time period of cone cell differentiation) to about 22,500 per mm^2 at fetal week 14, about 31,500 per mm^2 at fetal weeks 16–17, and about 36,000 per mm^2 at fetal week 25 (Diaz-Araya and Provis, 1992; Provis et al., 1985b, 1998). In the fetal area centralis, the large, cuboidal cone cell somata are arranged in a monolayer (Figs. 13A and 17A,B) (Bach and Seefelder, 1914). In the second phase, ranging from the formation of the foveal pit after fetal week 25 to birth, the photoreceptors in the peripheral retina and at the foveal rim, but not in the foveal center, are centripetally displaced (Fig. 13A) (Bach and Seefelder, 1914). In this phase, the immature cone cells in the foveal center are short and thick (as in the early area centralis; Fig. 13C) and barely functional (Abramov et al., 1982; Yuodelis and Hendrickson, 1986), while the cones near the foveal edge and in the peripheral retina begin to mature and become thinner (Fig. 13A) (Franz, 1913). There is a delay in the packing of central photoreceptors between fetal week 25 and birth (Provis et al., 2005, 2013; Bumsted O'Brien, 2008). In the third phase, during the postnatal development, the central and peripheral photoreceptors are displaced towards the center of the foveola (Fig. 13A) (Bach and Seefelder, 1914). The postnatal displacement of central photoreceptors results in an at least 4-fold increase in foveolar cone density (Fig. 13C) and is associated with a 4-fold reduction in the areas of the rod-free zone and the foveolar cone mosaic (Hendrickson and Kupfer, 1976; Yuodelis and Hendrickson, 1986; Diaz-Araya and Provis, 1992; Provis and Hendrickson, 2008; Springer et al., 2011). The postnatal displacement of the central photoreceptors proceeds faster than the displacement during the formation of the area centralis, and produces a higher photoreceptor density than in more peripheral areas (Provis et al., 2005; Bumsted O'Brien, 2008). In humans, the peak cone density is about 36,000 per mm^2 at birth, reaches the lower range of adult levels (98,000–324,000 per mm^2; Curcio et al., 1990) between 4 and 6 years, and continues to increase more slowly at least until the mid teenage years (Hendrickson and Yuodelis, 1984; Yuodelis and Hendrickson, 1986). While the visual capacity of newborn humans is mainly based on extrafoveal vision (Abramov et al., 1982), the rapid postnatal central cone packing contributes to the dramatic improvement of the visual acuity during the first few postnatal months (Dobson and Teller, 1978). A similar triphasic pattern of photoreceptor packing was described for marmosets and macaques (Hendrickson et al., 2006a, 2009; Springer et al., 2011). In all phases, peripheral rods and cones are displaced towards the foveal center (Diaz-Araya and Provis, 1992; Hendrickson and Provis, 2006). In humans between the fetal week 17 and postnatal week 6, even the photoreceptors near the optic disk are displaced towards the foveal center, suggesting that a very large retinal area is involved in photoreceptor redistribution (Hendrickson and Provis, 2006). The density of rods at a distance of 2 mm from the human foveal center increases from about 20 per mm^2 at fetal week 15 (when rods are inserted into the ONL) to about 600 per mm^2 at fetal week 24, and further to about

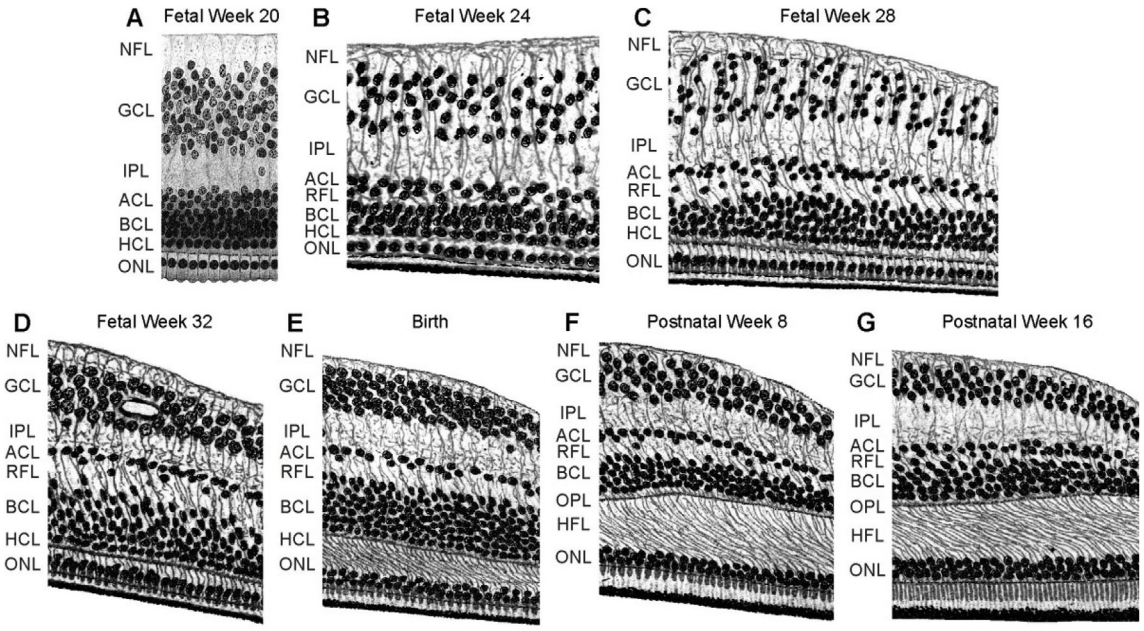

Fig. 17. Transitory radial fiber layer (RFL) during the development of the human fovea. **A.** Section through the retinal center at an early stage of the development of the area centralis (fetal week 20). Note the absence of a specialized RFL between the amacrine (ACL) and bipolar cell layers (BCL). **B.** Section through the retinal tissue at the edge of the area centralis (fetal week 24). Note the oblique arrangement of thick Müller cell processes in the RFL. In more vitreal layers (the inner plexiform [IPL], ganglion cell [GCL], and nerve fiber layers [NFL]), the Müller cell processes draw rather straight through the tissue. In the IPL, horizontal side processes of Müller cells are established. **C.** Section through the fovea wall during the formation of the foveal pit (fetal week 28). Note the oblique arrangement of Müller cell processes in the RFL and BCL, and of the bipolar cell nuclei rows in the BCL. **D.** Section through the fovea wall during the widening of the foveal pit (fetal week 32). Note the oblique arrangement of the nuclei rows in the GCL and the centripetally bended Müller cell processes and bipolar cell nuclei rows in the RFL and BCL. Note also the spindle-shaped nuclei of many bipolar cells and the increased density of neuronal somata in the GCL. **E.** Section through the fovea wall at birth. **F.** Section through the fovea wall during the formation of the foveola (postnatal week 8). The Müller cell processes in the IPL, GCL, and NFL are centrifugally bended, nearly parallel to the Müller cell fibers in the RFL and BCL. **G.** Section through the fovea wall during the formation of the fovea externa (postnatal week 16). The inner Müller cell processes begin to erect due to a centrifugal displacement of the tissue within the outer plexiform layer (OPL). This displacement contributes to the elongation of the Henle fibers in the Henle fiber layer (HFL) and is associated with a decrease in the thickness of the RFL. HCL, horizontal cell layer. Images are modified from Bach and Seefelder (1914).

140,000 per mm^2 in adults (Diaz-Araya and Provis, 1992; Curcio et al., 1990).

The high photoreceptor packing in the foveal center proceeds relatively late, after birth (Fig. 13C), because it (partly) depends on light stimulation and central information processing. The binocular vision starts to develop 6 weeks after birth, and the differentiation of binocular cells in the visual cortex peaks around the 3rd postnatal month. The visual acuity is low at birth. When the formation of foveal images at or shortly after birth is hindered (e.g., by cataract or corneal scarring), a high visual acuity may not develop, even though the opacity is removed later (Hendrickson and Provis, 2006). In marmosets which undergone experimental myopia shortly after birth, the central photoreceptor density is increased (Troilo, 1998).

The fovea externa represents the pyramid-like arrangement of the elongated cone segments in the center of the foveola; the tip of the fovea externa is located in the foveolar center (the site of the smallest thickness of the foveola) (Figs. 11B and 13C). It may be conceivable that the formation of the fovea externa is supported by a vertical contraction of (the outer processes of) Müller cells in the "Müller cell cone" (Figs. 11D and 18A,B). Because there is no correlation between the centrifugal shift of inner retinal layers and the length of central cone segments in humans (Tick et al., 2011), the vertical contraction of foveolar Müller cells may proceed relatively independent on the formation of the foveola. However, because the mean peak photoreceptor density is lower in albinotic human subjects with foveal hypoplasia compared to control subjects (Springer, 2014), and because prematurely born children with foveal hypoplasia have discrete deviations in the OLM contour of the fovea externa (Rosén et al., 2015), the formation of the fovea externa seems to be at least in part dependent on the development of the foveola. Possibly, the centrifugal pulling of Henle fibers contributes to the formation of the fovea externa (Fig. 11D) (Rosén et al., 2015); this pulling is less when the displacement of the inner retina is incomplete as in foveal hypoplasia.

The inner segments of foveal cones first appear between fetal weeks 20 and 26 (Yuodelis and Hendrickson, 1986; Provis et al., 1998). Thereafter, the inner segments elongate and become thinner; at fetal weeks 24–26, they are 6 µm in diameter and 9 µm in length (Yuodelis and Hendrickson, 1986). The outer segments of foveal cones are not present until fetal week 36, i.e., shortly before birth (Yamada and Ishikawa, 1965; Yuodelis and Hendrickson, 1986). The elongation of the central cone segments proceeds from birth until 17–25 years postnatally (Fig. 13C) (Yuodelis and Hendrickson, 1986; Vajzovic et al., 2012; Lee et al., 2015). Around postnatal month 45, the inner segments reach their adult length (30–35 µm), while the outer segments have reached only half of the adult length (Yuodelis and Hendrickson, 1986). The elongation of the central cones is associated with a thinning of the receptor segments, an increase of the receptor density (Fig. 13C), and a thickening of the central ONL that also proceeds up to 17–25 years postnatally (Lee et al., 2015). In humans, the diameter of foveal cones decreases from 7.5 to 2 µm during 45 months of postnatal development (Yuodelis and Hendrickson, 1986). The increasing receptor density contributes to the improvement of visual function until 21 years of age (Wang et al., 2009).

The postnatal thickening of the central ONL results from the increased stacking of cone cell somata (Fig. 13A,C). The thinning (to about 2 µm; Fig. 7G) and close spacing of the foveal cone inner segments enforces a stacking of the cone cell somata because their diameter is larger (about 5 µm) (Borwein et al., 1980; Ahnelt et al., 2004).

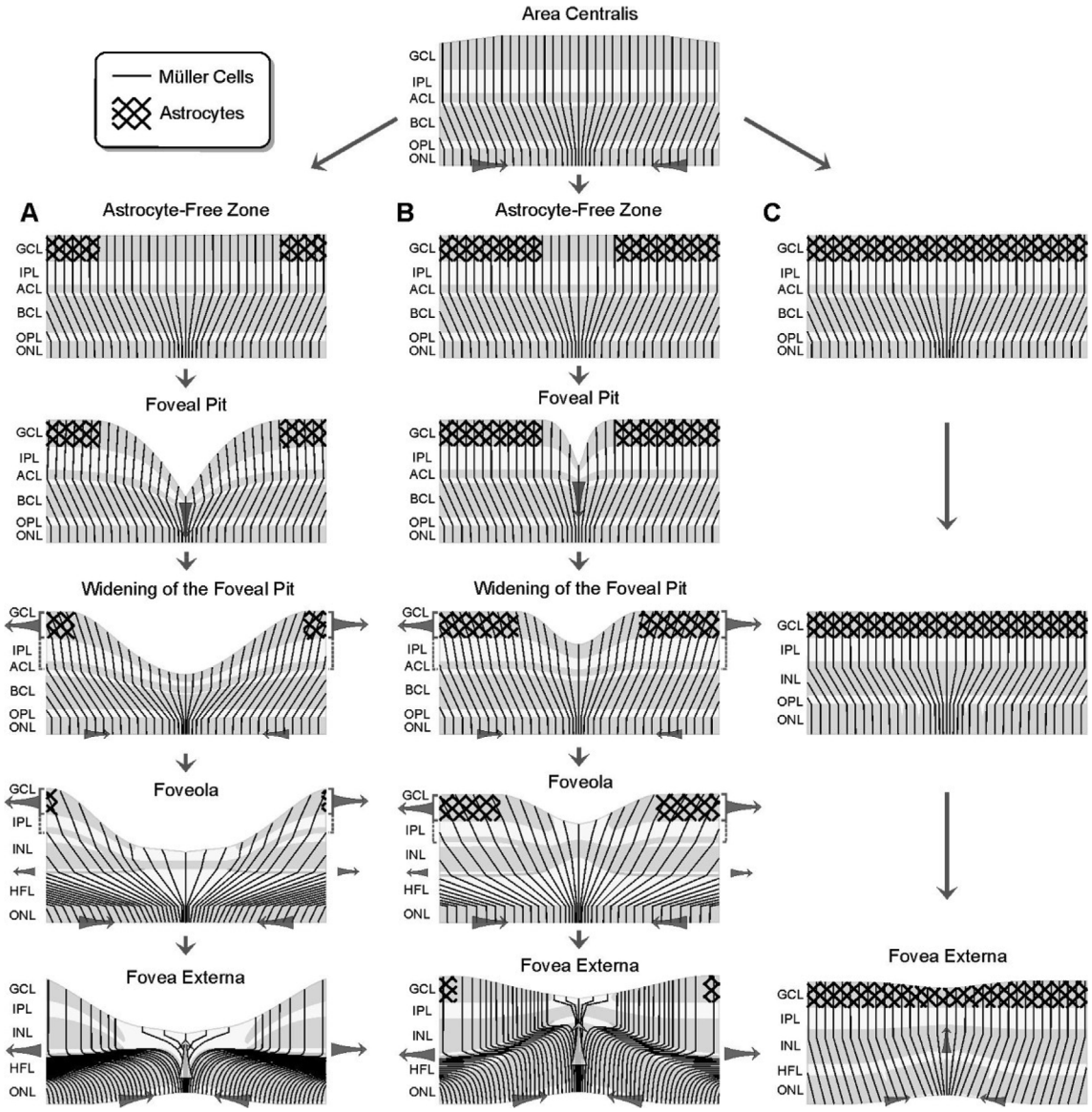

(caption on next page)

Fig. 18. Proposed model of the foveal development. In the area centralis, the photoreceptors are centripetally displaced; this results in a spatial shift between the inner and outer retina. This shift is compensated by the oblique arrangement of Müller and bipolar cell processes in the bipolar cell layer (BCL) and the transitory radial fiber layer (formed between the amacrine cell layer [ACL] and BCL). After formation of the astrocyte-free zone, a foveal pit is produced by a vertical contraction of the centralmost Müller cells. The foveal pit is widened by the centrifugal displacement of ganglion cells in the ganglion cell layer (GCL) which results in a tilting of the whole inner retinal tissue. Thereafter, the foveola is formed by an erection of the inner retinal tissue in the fovea walls; the erection likely results from a horizontal contraction of Müller cell side processes in the OPL. This contraction also contributes to the elongation of the Henle fibers in the Henle fiber layer (HFL). A horizontal contraction of Müller cell structures at the outer limiting membrane and a vertical contraction of central Müller cells in the foveola may contribute to the formation of the fovea externa. The foveal morphology varies with the size of the astrocyte-free zone. When the size of the astrocyte-free zone is large, a deep pit is formed (**A**). When the size of the astrocyte-free zone is small, a shallow pit is formed (**B**). When the astrocyte-free zone is very small or absent, no pit or a very shallow pit is formed, as observed in many cases of foveal hypoplasia (**C**). In cases of foveal hypoplasia, a fovea externa may be formed to a certain degree (**C**). INL, inner nuclear layer; IPL, inner plexiform layer; ONL, outer nuclear layer; OPL, outer plexiform layer.

During the first phase of photoreceptor packing, the somata rows in the ONL are vertically stacked, while during the second phase of central photoreceptor redistribution (along with the formation of the HFL), the somata in the inner part of the ONL are obliquely stacked (Figs. 11B and 13A,C). Foveal development may also involve a widening of the central ONL (see 2.2.). There is an inverse relation between the thickness of the central ONL and the magnitude of the centrifugal displacement of the inner retinal layers (Tick et al., 2011). In individuals with a small and thick foveola, the central ONL is thick, while in individuals with a large and thin foveola, the central ONL is thin and widened (Fig. 13D) (Tick et al., 2011). It is likely that the widening of the central ONL and the oblique stacking of cone cell somata are supported by centrifugal mechanical forces provided by the Müller cells of the fovea walls on the Henle fibers (Fig. 11D).

The developmental relocation of photoreceptors proceeds independently from the redistribution of RPE cells (Robinson and Hendrickson, 1995). At midgestation, one foveal RPE cell covers 5 cones (Krebs and Krebs, 1989; Robinson and Hendrickson, 1995). After birth, the number of cones per RPE cell changes rapidly; in the adult fovea, one foveal RPE cell covers 22–35 cones (Krebs and Krebs, 1989; Gao and Hollyfield, 1992; Robinson and Hendrickson, 1995). It has been suggested that the centripetal relocation of the (peri-) foveal photoreceptors is mediated by a radial contraction of the receptor segments (Packer et al., 1990; Provis et al., 2013). When the inner segments contract to become more slender and elongated, they move more closely together because they are bound to each other and to the outer Müller cell processes by adherent and tight junctions. This process will also drag the perifoveal photoreceptors and outer Müller cell processes towards the foveal center. The increase of the photoreceptor density may be mediated by contact signaling between cones, by the absence of signals derived from rods, and/or by FGF receptor signaling in photoreceptors (Cornish et al., 2004, 2005; Provis et al., 2013). Because the photoreceptors and their accompanying Müller cells are tightly glued together by heterotypic junctions composed of adherent junctions, tight junctions, and desmosomes (Omri et al., 2010), which form small bulbs at the OLM (Hendrickson et al., 2012), it is likely that the centripetal displacement of photoreceptors is supported by a horizontal contraction of Müller cell structures at the OLM (Fig. 18A and B). In addition, there are tight-like junctions between Müller cells and photoreceptor cell somata in the ONL (Omri et al., 2010). At the OLM, Müller cells contain contractile rings of filamentous actin that surround the photoreceptors; these actin rings are associated with the junctions between Müller and photoreceptor cells and form a structural meshwork in which photoreceptors are embedded (Del Priore et al., 1987). The cytoplasmic plaques of the junctions between Müller and photoreceptors contain actin, myosin, α-actinin, and vinculin (Drenckhahn and Wagner, 1985; Williams et al., 1990). It has been shown that stretching of the retinal tissue (as occurring during eye growth, for example) induces an expression of FGF2 in Müller cells (Lindqvist et al., 2010). Müller cell-derived FGF2 may be involved in inducing the elongation of the photoreceptor cell axons (Cornish et al., 2004, 2005; Provis et al., 2013).

4.5. Variations in foveal development

The foveal morphology in the normal human population shows substantial variations, e.g., in respect to the size of the foveola and of the foveal avascular zone, the depth of the foveal pit, the steepness and asymmetry of the fovea walls, and the magnitude of the centrifugal displacement of inner retinal layers (Fig. 13D) (Tick et al., 2011; Dubis et al., 2012a; Wilk et al., 2017). Generally, a lower depth of the foveal pit is associated with a lower magnitude of the centrifugal displacement of inner retinal layers resulting in smaller areas of the foveola and of the avascular zone, increased thickness of the foveola, and a decreased steepness of the foveal slope (Fig. 13D). A similar morphological variability can be observed in other primate species (Fig. 5A).

The morphological variability of the fovea mainly results from variations in the foveal development (Provis et al., 1998, 2013). The morphological variability of the fovea is strongly related to the size of the avascular zone (Provis et al., 1998, 2013). The foveal avascular zone in humans may have diameters between 200 μm and 1 mm (Adler, 1929; Dubis et al., 2012a). A wide and deep foveal pit (Fig. 13D) is typically seen in individuals of African descent (Wagner-Schuman et al., 2011); these subjects have foveal avascular zones with diameters between 0.8 and 1 mm. Subjects of Caucasian ancestry have a shallower foveal pit that is associated with smaller areas of the avascular zone and foveola (Fig. 13D) (Wagner-Schuman et al., 2011). The thickness of the foveola varies substantially as a function of the shape of the foveal pit (Fig. 13D) (Tick et al., 2011). In one study, the mean thickness of the foveola was 227 μm in preterm children and 90 μm in full-term children (Yanni et al., 2012). Because the largest distance over which oxygen can diffuse from the choriocapillaris is about 140 μm in the human retina (Dollery et al., 1969), there is little need for an internal retinal blood supply in thin foveolas of subjects with large avascular zones. In order to avoid metabolic stress, thicker foveolas need smaller foveal avascular zones. It may be conceivable that the Müller cell expression levels of molecules which inhibit the migration of astrocytes determine the size of the foveal astrocyte-free zone and thus the size of the avascular area. A large astrocyte-free zone results in a wide displacement of the inner retinal layers and thus the formation of a deep pit and a large-diameter foveola (Fig. 18A). A small astrocyte-free zone results in a small displacement of the inner retinal layers; therefore, remnants of inner retinal layers may persist in the foveal center, and the pit is shallow (Figs. 13D and 18B). Because the formation of the fovea externa is relatively independent from the development of the foveal pit, a regular fovea externa with elongated cone receptor segments is formed in both cases (Figs. 13D and 18A,B), resulting in normal visual acuities.

4.6. Improper foveal development

Foveal hypoplasia results from an arrest at different stages of foveal development (McAllister et al., 2010). Various different mutations and developmental conditions may lead to foveal malformation or hypoplasia. Foveal hypoplasia was associated with albinism, microcornea, familial and presenile cataracts, retinopathy of prematurity, and PAX6 mutations (Curran and Robb, 1976; Oliver et al., 1987; McGuire et al., 2003; Baker and Tasman, 2010). The morphology of the foveal pit and

the photoreceptor density in the foveal center vary greatly among albinotic subjects (Wilk et al., 2014). In the mean, the peak photoreceptor density is lower in human subjects with albinism compared to control subjects (Springer, 2014). The central retina of human albinos lacks a rod-free zone, cones are large, loosely packed and immature in shape, and the foveal pit is poorly formed or absent (Fulton et al., 1978; Mietz et al., 1992). In subjects with albinism, the length of the photoreceptor outer segments is the strongest predictor of the visual acuity (Mohammad et al., 2011). The varying photoreceptor densities in the foveal center of albinotic individuals could be partially explained with the different mechanisms of photoreceptor redistribution. The initial photoreceptor packing in the primate fovea is caused by the horizontal displacement at the OLM; this increases the foveal cone density but does not result in an elongation of the central photoreceptor segments. The postnatal cone packing may be supported by the vertical contraction of foveolar Müller cells (Figs. 11D and 18) which causes elongation of the foveolar photoreceptors that is associated with a further thinning of the photoreceptors and a further increase in the receptor density. Depending on the stage at which the foveal development is arrested, the fovea of albinotic subjects can lack or contain a fovea externa (Fig. 18C) that is associated with varying visual acuities.

When molecules, which inhibit the migration of astrocytes, are not expressed or at a very low level, a foveal astrocyte-free and avascular zone is not formed. The presence of astrocytes in the foveal center prevents the formation of a foveal pit (Fig. 18C), as observed in many cases of foveal hypoplasia. However, there are numerous other factors which may be dysregulated during development and thus may cause an arrest in foveal development with abnormal persistance of certain signs of early retinal structural organization. It has been shown, for example, that human subjects with foveal hypoplasia which lack a foveal avascular zone and a foveal pit may have a central bouquet of cones and a GCL dome (Querques et al., 2008); this suggests that, in this case, a nearly normal development of the fovea externa is associated with an arrest of the inner foveal development at the stage of the area centralis. The fact that albinotic subjects also lack a foveal rod-free zone (Usher, 1920; Mietz et al., 1992) suggests that the foveal development may be dysregulated at very early stages, e.g., by dysregulation of the expression or function of PAX6 which is involved in the specification of the foveal location, or by dysregulation of L-DOPA production which normally inhibits the proliferation of late progenitor cells (Ilia and Jeffery, 2000) that produce rods (Reichenbach, 1993; Reichenbach and Robinson, 1995).

5. Concluding remarks

The primate fovea is a retinal specialization for high-resolution color vision. The centrifugal displacement of the inner retinal layers away from the path of the incoming light and the absence of blood vessels may improve the quality of the visual image receipt by the highly packed cone photoreceptors in the foveola. There is increasing knowledge regarding the important roles of Müller cells and astrocytes in the foveal development and function, and the pathogenic role of Müller cell dysfunction in the development of age-related macular disorders. However, there are many questions related to the morphology, function, and development of the primate fovea. These questions involve, for example, the precise ratios between and spatial arrangements of different cell types in the central fovea, the (biomechanical and molecular) mechanisms of (improper) foveal development, the mechanical properties of the central fovea which have importance for the understanding of the pathogenesis of macular holes and the effects of ILM peeling, and the distinctive metabolic features of the fovea centralis, including its high susceptibility to age-related degeneration. It should be kept in mind that the structural and functional properties of the fovea described in this review alter in degenerative macular diseases and after foveal injury. The functional properties and the neuronal network of the retina also alter after vision-restoring therapies, e.g., after transfection of channelrhodopsins in animal models of photoreceptor degeneration (Bi et al., 2006; Thyagarajan et al., 2010). OCT, in combination with adaptive optics and other techniques such as two-photon microscopy which allows high-resolution imaging of the retina in the living eye close to the resolution of microscopy on histological preparations, may provide novel insights into the (patho-) mechanisms of foveal functioning and dysfunctioning which may also have importance for the understanding of macular alterations after implantation of electronic retina chips, for example.

Acknowledgements

The authors wish to thank Jens Grosche, Leipzig (effigos.com/de), for excellent graphics and the contributions to some data. Some of the work presented in this review was conducted with grants from the Deutsche Forschungsgemeinschaft (RE 948/17, RE 849/10, 11, 15, GRK 1097, to A.R.).

References

Abramov, I., Gordon, J., Hendrickson, A., Hainline, L., Dobson, V., LaBossiere, E., 1982. The retina of the newborn human infant. Science 217, 265–267.
Adler, F.H., 1929. The entoptic visibility of the capillary circulation in the retina. JAMA Ophthalmol 1, 91–98.
Agte, S., Junek, S., Matthias, S., Ulbricht, E., Erdmann, I., Wurm, A., Schild, D., Käs, J.A., Reichenbach, A., 2011. Müller glial cell-provided cellular light guidance through the vital Guinea-pig retina. Biophys. J. 101, 2611–2619.
Ahmad, K.M., Klug, K., Herr, S., Sterling, P., Schein, S., 2003. Cell density ratios in a foveal patch in macaque retina. Vis. Neurosci. 20, 189–209.
Ahnelt, P.K., 1998. The photoreceptor mosaic. Eye 12, 531–540.
Ahnelt, P.K., Pflug, R., 1986. Telodendrial contacts between foveolar cone pedicles in the human retina. Experientia 42, 298–300.
Ahnelt, P.K., Kolb, H., 1994. Horizontal cells and cone photoreceptors in human retina: a Golgi-electron microscopic study of spectral connectivity. J. Comp. Neurol. 343, 406–427.
Ahnelt, P.K., Kolb, H., 2000. The mammalian photoreceptor mosaic-adaptive design. Prog. Retin. Eye Res. 19, 711–777.
Ahnelt, P.K., Kolb, H., Pflug, R., 1987. Identification of a subtype of cone photoreceptor, likely to be blue sensitive, in the human retina. J. Comp. Neurol. 255, 18–34.
Ahnelt, P., Schubert, C., Anger, E., 2004. Macular photoreceptor organization. Modular substructuring – a consistent feature along all foveal cone elements. In: Binder, S. (Ed.), The Macula. Diagnosis, Treatment and Future Trends. Springer, Wien, pp. 1–5.
Almeida, D.R., Chin, E.K., Tarantola, R.M., Folk, J.C., Boldt, H.C., Skeie, J.M., Mullins, R.F., Russell, S.R., Mahajan, V.B., 2015. Effect of internal limiting membrane abrasion on retinal tissues in macular holes. Invest. Ophthalmol. Vis. Sci. 56, 2783–2789.
Azuma, N., Tadokoro, K., Asaka, A., Yamada, M., Yamaguchi, Y., Handa, H., Matsushima, S., Watanabe, T., Kohsaka, S., Kida, Y., Shiraishi, T., Ogura, T., Shimamura, K., Nakafuku, M., 2005. The Pax6 isoform bearing an alternative spliced exon promotes the development of the neural retinal structure. Hum. Mol. Genet. 14, 735–745.
Babbitt, E.D., 1878. The Principles of Light and Color. Babbitt & Co., New York.
Bach, L., Seefelder, R., 1914. Atlas zur Entwicklungsgeschichte des menschlichen Auges. Engelmann, Leipzig, Germany.
Baker, P.S., Tasman, W., 2010. Optical coherence tomography imaging of the fovea in retinopathy of prematurity. Ophthalmic Surg. Lasers Imaging 41, 201–206.
Balaratnasingam, C., Chae, B., Remmer, M.H., Gomez, E., Suzuki, M., Engelbert, M., Spaide, R.F., 2015. The spatial profile of macular pigments is related to the topological characteristics of the foveal avascular zone. Invest. Ophthalmol. Vis. Sci. 56, 7859–7865.
Balazs, E.A., 1984. Functional anatomy of the vitreous. In: Duane, T.D., Jaeger, E.A. (Eds.), Biomedical Foundations of Ophthalmology. JB Lippincott, Philadelphia, PA.
Barishak, Y., 1992. Embryology of the Eye and its Adnexae. Karger, New York.
Belloni, L., 1983. Der Beitrag von Francesco Buzzi zur Entdeckung der "Macula lutea" und der "Fovea centralis" des menschlichen auges. Gesnerus 40, 23–30.
Beltran, W.A., Cideciyan, A.V., Guziewicz, K.E., Iwabe, S., Swider, M., Scott, E.M., Savina, S.V., Ruthel, G., Stefano, F., Zhang, L., Zorger, R., Sumaroka, A., Jacobson, S.G., Aguirre, G.D., 2014. Canine retina has a primate fovea-like bouquet of cone photoreceptors which is affected by inherited macular degenerations. PLoS One 9 e90390.
Bi, A., Cui, J., Ma, Y.P., Olshevskaya, E., Pu, M., Dizhoor, A.M., Pah, Z.H., 2006. Ectopic expression of a microbial-type rhodopsin restores visual responses in mice with photoreceptor degeneration. Neuron 50, 23–33.
Bonds, A.B., MacLeod, D.I.A., 1978. A displaced Stiles-Crawford effect associated with an eccentric pupil. Invest. Ophthalmol. Vis. Sci. 17, 754–761.
Borwein, B., Borwein, D., Medeiros, J., McGowan, J.W., 1980. The ultrastructure of monkey foveal photoreceptors, with special reference to the structure, shape, size, and spacing of the foveal cones. Am. J. Anat. 159, 125–146.
Boycott, B.B., Dowling, J.E., 1969. Organization of the primate retina: light microscopy. Philos. Trans. Royal Soc. Lond. B 255, 109–184.
Boycott, B.B., Wässle, H., 1991. Morphological classification of bipolar cells of the primate retina. Eur. J. Neurosci. 3, 1069–1088.
Breckler, J., Au, K., Cheng, J., Hasson, T., Burnside, B., 2000. Novel myosin VI isoform is

abundantly expressed in retina. Exp. Eye Res. 70, 121–134.
Bringmann, A., Reichenbach, A., Wiedemann, P., 2004. Pathomechanisms of cystoid macular edema. Ophthalmic Res. 36, 241–249.
Bringmann, A., Pannicke, T., Grosche, J., Francke, M., Wiedemann, P., Skatchkov, S.N., Osborne, N.N., Reichenbach, A., 2006. Müller cells in the healthy and diseased retina. Prog. Retin. Eye Res. 25, 397–424.
Bringmann, A., Iandiev, I., Pannicke, T., Wurm, A., Hollborn, M., Wiedemann, P., Osborne, N.N., Reichenbach, A., 2009. Cellular signaling and factors involved in Müller cell gliosis: neuroprotective and detrimental effects. Prog. Retin. Eye Res. 28, 423–451.
Bringmann, A., Grosche, A., Pannicke, T., Reichenbach, A., 2013. GABA and glutamate uptake and metabolism in retinal glial (Müller) cells. Front. Endocrinol. (Lausanne) 4, 48.
Bumsted, K., Hendrickson, A., 1999. Distribution and development of short-wavelength cones differ between *Macaca* monkey and human fovea. J. Comp. Neurol. 403, 502–516.
Bumsted O'Brien, K.M., 2008. Development of the foveal specialization. In: Tombran-Tink, J., Barnstable, C.J. (Eds.), Visual Transduction and Non-visual Light Perception. Humana Press, Totowa, NJ, pp. 17–34.
Bumsted O'Brien, K.M., Cheng, H., Jiang, Y., Schulte, D., Swaroop, A., Hendrickson, A.E., 2004. Expression of photoreceptor-specific nuclear receptor NR2E3 in rod photoreceptors of fetal human retina. Invest. Ophthalmol. Vis. Sci. 45, 2807–2812.
Burns, M.S., Tyler, N.K., 1990. Interglial cell gap junctions increase in urethane-induced photoreceptor degeneration in rats. Invest. Ophthalmol. Vis. Sci. 31, 1690–1701.
Burris, C.J., Klug, K., Ngo, I.T., Sterling, P., Schein, S., 2002. How Müller glial cells in macaque fovea coat and isolate the synaptic terminals of cone photoreceptors. J. Comp. Neurol. 453, 100–111.
Buzzi, F., 1782. Nuove sperienze fatte sull'occhio umano. Opuscoli Scelti Sulle Scienze e Sulle Arti 5, 87–95.
Buzzi, F., 1795. Lettera del dott. Paolo Antonio Venini al sig. dott. A.C. medico in Milano. Nuovo giornale della píù recente letteratura medico-chírurgica d'Europa 9, 370–376.
Byon, I.S., Kwon, H.J., Park, G.H., Park, S.W., Lee, J.E., 2014. Macular hole formation in rhegmatogenous retinal detachment after scleral buckling. Korean J. Ophthalmol. Times 28, 364–372.
Campbell, F.W., Gubisch, R.W., 1966. Optical quality of the human eye. J. Physiol 186, 558–578.
Chew, B.P., Brown, C.M., Park, J.S., Mixter, P.F., 2003. Dietary lutein inhibits mouse mammary tumor growth by regulating angiogenesis and apoptosis. Anticancer Res. 23, 3333–3339.
Chievitz, J.H., 1887. Die Area und Fovea centralis retinae beim menschlichen Foetus. Int. Monatsschrift f. Anat. U. Physiol 4, 201.
Chievitz, J.H., 1888. Entwickelung der Fovea centralis retinae. Anat. Anzeiger 3, 579–583.
Chun, M.H., Grünert, U., Martin, P.R., Wässle, H., 1996. The synaptic complex of cones in the fovea and in the periphery of the macaque monkey retina. Vision Res. 36, 3383–3395.
Chung, H., Byeon, S.H., 2017. New insights into the pathoanatomy of macular holes based on features of optical coherence tomography. Surv. Ophthalmol. 62, 506–521.
Conradi, N., Sjöstrand, J., 1993. A morphometric and stereologic analysis of ganglion cells of the central human retina. Graefes Arch. Clin. Exp. Ophthalmol. Times 231, 169–174.
Cornish, E.E., Natoli, R.C., Hendrickson, A., Provis, J.M., 2004. Differential distribution of fibroblast growth factor receptors (FGFRs) on foveal cones: FGFR-4 is an early marker of cone photoreceptors. Mol. Vis. 10, 1–14.
Cornish, E.E., Madigan, M.C., Natoli, R., Hales, A., Hendrickson, A.E., Provis, J.M., 2005. Gradients of cone differentiation and FGF expression during development of the foveal depression in macaque retina. Vis. Neurosci. 22, 447–459.
Ctori, I., Huntjens, B., 2017. The association between foveal morphology and macular pigment spatial distribution: an ethnicity study. PLoS One 12 e0169520.
Curcio, C.A., Allen, K.A., 1990. Topography of ganglion cells in human retina. J. Comp. Neurol. 300, 5–25.
Curcio, C.A., Sloan, K.R.J., Packer, O., Hendrickson, A.E., Kalina, R.E., 1987. Distribution of cones in human and monkey retina: individual variability and radial asymmetry. Science 236, 579–582.
Curcio, C.A., Sloan, K.R.J., Kalina, R.E., Hendrickson, A.E., 1990. Human photoreceptor topography. J. Comp. Neurol. 292, 497–523.
Curcio, C.A., Allen, K.A., Sloan, K.R., Lerea, C.L., Hurley, J.B., Klock, I.B., Milam, A.H., 1991. Distribution and morphology of human cone photoreceptors stained with anti-blue opsin. J. Comp. Neurol. 312, 610–624.
Curcio, C.A., Messinger, J.D., Sloan, K.R., Mitra, A., McGwin, G., Spaide, R.F., 2011. Human chorioretinal layer thicknesses measured in macula-wide, high-resolution histologic sections. Invest. Ophthalmol. Vis. Sci. 52, 3943–3954.
Curran, R.E., Robb, R.M., 1976. Isolated foveal hypoplasia. Arch. Ophthalmol. 94, 48–50.
Dacey, D.M., 1993. The mosaic of midget ganglion cells in the human retina. J. Neurosci. 13, 5334–5355.
Dacey, D.M., Lee, B.B., 1994. The 'blue-on' opponent pathway in primate retina originates from a distinct bistratified ganglion cell type. Nature 367, 731–735.
Da Silva, S., Cepko, C.L., 2017. Fgf8 expression and degradation of retinoic acid are required for patterning a high-acuity area in the retina. Dev. Cell 42, 68–81 e6.
Del Priore, L.V., Lewis, A., Tan, S., Carley, W.W., Webb, W.W., 1987. Fluorescence light microscopy of F-actin in retinal rods and glial cells. Invest. Ophthalmol. Vis. Sci. 28, 633–639.
De Monasterio, F.M., McCrane, E.P., Newlander, J.K., Schein, S.J., 1985. Density profile of blue-sensitive cones along the horizontal meridian of macaque retina. Invest. Ophthalmol. Vis. Sci. 26, 289–302.
Detwiler, S.R., 1943. Vertebrate Photoreceptors. Macmillan, New York.
Diaz-Araya, C., Provis, J.M., 1992. Evidence of photoreceptor migration during early foveal development: a quantitative analysis of human fetal retinae. Vis. Neurosci. 8, 505–514.
Distler, C., Dreher, Z., 1996. Glia cells of the monkey retina - II. Müller cells. Vision Res. 36, 2381–2394.
Distler, C., Kirby, M.A., 1996. Transience of astrocytes in the newborn macaque monkey retina. Eur. J. Neurosci. 8, 847–851.
Distler, C., Weigel, H., Hoffmann, K.P., 1993. Glia cells of the monkey retina. I. Astrocytes. J. Comp. Neurol. 333, 134–147.
Distler, C., Kopatz, K., Telkes, I., 2000. Developmental changes in astrocyte density in the macaque perifoveal region. Eur. J. Neurosci. 12, 1331–1341.
Dobson, V., Teller, D.Y., 1978. Visual acuity in human infants: a review and comparison of behavioral and electrophysiological studies. Vision Res. 18, 1469–1483.
Dollery, C.T., Bulpitt, C.J., Kohner, E.M., 1969. Oxygen supply to the retina from the retinal and choroidal circulation at normal and increased arterial oxygen tensions. Invest. Ophthalmol. 8, 588–594.
Drasdo, N., Millican, C.L., Katholi, C.R., Curcio, C.A., 2007. The length of Henle fibers in the human retina and a model of ganglion receptive field density in the visual field. Vision Res. 47, 2901–2911.
Drenckhahn, D., Wagner, H.J., 1985. Relation of retinomotor responses and contractile proteins in vertebrate retinas. Eur. J. Cell Biol. 37, 156–168.
Dubis, A.M., Hansen, B.R., Cooper, R.F., Beringer, J., Dubra, A., Carroll, J., 2012a. Relationship between the foveal avascular zone and foveal pit morphology. Invest. Ophthalmol. Vis. Sci. 53, 1628–1636.
Dubis, A.M., Costakos, D.M., Subramaniam, C.D., Godara, P., Wirostko, W.J., Carroll, J., Provis, J.M., 2012b. Evaluation of normal human foveal development using optical coherence tomography and histologic examination. Arch. Ophthalmol. 130, 1291–1300.
Duke-Elder, S., 1958. The Eye in Evolution. Kimpton, London.
Dyer, M.A., Martins, R., Da Silva Filho, M., Muniz, J.A., Silveira, L.C., Cepko, C.L., Finlay, B.L., 2009. Developmental sources of conservation and variation in the evolution of the primate eye. Proc. Natl. Acad. Sci. U. S. A 106, 8963–8968.
Elsner, A.E., Burns, S.A., Beausencourt, E., Weiter, J.J., 1998. Foveal cone photopigment distribution: small alterations associated with macular pigment distribution. Invest. Ophthalmol. Vis. Sci. 39, 2394–2404.
Engerman, R.L., 1976. Development of the macular circulation. Invest. Ophthalmol. 15, 835–840.
Enoch, J.M., Van Loo Jr., J.A., Okun, E., 1973. Realignment of photoreceptors disturbed in orientation secondary to retinal detachment. Invest. Ophthalmol. 12, 849–853.
Finlay, B.L., De Lima Silveira, C.L., Reichenbach, A., 2005. Comparative aspects of visual system development. In: Kremers, J. (Ed.), The Primate Visual System. A Comparative Approach. John Wiley & Sons, Chichester, pp. 37–72.
Finlay, B.L., Franco, E.C., Yamada, E.S., Crowley, J.C., Parsons, M., Muniz, J.A., Silveira, L.C., 2008. Number and topography of cones, rods and optic nerve axons in New and Old World primates. Vis. Neurosci. 25, 289–299.
Fite, K.V., Rosenfield-Wessels, S., 1975. A comparative study of deep avian foveas. Brain Behav. Evol. 12, 97–115.
Foos, R.Y., 1972. Posterior vitreous detachment. Trans. Am. Acad. Ophthalmol. Otolaryngol. 76, 480.
Franco, E.C., Finlay, B.L., Silveira, L.C., Yamada, E.S., Crowley, J.C., 2000. Conservation of absolute foveal area in New World monkeys. A constraint on eye size and conformation. Brain Behav. Evol. 56, 276–286.
Franz, V., 1913. Sehorgan. In: Oppel, A. (Ed.), Lehrbuch der vergleichenden mikroskopischen Anatomie der Wirbeltiere. Siebenter Teil. G. Fischer, Jena.
Franze, K., Grosche, J., Skatchkov, S.N., Schinkinger, S., Foja, C., Schild, D., Uckermann, O., Travis, K., Reichenbach, A., Guck, J., 2007. Müller cells are living optical fibers in the vertebrate retina. Proc. Natl. Acad. Sci. U. S. A 104, 8287–8292.
Frey, K., Zimmerling, B., Scheibe, P., Rauscher, F.G., Reichenbach, A., Francke, M., Brunner, R., 2017. Does the foveal shape influence the image formation in human eyes? Adv. Opt. Techn 6, 403–410.
Fukuda, Y.H., Sawai, M., Watanabe, K., Wakakuwa, K., Morigawa, K., 1989. Nasotemporal overlap of crossed and uncrossed retinal ganglion cell projections in the Japanese monkey (*Macaca fuscata*). J. Neurosci. 9, 2353–2373.
Fulton, A.B., Albert, D.M., Craft, J.L., 1978. Human albinism: light and electron microscopy. Arch. Ophthalmol. 96, 305–310.
Gandorfer, A., Rohleder, M., Sethi, C., Eckle, D., Welge-Lüssen, U., Kampik, A., Luthert, P., Charteris, D., 2004. Posterior vitreous detachment induced by microplasmin. Invest. Ophthalmol. Vis. Sci. 45, 641–647.
Gao, H., Hollyfield, J.G., 1992. Aging of the human retina. Differential loss of neurons and retinal pigment epithelial cells. Invest. Ophthalmol. Vis. Sci. 33, 1–17.
Gariano, R.F., 2010. Special features of human retinal angiogenesis. Eye 24, 401–407.
Gariano, R.F., Iruela-Arispe, M.L., Hendrickson, A.E., 1994. Vascular development in primate retina: comparison of laminar plexus formation in monkey and human. Invest. Ophthalmol. Vis. Sci. 35, 3442–3455.
Gariano, R.F., Sage, E.H., Kaplan, H.J., Hendrickson, A.E., 1996. Development of astrocytes and their relation to blood vessels in fetal monkey retina. Invest. Ophthalmol. Vis. Sci. 37, 2367–2375.
Gass, J.D.M., 1999. Müller cell cone, an overlooked part of the anatomy of the fovea centralis. Arch. Ophthalmol. 117, 821–823.
Georges, P., Madigan, M.C., Provis, J.M., 1999. Apoptosis during development of the human retina: relationship to foveal development and retinal synaptogenesis. J. Comp. Neurol. 413, 198–208.
Gong, D., Zou, X., Zhang, X., Yu, W., Qu, Y., Dong, F., 2016. The influence of age and central foveal thickness on foveal zone size in healthy people. Ophthalmic Surg. Lasers Imaging Retina 47, 142–148.
Gorrand, J.-M., 1979. Diffusion of the human retina and quality of the optics of the eye on

the fovea and the peripheral retina. Vision Res. 19, 907–912.
Greeff, R., 1900. Die mikroskopische Anatomie des Sehnerven und der Netzhaut. In: Von Graefe-saemisch Handb. D. Augenheilk., Bd. 1, Abt. 2, Kap. 5. Engelmann, Leipzig.
Grünert, U., Greferath, U., Boycott, B.B., Wässle, H., 1993. Parasol (Pα) ganglion-cells of the primate fovea: immunocytochemical staining with antibodies against $GABA_A$-receptors. Vision Res. 33, 1–14.
Halfter, W., Sebag, J., Cunningham Jr., E.T., 2014. Vitreoretinal interface and inner limiting membrane. In: Sebag, J. (Ed.), Vitreous: in Health and Disease. Springer Science + Business Media, New York, pp. 165–191.
Harkness, L., Bennet-Clark, H.C., 1978. The deep fovea as a focus indicator. Nature 272, 814–816.
Hecht, S., Verrijp, C.D., 1933. Intermittent stimulation by light: III. The relation between intensity and critical fusion frequency for different retinal locations. J. Gen. Physiol. 17, 251–268.
Hendrickson, A.E., 1992. A morphological comparison of foveal development in man and monkey. Eye 6, 136–144.
Hendrickson, A., 2005. Organization of the adult primate fovea. In: Penfold, P.L., Provis, J.M. (Eds.), Macular Degeneration. Springer, Berlin, Heidelberg, pp. 1–23.
Hendrickson, A.E., Kupfer, C., 1976. The histogenesis of the fovea in the macaque monkey. Invest. Ophthalmol. Vis. Sci. 15, 746–756.
Hendrickson, A.E., Yuodelis, C., 1984. The morphological development of the human fovea. Ophthalmology 91, 603–612.
Hendrickson, A., Drucker, D., 1992. The development of parafoveal and mid-peripheral human retina. Behav. Brain Res. 49, 21–31.
Hendrickson, A., Provis, J., 2006. Comparison of the development of the primate fovea centralis with peripheral retina. In: Sernagor, E., Eglen, S., Harris, B., Wong, R. (Eds.), Retinal Development. Cambridge University Press, Cambridge, UK, pp. 126–149.
Hendrickson, A., Djajadi, H.R., Nakamura, L., Possin, D.E., Sajuthi, D., 2000. Nocturnal tarsier retina has both short and long/medium-wavelength cones in an unusual topography. J. Comp. Neurol. 424, 718–730.
Hendrickson, A., Troilo, D., Possin, D., Springer, A., 2006a. Development of the neural retina and its vasculature in the marmoset *Callithrix jacchus*. J. Comp. Neurol. 497, 270–286.
Hendrickson, A., Djajadi, H., Erickson, A., Possin, D., 2006b. Development of the human retina in the absence of ganglion cells. Exp. Eye Res. 83, 920–931.
Hendrickson, A., Possin, D., Vajzovic, L., Toth, C.A., 2012. Histologic development of the human fovea from midgestation to maturity. Am. J. Ophthalmol. 154, 767–778.
Henrich, P.B., Monnier, C.A., Halfter, W., Haritoglou, C., Strauss, R.W., Lim, R.Y., Loparic, M., 2012. Nanoscale topographic and biomechanical studies of the human internal limiting membrane. Invest. Ophthalmol. Vis. Sci. 53, 2561–2570.
Hogan, M.J., Alvarado, J.A., Wendell, J.E., 1971. Histology of the Human Eye: an Atlas and Textbook. W.B. Saunders, Toronto, Canada.
Holländer, H., Makarov, F., Dreher, Z., Van Driel, D., Chan-Ling, T.L., Stone, J., 1991. Structure of the macroglia of the retina: sharing and division of labour between astrocytes and Müller cells. J. Comp. Neurol. 313, 587–603.
Hollenberg, M.J., Spira, A.W., 1973. Human retinal development: ultrastructure of the outer retina. Am. J. Anat. 137, 357–385.
Ilia, M., Jeffery, G., 2000. Retinal cell addition and rod production depend on early stages of ocular melanin synthesis. J. Comp. Neurol. 420, 437–444.
Izumi-Nagai, K., Nagai, N., Ohgami, K., Satofuka, S., Ozawa, Y., Tsubota, K., 2007. Umezawa K, Ohno S, Oike Y, Ishida S. Macular pigment lutein is antiinflammatory in preventing choroidal neovascularization. Arterioscler. Thromb. Vasc. Biol. 27, 2555–2562.
Jacobs, G.H., 1998. Photopigments and seeing – lessons from natural experiments – the proctor lecture. Invest. Ophthalmol. Vis. Sci. 39, 2205–2216.
Jacobs, G.H., Deegan, J.F., 2001. Photopigments and colour vision in New World monkeys from the family atelidae. Proc. Royal Soc. Lond. B 268, 695–702.
Kaplan, E., Lee, B.B., Shapley, R.M., 1990. New views of primate retinal function. Prog. Retin. Res. 9, 273–336.
Kawano, K., Uehara, F., Sameshima, M., Ohba, N., 1984. Binding sites of peanut agglutinin in mammalian retina. Jpn. J. Ophthalmol. 28, 205–214.
Kelling, S.T., Sengelaub, D.R., Wikler, K.C., Finlay, B.L., 1989. Differential elasticity of the immature retina: a contribution to the development of the area centralis? Vis. Neurosci. 2, 117–120.
Kinnear, P.E., Jay, B., Witkop, C.J., 1985. Albinism. Surv. Ophthalmol 30, 75–101.
Kirby, M.A., Steineke, T.C., 1992. Morphogenesis of retinal ganglion cells during formation of the fovea in the Rhesus macaque. Vis. Neurosci. 9, 603–616.
Klug, K., Herr, S., Ngo, I.T., Sterling, P., Schein, S., 2003. Macaque retina contains an S-cone OFF midget pathway. J. Neurosci. 23, 9881–9887.
Kolb, H., Famiglietti, E.V., 1974. Rod and cone pathways in the inner plexiform layer of cat retina. Science 186, 47–49.
Kolb, H., Marshak, D., 2003. The midget pathways of the primate retina. Doc. Ophthalmol. 106, 67–81.
Kolb, H., Boycott, B.B., Dowling, J.E., 1969. A second type of midget bipolar cell in the primate retina. Philos. Trans. Royal Soc. Lond. B 255, 177–184.
Kolmer, W., 1930. Zur Kenntnis des Auges der Primaten. Z. Anat. Entwicklungsgesch 93, 679–722.
Kolmer, W., Lauber, H., 1936. Haut und Sinnesorgane. Zweiter Teil: Auge. Springer, Heidelberg.
König, A., 1894. Über den menschlichen Sehpurpur und seine Bedeutung für das Sehen. S. B. Akad Wiss Berlin. pp. 577–598.
Kouyama, N., Marshak, D.W., 1992. Bipolar cells specific for blue cones in the macaque retina. J. Neurosci. 12, 1233–1252.
Kozulin, P., Natoli, R., Bumsted O'Brien, K.M., Madigan, M.C., Provis, J.M., 2010. The cellular expression of antiangiogenic factors in fetal primate macula. Invest. Ophthalmol. Vis. Sci. 51, 4298–4306.
Krebs, W., Krebs, I.P., 1989. Quantitative morphology of the central retina in the primate retina. Am. J. Anat. 184, 225–236.
Kreysing, M., Boyde, L., Guck, J., Chalut, K.J., 2010. Physical insight into light scattering by photoreceptor cell nuclei. Opt. Lett. 35, 2639–2641.
Kuhrt, H., Gryga, M., Wolburg, H., Joffe, B., Grosche, J., Reichenbach, A., Noori, H.R., 2012. Postnatal mammalian retinal development: Quantitative data and general rules. Prog. Retin. Eye Res. 31, 605–621.
Labin, A.M., Safuri, S.K., Ribak, E.N., Perlman, I., 2014. Müller cells separate between wavelengths to improve day vision with minimal effect upon night vision. Nat. Commun. 5, 4319.
Lamb, T.D., 2013. Evolution of phototransduction, vertebrate photoreceptors and retina. Prog. Retin. Eye Res. 36, 52–119.
Lamb, T.D., Collin, S.P., Pugh Jr., E.N., 2007. Evolution of the vertebrate eye: opsins, photoreceptors, retina and eye cup. Nat. Rev. Neurosci. 8, 960–976.
Land, M.F., 1972. The physics and biology of animal reflectors. Prog. Biophys. Mol. Biol. 24, 75–106.
LaVail, M.M., Rapaport, D.H., Rakic, P., 1991. Cytogenesis in the monkey retina. J. Comp. Neurol. 309, 86–114.
Lee, H., Purohit, R., Patel, A., Papageorgiou, E., Sheth, V., Maconachie, G., Pilat, A., McLean, R.J., Proudlock, F.A., Gottlob, I., 2015. *In vivo* foveal development using optical coherence tomography. Invest. Ophthalmol. Vis. Sci. 56, 4537–4545.
Leventhal, A.G., Ault, S.J., Vitek, D.J., 1988. The nasotemporal division in primate retina: the neural bases of macular sparing and splitting. Science 240, 66–67.
Lindqvist, N., Liu, Q., Zajadacz, J., Franze, K., Reichenbach, A., 2010. Retinal glial (Müller) cells: sensing and responding to tissue stretch. Invest. Ophthalmol. Vis. Sci. 51, 1683–1690.
Locket, N.A., 1992. Problems of deep foveas. Aust. N. Z. J. Ophthalmol. 20, 281–295.
Lu, Y.-B., Franze, K., Seifert, G., Steinhäuser, C., Kirchhoff, F., Wolburg, H., Guck, J., Janmey, P., Wie, E.-Q., Käs, J., Reichenbach, A., 2006. Viscoelastic properties of individual glial cells and neurons in the CNS. Proc. Natl. Acad. Sci. U. S. A 103, 17759–17764.
Lu, Y.B., Iandiev, I., Hollborn, M., Körber, N., Ulbricht, E., Hirrlinger, P.G., Pannicke, T., Wie, E.Q., Bringmann, A., Wolburg, H., Wilhelmsson, U., Pekny, M., Wiedemann, P., Reichenbach, A., Käs, J.A., 2011. Reactive glial cells: increased stiffness correlates with increased intermediate filament expression. FASEB J 25, 624–631.
Lujan, B.J., Roorda, A., Knighton, R.W., Carroll, J., 2011. Revealing Henle's fiber layer using spectral domain optical coherence tomography. Invest. Ophthalmol. Vis. Sci. 52, 1486–1492.
Lundkvist, A., Reichenbach, A., Betsholtz, C., Carmeliet, P., Wolburg, H., Pekny, M., 2004. Under stress, the absence of intermediate filaments from Müller cells in the retina has structural and functional consequences. J. Cell Sci. 117, 3481–3488.
MacDonald, R.B., Randlett, O., Oswald, J., Yoshimatsu, T., Franze, K., Harris, W.A., 2015. Müller glia provide essential tensile strength to the developing retina. J. Cell Biol. 210, 1075–1083.
Mann, I., 1964. The Development of the Human Eye. Grune and Stratton, New York.
Mansour, A.M., Schachat, A., Bodiford, G., Haymond, R., 1993. Foveal avascular zone in diabetes mellitus. Retina 13, 125–128.
Marmor, M.F., Choi, S.S., Zawadzki, R.J., Werner, J.S., 2008. Visual insignificance of the foveal pit: reassessment of foveal hypoplasia as fovea plana. Arch. Ophthalmol. 126, 907–913.
Martin, P.R., Grünert, U., 1992. Spatial density and immunoreactivity of bipolar cells in the macaque monkey retina. J. Comp. Neurol. 323, 269–287.
Martin, P.R., Grünert, U., 1999. Analysis of the short wavelength-sensitive ("blue") cone mosaic in the primate retina: Comparison of New World and Old World monkeys. J. Comp. Neurol. 406, 1–14.
Mastronarde, D.N., Thibeault, M.A., Dubin, M.W., 1984. Non-uniform postnatal growth of the cat retina. J. Comp. Neurol. 228, 598–608.
Matet, A., Savastano, M.C., Rispoli, M., Bergin, C., Moulin, A., Crisanti, P., Behar-Cohen, F., Lumbroso, B., 2015. *En face* optical coherence tomography of foveal microstructure in full-thickness macular hole: a model to study perifoveal Müller cells. Am. J. Ophthalmol. 159, 1142–1151.
McAllister, J.T., Dubis, A.M., Tait, D.M., Ostler, S., Rha, J., Stepien, K.E., Summers, C.G., Carroll, J., 2010. Arrested development: high-resolution imaging of foveal morphology in albinism. Vision Res. 50, 810–817.
McCafferty, B.K., Wilk, M.A., McAllister, J.T., Stepien, K.E., Dubis, A.M., Brilliant, M.H., Anderson, J.L., Carroll, J., Summers, C.G., 2015. Clinical insights into foveal morphology in albinism. J. Pediatr. Ophthalmol. Strabismus 52, 167–172.
McGuire, D.E., Weinreb, R.N., Goldbaum, M.H., 2003. Foveal hypoplasia demonstrated *in vivo* with optical coherence tomography. Am. J. Ophthalmol. 135, 112–114.
Mietz, H., Green, W.R., Wolff, S.M., Abundo, G.P., 1992. Foveal hypoplasia in complete oculocutaneous albinism. A histopathologic study. Retina 12, 254–260.
Mohammad, S., Gottlob, I., Kumar, A., Thomas, M., Degg, C., Sheth, V., Proudlock, F.A., 2011. The functional significance of foveal abnormalities in albinism measured using spectral-domain optical coherence tomography. Ophthalmology 118, 1645–1652.
Mollon, J.D., Bowmaker, J.K., 1992. The spatial arrangement of cones in the primate fovea. Nature 360, 677–679.
Moritz, G.L., Melin, A.D., Tuh Yit Yu, F., Bernard, H., Ong, P.S., Dominy, N.J., 2014. Niche convergence suggests functionality of the nocturnal fovea. Front. Integr. Neurosci. 8, 61.
Müller, H., 1851. Zur Histologie der Netzhaut. Z. Wiss. Zool. 3, 234–237.
Müller, H., 1856. Anatomisch-physiologische Untersuchungen über die Retina des Menschen und der Wirbelthiere. Z. Wiss. Zool. 8, 1–122.
Müller, H., 1861. Ueber das ausgedehnte Vorkommen einer dem gelben Fleck der Retina entsprechenden Stelle bei Thieren. Vorläufige Notiz. Würzb. Naturwiss. Zeitschr 2, 139.
Müller, H., 1862. Ueber das Auge des Chamäleon mit vergleichenden Bemerkungen.

Würzb. Naturwiss. Zeitschr 3, 10–42.
Müller, H., 1863. Ueber das Vorhandensein zweier Foveae in der Netzhaut vieler Vogelaugen. Zehender's Klin. Monatsbl 438–440.
Nishikawa, S., 2006–07. The pathology of Müller cells under different disease conditions. Neuroembryol. Aging 4, 61–75.
Nishikawa, S., Tamai, M., 2001. Müller cells in the human foveal region. Curr. Eye Res. 22, 34–41.
Nishimura, Y., Rakic, P., 1985. Development of the rhesus monkey retina. I. Emergence of the inner plexiform layer and its synapses. J. Comp. Neurol. 241, 420–434.
Oliver, M.D., Dotan, S.A., Chemke, J., Abraham, F.A., 1987. Isolated foveal hypoplasia. Br. J. Ophthalmol. 71, 926–930.
Omri, S., Omri, B., Savoldelli, M., Jonet, L., Thillaye-Goldenberg, B., Thuret, G., Gain, P., Jeanny, J.C., Crisanti, P., Behar-Cohen, F., 2010. The outer limiting membrane (OLM) revisited: clinical implications. Clin. Ophthalmol. 4, 183–195.
Oppel, O., 1967. Untersuchungen über die Verteilung und Zahl der retinalen Ganglienzellen beim Menschen. Graefes Arch. Clin. Exp. Ophthalmol. 172, 1–22.
Packer, O., Hendrickson, A.E., Curcio, C.A., 1989. Photoreceptor topography of the adult pigtail macaque (*Macaca nemestrina*) retina. J. Comp. Neurol. 288, 165–183.
Packer, O., Hendrickson, A.E., Curcio, C.A., 1990. Development redistribution of photoreceptors across the *Macaca nemestrina* (pigtail macaque) retina. J. Comp. Neurol. 298, 472–493.
Packer, O.S., Verweij, J., Li, P.H., Schnapf, J.L., Dacey, D.M., 2010. Blue-yellow opponency in primate S cone photoreceptors. J. Neurosci. 30, 568–572.
Penfold, P.L., Provis, J.M., 1986. Cell death in human retinal development: Phagocytosis of pyknotic and apoptotic bodies by retinal cells. Graefes Arch. Clin. Exp. Ophthalmol. 224, 549–553.
Penfold, P.L., Provis, J.M., 1991. Antibodies to human leucocyte antigens indicate subpopulations of microglia in human retina. Vis. Neurosci. 7, 383–388.
Percival, K.A., Martin, P.R., Grünert, U., 2013. Organisation of koniocellular-projecting ganglion cells and diffuse bipolar cells in the primate fovea. Eur. J. Neurosci. 37, 1072–1089.
Perry, V.H., Cowey, A., 1985. The ganglion cell and cone distributions in the monkey's retina: Implications for central magnification factors. Vision Res. 25, 1795–1810.
Perry, V.H., Cowey, A., 1988. The length of the fibres of Henle in the retina of macaque monkeys: Implications for vision. Neuroscience 25, 225–236.
Perry, V.H., Oehler, R., Cowey, A., 1984. Retinal ganglion cells that project to the dorsal lateral geniculate nucleus in the macaque monkey. Neuroscience 12, 1101–1123.
Piersol, G.A., 1897. The microscopical anatomy of the eyeball. In: Norris, W.F., Oliver, C.A. (Eds.), System of Diseases of the Eye. Vol. I. Embryology, Anatomy, and Physiology of the Eye. J.B. Lippincott Company, Philadelphia, PA, pp. 217–382.
Polyak, S.L., 1941. The Retina. University of Chicago Press, Chicago.
Polyak, S.L., 1957. The Vertebrate Visual System. University of Chicago Press, Chicago.
Ponsioen, T.L., Van Luyn, M.J.A., Van der Worp, R.J., Pas, H.H., Hooymans, J.M.M., Los, L.I., 2008. Human retinal Müller cells synthesize collagens of the vitreous and vitreoretinal interface *in vitro*. Mol. Vis. 14, 652–660.
Provis, J.M., 1987. Patterns of cell death in the ganglion cell layer of the human fetal retina. J. Comp. Neurol. 259, 237–246.
Provis, J.M., 2001. Development of the primate retinal vasculature. Prog. Retin. Eye Res. 20, 799–821.
Provis, J.M., Hendrickson, A.E., 2008. The foveal avascular region of developing human retina. Arch. Ophthalmol. 126, 507–511.
Provis, J.M., Van Driel, D., Billson, F.A., Russell, P., 1985a. Development of the human retina: Patterns of cell distribution and redistribution in the ganglion cell layer. J. Comp. Neurol. 233, 429–451.
Provis, J.M., Van Driel, D., Billson, F.A., Russell, P., 1985b. Human fetal optic nerve: Overproduction and elimination of retinal axons during development. J. Comp. Neurol. 238, 92–100.
Provis, J.M., Diaz, C.M., Dreher, B., 1998. Ontogeny of the primate fovea: A central issue in retinal development. Prog. Neurobiol. 54, 549–580.
Provis, J.M., Sandercoe, T., Hendrickson, A.E., 2000. Astrocytes and blood vessels define the foveal rim during primate retinal development. Invest. Ophthalmol. Vis. Sci. 41, 2827–2836.
Provis, J.M., Penfold, P.L., Cornish, E.E., Sandercoe, T.M., Madigan, M.C., 2005. Anatomy and development of the macula: specialisation and the vulnerability to macular degeneration. Clin. Exp. Optom. 88, 269–281.
Provis, J.M., Dubis, A.M., Maddess, T., Carroll, J., 2013. Adaptation of the central retina for high acuity vision: cones, the fovea and the avascular zone. Prog. Retin. Eye Res. 35, 63–81.
Pum, D., Ahnelt, P.K., Grasl, M., 1990. Iso-orientation areas in the foveal cone mosaic. Vis. Neurosci. 5, 511–523.
Pumphrey, R.J., 1948. The theory of the fovea. J. Exp. Biol. 25, 299–312.
Querques, G., Bux, A.V., Iaculli, C., Delle Noci, N., 2008. Isolated foveal hypoplasia. Retina 28, 1552–1553.
Ramírez, J.M., Triviño, A., Ramírez, A.I., Salazar, J.J., García-Sánchez, J., 1996. Structural specializations of human retinal glial cells. Vision Res. 36, 2029–2036.
Ramón y Cajal, S., 1891. Significación fisiológica de las expansiones protoplásmicas y nerviosas de las células de la substancia gris. Revista de Ciencias Médicas. In: Memoria leída en el Congreso Médico de Valencia. Sesión de 24 de junio de 1891 con cinco grabados, Barcelona, 22, XVII: 1–15.
Ramón y Cajal, S., 1894. Die Retina der Wirbelthiere. J.F. Bergmann, Wiesbaden.
Rapaport, D.H., Fletcher, J.T., LaVail, M.M., Rakic, P., 1992. Genesis of neurons in the retinal ganglion cell layer of the monkey. J. Comp. Neurol. 322, 577–588.
Reading, V.M., Weale, R.A., 1974. Macular pigment and chromatic aberration. J. Opt. Soc. Am. 64, 231–234.
Reichenbach, A., 1989. Attempt to classify glial cells by means of their process specialization using the rabbit retinal Müller cell as an example of cytotopographic specialization of glial cells. Glia 2, 250–259.
Reichenbach, A., 1993. Two types of neuronal precursor cells in the mammalian retina – a short review. J. Hirnforsch. 34, 335–341.
Reichenbach, A., Pritz-Hohmeier, S., 1995. Normal and disturbed early development of the eye anlagen. Prog. Retin. Eye Res. 14, 1–46.
Reichenbach, A., Robinson, S.R., 1995. Phylogenetic constraints on retinal organization and development: an Haeckelian perspective. Prog. Retin. Eye Res. 15, 139–171.
Reichenbach, A., Bringmann, A., 2010. Müller Cells in the Healthy and Diseased Retina. Springer, New York, Dordrecht, Heidelberg, London.
Reichenbach, A., Bringmann, A., 2016. Retinal Glia. In: Verkhratsky, A., Parpura, V. (Eds.), Colloquium Series on Neuroglia in Biology and Medicine: from Physiology to Disease. Morgan & Claypool Life Sciences, Philadelphia, PA.
Reichenbach, A., Bringmann, A., 2017. Comparative anatomy of glial cells in mammals. In: In: Kaas, J. (Ed.), Evolution of Nervous Systems, 2nd Edition, vols. 2.I. Elsevier, Oxford, pp. 309–348.
Reichenbach, A., Schnitzer, J., Friedrich, A., Ziegert, W., Brückner, G., Schober, W., 1991. Development of the rabbit retina. I. Size of eye and retina, and postnatal cell proliferation. Anat. Embryol. 183, 287–297.
Reichenbach, A., Ziegert, M., Schnitzer, J., Pritz-Hohmeier, S., Schaaf, P., Schober, W., Schneider, H., 1994. Development of the rabbit retina. V. The question of 'columnar units' Dev. Brain Res. 79, 72–84.
Robinson, S.R., Hendrickson, A., 1995. Shifting relationships between photoreceptors and pigment epithelial cells in monkey retina: implications for the development of retinal topography. Vis. Neurosci. 12, 767–778.
Rochon-Duvigneaud, A., 1907. Recherches sur la fovea de la retine humaine et particulierement sur le bouquet des cones centraux. Arch. d'Anat. Microscop 9, 315–342.
Rohen, J.W., Castenholtz, A., 1967. Über die Zentralisation der Retina bei Primaten. Folia Primat 5, 92–147.
Röll, B., 2001. Gecko vision – retinal organization, foveae and implications for binocular vision. Vision Res. 41, 2043–2056.
Roorda, A., Metha, A.B., Lennie, P., Williams, D.R., 2001. Packing arrangement of the three cone classes in primate retina. Vision Res. 41, 1291–1306.
Rosén, R., Sjöstrand, J., Nilsson, M., Hellgren, K., 2015. A methodological approach for evaluation of foveal immaturity after extremely preterm birth. Ophthalmic Physiol. Optics 433–441.
Ross, C.F., 2004. The tarsier fovea: Functionless vestige or nocturnal adaptation? In: Ross, C.F., Kay, R.F. (Eds.), Anthropoid Origins: New Visions. Kluwer Academic/Plenum Publishers, New York, pp. 477–537.
Rossi, E.A., Roorda, A., 2010. The relationship between visual resolution and cone spacing in the human fovea. Nat. Neurosci. 13, 156–157.
Rowe, M.H., Dreher, B., 1982. Functional morphology of beta cells in the area centralis of the cat's retina: A model for the evolution of central retinal specializations. Brain Behav. Evol. 21, 1–23.
Rudich, D.S., Curcio, C.A., Wasserstein, M., Brodie, S.E., 2013. Inner macular hyperreflectivity demonstrated by optical coherence tomography in niemann-pick disease. JAMA Ophthalmol 131, 1244–1246.
Salzmann, M., 1912. Anatomie und Histologie des menschlichens Augapfels im Normalzustande. (seine Entwicklung und sein Altern. Leipzig).
Sandercoe, T.M., Geller, S.F., Hendrickson, A.E., Stone, J., Provis, J.M., 2003. VEGF expression by ganglion cells in central retina before formation of the foveal depression in monkey retina: evidence of developmental hypoxia. J. Comp. Neurol. 462, 42–54.
Savy, C., Simon, A., Nguyen-Legros, J., 1991. Spatial geometry of the dopamine innervation in the avascular area of the human fovea. Vis. Neurosci. 7, 487–498.
Schein, S.J., 1988. Anatomy of macaque fovea and spatial densities of neurons in foveal representation. J. Comp. Neurol. 269, 479–505.
Schnitzer, J., 1987. Retinal astrocytes: their restriction to vascularized parts of the mammalian retina. Neurosci. Lett. 78, 29–34.
Schulte, D., Peters, M.A., Sen, J., Cepko, C.L., 2005. The rod photoreceptor pattern is set at the optic vesicle stage and requires spatially restricted cVax expression. J. Neurosci. 25, 2823–2831.
Schultze, M., 1866. Zur Anatomie und Physiologie der Retina. Arch. Mikrosk. Anat. 2, 165–286.
Schultze, M., 1867. Ueber Stäbchen und Zapfen der Retina. Arch. Mikrosk. Anat. 3, 215–247.
Sinha, R., Hoon, M., Baudin, J., Okawa, H., Wong, R.O., Rieke, F., 2017. Cellular and circuit mechanisms shaping the perceptual properties of the primate fovea. Cell 168, 413–426.
Sivak, J.G., Mandelman, T., 1982. Chromatic dispersion of the ocular media. Vision Res. 22, 997–1003.
Sjöstrand, J., Conradi, N., Klaren, L., 1994. How many ganglion cells are there to a foveal cone? Graefes Arch. Clin. Exp. Ophthalmol. Times 232, 432–437.
Sjöstrand, J., Olsson, V., Popovic, Z., Conradi, N., 1999Fa. Quantitative estimations of foveal and extra-foveal retinal circuitry in humans. Vision Res. 39, 2987–2998.
Sjöstrand, J., Popovic, Z., Conradi, N., Marshall, J., 1999Fb. Morphometric study of the displacement of retinal ganglion cells subserving cones within the human fovea. Graefes Arch. Clin. Exp. Ophthalmol. Times 237, 1014–1023.
Slonacker, J.R., 1897. A Comparative Study of the Area of Acute Vision in Vertebrates. Harvard University Press, Cambridge, MA.
Smelser, G.K., Ozanics, V., Rayborn, M., Sagun, D., 1973. The fine structure of the retinal transient layer of chievitz. Invest. Ophthalmol. 12, 504–512.
Snodderly, D.M., Auran, J.D., Delori, F.C., 1984. The macular pigment. II. Spatial distribution in primate retinas. Invest. Ophthalmol. Vis. Sci. 25, 674–685.
Snodderly, D.M., Weinhaus, R.S., Choi, J.C., 1992. Neural-vascular relationships in the central retina of macaque monkeys (*Macaca fascicularis*). J. Neurosci. 12, 1169–1193.
Snow, D.M., Watanabe, M., Letourneau, P.C., Silver, J., 1991. A chondroitin sulfate proteoglycan may influence the direction of retinal ganglion cell outgrowth.

Development 113, 1473–1485.
Snyder, A.W., Miller, W.H., 1978. Telephoto lens system of falconiform eyes. Nature 275, 127–129.
Solovei, I., Kreysing, M., Lanctot, C., Kösem, S., Peichl, L., Cremer, T., Guck, J., Joffe, B., 2009. Nuclear architecture of rod photoreceptor cells adapts to vision in mammalian evolution. Cell 137, 356–368.
Sömmerring, S.T., 1795. Foramilunum centrale retinae. Göttingische Anzeigen von gelehrten Sachen unter der Aufsicht der Königl. Gesellschaft der Wissenschaften 2, 1401–1402.
Springer, A.D., 2014. Relationship between foveal cone specialization and pit morphology in albinism. Invest. Ophthalmol. Vis. Sci. 55, 5922.
Springer, A.D., Hendrickson, A.E., 2004a. Development of the primate area of high acuity: 1. Use of finite element analysis models to identify mechanical variables affecting pit formation. Vis. Neurosci. 21, 53–62.
Springer, A.D., Hendrickson, A.E., 2004b. Development of the primate area of high acuity: 2. Quantitative morphological changes associated with retinal and pars plana growth. Vis. Neurosci. 21, 775–790.
Springer, A.D., Hendrickson, A.E., 2005. Development of the primate area of high acuity: 3. Temporal relationships between pit formation, retinal elongation and cone packing. Vis. Neurosci. 22, 171–185.
Springer, A., Troilo, D., Possin, D., Hendrickson, A., 2011. Foveal cone density shows a rapid postnatal maturation in the marmoset monkey. Vis. Neurosci. 28, 473–484.
Stuermer, C.A., Bastmeyer, M., 2000. The retinal axon's pathfinding to the optic disk. Prog. Neurobiol. 62, 197–214.
Syrbe, S., Kuhrt, H., Gärtner, U., Habermann, G., Wiedemann, P., Bringmann, A., Reichenbach, A., 2018. Müller glial cells of the primate foveola: An electron microscopical study. Exp. Eye Res. 167, 110–117.
Thomas, M.G., Kumar, A., Mohammad, S., Proudlock, F.A., Engle, E.C., Andrews, C., Chan, W.M., Thomas, S., Gottlob, I., 2011. Structural grading of foveal hypoplasia using spectral-domain optical coherence tomography a predictor of visual acuity? Ophthalmology 118, 1653–1660.
Thyagarajan, S., van Wyk, M., Lehmann, K., Löwel, S., Feng, G., Wässle, H., 2010. Visual function in mice with photoreceptor degeneration and transgenic expression of channelrhodopsin 2 in ganglion cells. J. Neurosci. 30, 8745–8758.
Tick, S., Rossant, F., Ghorbel, I., Gaudric, A., Sahel, J.A., Chaumet-Riffaud, P., Paques, M., 2011. Foveal shape and structure in a normal population. Invest. Ophthalmol. Vis. Sci. 52, 5105–5110.
Toates, F.M., 1972. Accommodation function of the human eye. Physiol. Rev. 52, 828–863.
Troilo, D., 1998. Changes in retinal morphology following experimentally induced myopia. OSA Techn. Digest 1, 206–209.
Tuchin, V.V., 2000. Tissue Optics. SPIE Press, Bellingham, WA.
Tucker, V.A., 2000. The deep fovea, sideways vision and spiral flight paths in raptors. J. Exp. Biol. 203, 3745–3754.
Usher, C.H., 1920. Histological examination of a human albino's eyeball, with a note on mesoblastic pigmentation in foetal eyes. Biometrika 13, 46–56.
Vajzovic, L., Hendrickson, A.E., O'Connell, R.V., Clark, L.A., Tran-Viet, D., Possin, D., Chiu, S.J., Farsiu, S., Toth, C.A., 2012. Maturation of the human fovea: correlation of spectral-domain optical coherence tomography findings with histology. Am. J. Ophthalmol. 154, 779–789.
Valentin, G., 1879. Ein Beitrag zur Kenntniss der Brechungsverhältnisse der Thiergewebe. Arch. Physiol. 19, 78–105.
Van Buren, J.M., 1963. The Retinal Ganglion Cell Layer. C.C. Thomas, Springfield.
Van Essen, D.C., 1997. A tension-based theory of morphogenesis and compact wiring in the central nervous system. Nature 385, 313–318.
Verardo, M., Lewis, G.P., Takeda, M., Linberg, K.A., Byun, J., Luna, G., Wilhelmsson, U., Pekny, M., Chen, D.F., Fisher, S.K., 2008. Abnormal reactivity of Müller cells after retinal detachment in mice deficient in GFAP and vimentin. Invest. Ophthalmol. Vis. Sci. 49, 3659–3665.
Wagner-Schuman, M., Dubis, A.M., Nordgren, R.N., Lei, Y., Odell, D., Chiao, H., Weh, E., Fischer, W., Sulai, Y., Dubra, A., Carroll, J., 2011. Race- and sex-related differences in retinal thickness and foveal pit morphology. Invest. Ophthalmol. Vis. Sci. 52, 625–634.
Walls, G.L., 1942. The Vertebrate Eye and its Adaptive Radiation. Cranbrook Press, Bloomfield Hills, MI.
Walsh, M.K., Goldberg, M.F., 2007. Abnormal foveal avascular zone in nanophthalmos. Am. J. Ophthalmol. 143, 1067–1068.
Wang, Y.Z., Morale, S.E., Cousins, R., Birch, E.E., 2009. Course of development of global hyperacuity over lifespan. Optom. Vis. Sci. 86, 695–700.
Wässle, H., Boycott, B., 1991. Functional architecture of mammalian retina. Physiol. Rev. 71, 447–480.
Wässle, H., Grünert, U., Röhrenbeck, J., Boycott, B.B., 1989. Cortical magnification factor and the ganglion cell density of the primate fovea. Nature 341, 643–646.
Wässle, H., Grünert, U., Röhrenbeck, J., Boycott, B.B., 1990. Retinal ganglion cell density and the cortical magnification factor in the primate. Vision Res. 30, 1897–1911.
Wässle, H., Grünert, U., Martin, P.R., Boycott, B.B., 1994. Immunohistochemical characterization and spatial distribution of midget bipolar cells in the macaque monkey retina. Vision Res. 34, 561–579.
Weale, R.A., 1966. Why does the human retina possess a fovea? Nature 212, 255–256.
Webb, S.V., Kaas, J.H., 1976. The sizes and distribution of ganglion cells in the retina of the owl monkey, *Aotus trivirgatus*. Vision Res. 16, 1247–1254.
Wikler, K.C., Rakic, P., 1990. Distribution of photoreceptor subtypes in the retina of diurnal and nocturnal primates. J. Neurosci. 10, 3390–3401.
Wikler, K.C., Williams, R.W., Rakic, P., 1990. Photoreceptor mosaic: Number and distribution of rods and cones in the rhesus monkey retina. J. Comp. Neurol. 297, 499–508.
Wilder, H.D., Grünert, U., Lee, B.B., Martin, P.R., 1996. Topography of ganglion cells and photoreceptors in the retina of a New World monkey: the marmoset *Callithrix jacchus*. Vis. Neurosci. 13, 335–352.
Wilk, M.A., McAllister, J.T., Cooper, R.F., Dubis, A.M., Patitucci, T.N., Summerfelt, P., Anderson, J.L., Stepien, K.E., Costakos, D.M., Connor Jr., T.B., Wirostko, W.J., Chiang, P.W., Dubra, A., Curcio, C.A., Brilliant, M.H., Summers, C.G., Carroll, J., 2014. Relationship between foveal cone specialization and pit morphology in albinism. Invest. Ophthalmol. Vis. Sci. 55, 4186–4198.
Wilk, M.A., Dubis, A.M., Cooper, R.F., Summerfelt, P., Dubra, A., Carroll, J., 2017. Assessing the spatial relationship between fixation and foveal specializations. Vision Res. 132, 53–61.
Williams, D.R., 1980. Visual consequences of the foveal pit. Invest. Opthalmol. Vis. Sci. 19, 653–667.
Williams, D.S., Arikawa, K., Paallysaho, T., 1990. Cytoskeletal components of the adherens junctions between the photoreceptors and the supportive Müller cells. J. Comp. Neurol. 295, 155–164.
Wilmer, E.N., Wright, W.D., 1945. Colour sensitivity of the fovea centralis. Nature 156, 119–121.
Wilson, H.R., Mets, M.B., Nagy, S.E., Kressel, A.B., 1988. Albino spatial vision as an instance of arrested visual development. Vision Res. 28, 979–990.
Wolf-Schnurrbusch, U.E., Röösli, N., Weyermann, E., Heldner, M.R., Höhne, K., Wolf, S., 2007. Ethnic differences in macular pigment density and distribution. Invest. Ophthalmol. Vis. Sci. 48, 3783–3787.
Wolin, L.R., Massopust, L.C., 1970. Morphology of the primate retina. In: In: Noback, C.R., Montagna, W. (Eds.), The Primate Brain, vol. 1. Appleton-Century-Crofts, New York, pp. 1–27.
Wood, C.A., 1917. The Fundus Oculi of Birds Especially as Viewed by the Ophthalmoscope. Lakeside Press, Chicago.
Wood, C.A., Woodruff, T.A., 1904. The Commoner Diseases of the Eye: How to Detect and How to Treat Them. G. P. Engelhard & Co., Chicago.
Woollard, H.H., 1927. The differentiation of the retina in primates. Proc. Zool. Soc. Lond. 1, 1–17.
Yamada, E., 1969. Some structural features of the fovea centralis in the human retina. Arch. Ophthalmol. 82, 151–159.
Yamada, E., Ishikawa, T., 1965. Some observations on the submicroscopic morphogenesis of the human retina. In: Rohen, J.W. (Ed.), The Structure of the Eye: II. Symposium. Schattauer, Stuttgart, pp. 5–16.
Yanni, S.E., Wang, J., Chan, M., Carroll, J., Farsiu, S., Leffler, J.N., Spencer, R., Birch, E.E., 2012. Foveal avascular zone and foveal pit formation after preterm birth. Br. J. Ophthalmol. 96, 961–966.
Yokotsuka, K., Kishi, S., Shimizu, K., 1997. White dot fovea. Am. J. Ophthalmol. 123, 76–83.
Yuodelis, C., Hendrickson, A., 1986. A qualitative and quantitative analysis of the human fovea during development. Vision Res. 26, 847–855.
Zernike, F., 1955. How I discovered phase contrast. Science 121, 345–349.
Zueva, L., Makarov, V., Zayas-Santiago, A., Golubeva, T., Korneeva, E., Savvinov, A., Eaton, M., Skatchkov, S., Inyushin, M., 2014. Müller cell alignment in bird fovea: possible role in vision. J. Neurosci. Neuroeng 3, 85–91.

View publication stats